DESIGN & IMPLEMENTATION OF A CONTROL SYSTEM
FOR USE OF GALVANOMETRIC SCANNERS
IN LASER MICROMACHINING APPLICATIONS

by
GÖNENÇ ÜLKER

Submitted to the Graduate School of Engineering and Natural Sciences
in partial fulfillment of
the requirements for the degree of
Master of Science

SABANCI UNIVERSITY
Spring 2011

DESIGN & IMPLEMENTATION OF A CONTROL SYSTEM
FOR USE OF GALVANOMETRIC SCANNERS
IN LASER MICROMACHINING APPLICATIONS

APPROVED BY:

Prof. Dr. ASIF ŞABANOVİÇ

(Thesis Advisor)
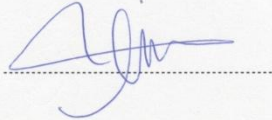
Associate Prof. KEMALETTİN ERBATUR

Associate Prof. ALİ KOŞAR

Associate Prof. AYHAN BOZKURT

Associate Prof. İBRAHİM TEKİN

DATE OF APPROVAL: 09.08.2011

DESIGN & IMPLEMENTATION OF A CONTROL SYTEM

FOR USE OF GALVANOMETRIC SCANNERS

IN LASER MICROMACHINING APPLICATIONS

Gönenç Ülker

Mechatronics, MSc Thesis, 2011

Thesis Supervisor: Prof. Dr. Asıf Şabanoviç

Keywords: Laser Micromachining, Galvanometric Scanner, Telecentric Lens, Raster
Scanning

ABSTRACT

In the recent years, laser machining technology has been used widely in industrial applications usually with the aim of increasing the production capability of mass production lines - especially for fast marking, engraving type of applications where speed is an important concern - or manufacturing quality of a certain facility by increasing the level of accuracy in material processing applications such as drilling, cutting; or any scientific research oriented work where high precision machining of parts in sub millimeter scale might be required.

A galvanometric scanner is a high precision device that is able to steer a laser beam with a mirror attached to a motor, whose rotor angular range is usually limited with tens of degrees in both directions of rotation; and position is controlled either by voltage or current. Due to their lightness, the rotor and the mirror can move very fast, allowing fast marking (burning out) operation with the laser beam. This can be evaluated as a great advantage compared to slower mechanical appliances used for cutting/machining of different materials.

This study concentrates on the analysis of galvanometric scanner system components; and the design and implementation of a hardware and software based control system for a dual-axis galvo setup; and their adaptation for use in laser micromachining applications either as a standalone system or a modular subsystem. Analysis part of the thesis work contains: evaluation of dominant laser micromachining techniques, an overview of the galvanometric scanner system based approach and related components (e.g. electromechanical, electrical, optical), understanding of working principles and related simulation work, compatibility issues with the target micromachining applications. Design part of the thesis work includes: the design and implementation of electronic controller board, intermediate drive electronics stage, microcontroller programming for machining control algorithm, interfacing with graphical user interface based control software and production of necessary mechanical parts. The study has been finalized with experimental work and evaluation of obtained results.

The results of these studies are promising and motivate the use of laser galvanometric scanner systems in laser micromachining applications.

LAZER MİKROİŞLEME AMAÇLI

GALVANOMETRİK TARAYICI

KONTROL SİSTEMİ TASARIMI VE UYGULANMASI

Gönenç Ülker

Mekatronik, Yüksek Lisans Tezi, 2011

Tez Danışmanı: Prof. Dr. Asıf Şabanoviç

Anahtar Kelimeler: Lazer Mikroişleme, Galvanometrik Tarayıcı, Telesentrik Lens, Raster Tarama

ÖZET

Lazer mikro işleme teknolojisi, son yıllarda, kimi zaman endüstriyel alanlarda – özellikle markalama, engravür gibi hızın önemli olduğu uygulamalarda – seri üretim hatlarının üretim kapasitesini arttırmakta; kimi zaman belli bir tesisteki üretim kalitesini delme, kesme gibi malzeme işleme uygulamalarındaki kesinlik seviyesini geliştirerek yükseltmekte; kimi zamansa bilimsel odaklı çalışmalarda milimetre altı boyutlardaki malzemelerin yüksek hassasiyetle üretilmesinde ve işlenmesinde, yaygın olarak kullanılmaktadır.

Galvanometrik tarayıcı, lazer ışınını motora bağlı bir ayna marifetiyle yönlendirebilen, rotor açısal hareket kabiliyeti her iki yönde de genellikle onlu derecelerle sınırlı, konumu voltaj ya da akım ile kontrol edilebilen, yüksek hassasiyetli bir cihazdır. Düşük ağırlıkları sayesinde rotor ve ayna çok hızlı hareket edebilir ve bu durum lazer ışını ile markalama işlemlerine imkan tanımaktadır. Bu durum farklı malzemeleri kesme ve işlemede kullanılan ve görece yavaş çalışan mekanik sistemlere kıyasla avantaj sayılabilir.

Bu çalışma, galvanometrik tarayıcı sistem bileşenlerinin analizine; ikili eksen galvo düzeneğine yönelik donanımın ve yazılım tabanlı kontrol sisteminin tasarlanmasına ve uygulanmasına; ve bunların lazer mikroişleme uygulamalarına yönelik bağımsız sistem ya da modüler alt sistem olarak kullanımına odaklanmaktadır. Söz konusu tez çalışmasının analiz kısmı: baskın lazer mikroişleme tekniklerinin değerlendirilmesini, galvanometrik tarayıcı sistemi tabanlı yaklaşımın ve ilgili elemanların gözden geçirilmesini (ör: elektromekanik, elektronik, optik), çalışma prensiplerinin anlaşılmasını, ilgili benzeşim çalışmasını ve uyumluluk ile ilgili konuların ele alınmasını kapsamaktadır. Tezin tasarım kısmı: elektronik kontrol kartının ve yardımcı sürücü kartın tasarlanmasını-uygulanmasını, işlem kontrol algoritmasının mikrokontrolöre uyarlanmasını, grafik kullanıcı arayüzü tabanlı kontrol yazılımını ve gerekli mekanik parçaların üretilmesini kapsamaktadır. Çalışma, deneysel sürecin ele alınması ve elde edilen sonuçların değerlendirilmesi ile sonlandırılmıştır.

Bu çalışmanın sonuçları olumlu ve galvanometrik tarayıcı sistemlerinin lazer mikroişleme uygulamalarında kullanımını teşvik eder niteliktedir.

Dedicated To;

Zeliha Ercan & Demir Ülker (parents),

and *Erkan Oğur*

for their "being the lights on my way"

TABLE OF CONTENTS

LIST OF FIGURES

1 INTRODUCTION

1.1 Motivation

With the effect of technological advances, micro level material processing techniques have been developed considerably over the last few decades, thus also paving the way going to the production of extremely tiny and complex structures for variety of applications. Micromachining methods might differ in terms of functionality as well as application specific performance such that there are several methods that have been frequently used to fabricate or machine in micro scale, including electron beam lithography, optical lithography, nanoimprint lithography, soft lithography, etc. Each method has its advantages and disadvantages when certain type of an application is the concern. Laser micromachining is one of these methods that have been used in various applications, ranging from medical (e.g. stent production) (see Fig. 1.1) to semiconductor industry (e.g. solar cell processing, resistor trimming) due to its unique advantages compared to other micro production methods. Above all, the major advantage is being able to machine directly using a simple aperture instead of a masking process which also increases the flexibility of the procedure. Furthermore, various materials ranging from soft tissue to metals can be machined by laser.
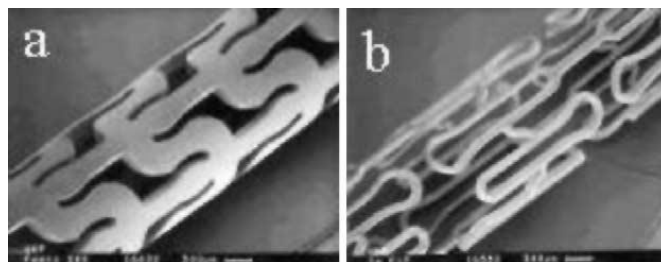
Fig. 1.1 Prototypes of stents made of: (a) bio-resorbable polymer and (b) tantalum.

In laser micromachining systems, material processing performance can be expected to be directly tied with laser beam operational parameters (e.g. beam intensity, pulse repetition rate, beam wavelength) and functional design of the system (e.g. accuracy of the control and design of mechanical elements).

1.2   Objectives

In this thesis, it has been primarily focused on realization of a galvanometric scanner based, sub-millimeter level material processing system that includes a high power pulsed-fiber laser, steered beam focusing optics and commercially available dual-axis galvo modules and related electronics. System controlled by using the designed electronic controller hardware and developed software interface. Formation of micro patterns on different kind of materials has been the target experimental work. In addition to all those, the relation between laser beam machining parameters and material removal rate depending on material properties has been evaluated as much as possible during this study. So that proposed system can find future use in both academic and industrial areas.

For this thesis a galvanometer is basically defined as an integrated system consisting of a brushed DC motor having a limited rotational action and with an attached mirror on rotor shaft and a position feedback mechanism. Two galvanometers together with two scanning mirrors can be driven to steer a laser beam emitted by a laser source such that after focusing with an appropriate mechanism (typically a telecentric scanning lens) the laser beam can be diverted on a target work piece. Figure 1.2 below illustrates the specified procedure in general.
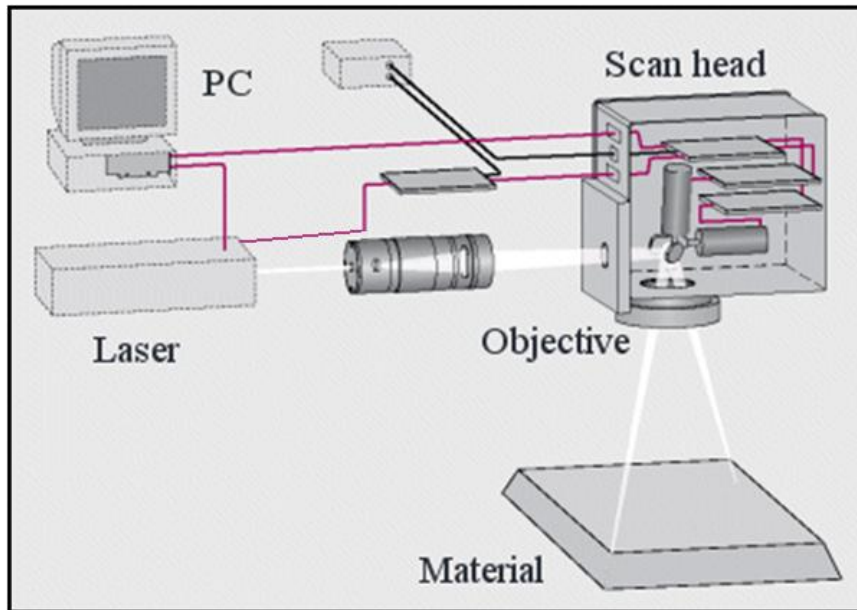
Fig. 1.2 Laser Micromachining General View

Changes in rotor position occurring due to angular rotations of X and Y mirrors can be followed by optical rotary encoders of the galvos; so by applying proper control (usually closed-loop) desired machining patterns can be transferred on to a two dimensional coordinate plane. Two main beam steering methods used in machining applications are called "*raster scanning*" and "*vector scanning*".

Raster scanning, can be defined as the process where the laser beam makes a series of bi-directional, horizontal or vertical scan lines to produce an image. With a suitable data processing and software interface, fills and bitmaps can be turned into data formats, which can be automatically raster scanned by the laser system. A good example of it can be "marking", where laser power set to a value that is low enough to only remove layers from the surface of the material (also called "etching"). On the other hand in vector scanning type of processing the laser beam follows the path of the outline (if present) of the graphic. That type of scanning is suitable especially for "cutting", "drilling" type of operations, where the laser power set to a high enough value to cut or to penetrate all the way through the material. That setting of the laser power to a certain value can be related with intensity control and operational modes of the designed software interface.

Intensity control of the laser beam through setting of laser beam parameters such as pulse duty factor, pulse repetition rate gives the ability to adjust the optical power output level of the laser such that by adjusting the energy transferred to the work piece, the material in a certain region can either be vaporized completely (e.g. cutting, drilling processes) or partially removing a layer of material (e.g. engraving, etching). In that context, "Black-White" mode operation supported by the designed GUI might be seen as suitable for cutting, drilling operations whereas "Gray-Scale" mode - also depending on the linear power adjustment capability of the laser - might provide advantage in laser scribing and engraving type of operations.

1.3   Thesis Organization

This thesis is organized as follows:

Chapter 1 introduces basic principles and application areas of laser micromachining. It also introduces several micro/nano fabrication methods.

Chapter 2 covers literature review on laser micromachining, common approaches and related topics.

Chapter 3 gives analysis of hardware components (electromechanical, electronic, and optic) together with related theoretical background and simulation work.

Chapter 4 summarizes designed hardware and software (embedded hardware software development and GUI based control software)

Chapter 5 contains experimental work and conclusion

Chapter 6 handles the possible future work

2 LITERATURE REVIEW

In this chapter, several micro scale fabrication methods - also including laser micromachining - that can be used in micro level production have been introduced with also elaborating on their principle of operation and application areas. Furthermore, advantages and disadvantages of laser beam machining for fabrication of microstructures will be discussed within comparison to other fabrication methods.

2.1 Production in Micro Scale

Micro structures and systems provide a lot of advantages in various areas, because compared to the macro level structures; they can contain more functionality in same limited volume, thus also leading to a dramatical decrease in overall system size. However, this "creating tiny structures and systems in the limited area" is an important challenge itself. Micro fabrication consists of material adding, removal and bonding as most conventional manufacturing processes. However, due to small size of micro systems, traditional processes may not be used for it. Wet and dry etchings can be counted between the most frequently used methods for the fabrication of micro structures, with lots of recipes available for various materials. Wet chemical etching involves a chemical interaction between an etchant and a target substrate to remove material and in order to create a certain structure, a masking process is also necessary to separate target (the areas to be etched) and protected areas on the substrate. On the other hand, dry etching uses physical bombardment or the chemical interaction using plasma technology. It is easy to control the etching parameters and produced much less toxic material compared to wet chemical etching. Plasma etching, reactive ion etching and deep reactive ion etching are the major dry etching methods. Dry etching methods also need a masking process such as photolithography, which is mainly used in

semiconductor industries. One other lithography based method is soft lithography, which is a fabrication method based on the usage of an elastomeric mask for patterns [1]. In general, soft lithography includes micro contact printing, replica molding (REM), micro transfer molding (μTM), micro molding in capillaries, and solvent-assisted micro molding and it can create the structures with feature sizes ranging from 30nm to 100μm [2]. Basically, soft lithography uses self-assembly or replicates a pre-fabricated mold. Tip-based lithography methods contain Dip-Pen nanolithography; the most well-known tip-based nanolithography. To start the process, the target material is coated on the AFM tip and patterned on a certain substrate. On the other hand, nanoscratching is a material removal process in which, instead of adding materials, a diamond AFM tip has been used [3]. It is similar to the conventional milling machining. However, it provides very limited accessibility due to the tip geometry (pyramid shape). Anodization nanolithography (ANL) is also a method based on AFM [4]. When voltage is applied between the AFM tip and the hydrogenated surface, the local oxidation on the silicon surface is grown. Electron beam lithography (EBL) is a direct writing method without an additional process. It is a material removal process using electron beam which generally provides very high resolutions [5]. However, it cannot provide a high fabrication rate. Photolithography and X-ray lithography use a light source to fabricate micro structures. Photolithography is the method to transfer certain structures on the mask material using UV light before etching technology. Currently, it is the most popular method in the semiconductor industries. On the other hand, X-ray lithography uses X-ray to transfer the structures on the base substrate through masks. X-ray has ultra-short wave length, so it allows the structure size to achieve much smaller than the size fabricated by photolithography, however, it does not allow image reduction contrary to photolithography which usually allows image reduction during mask transfer processes. So when the end shape is very small, the mask generation might turn in to a challenging problem [1]. Besides above several processes, a lot of processes for material removal still exist. Furthermore, material adding processes such as chemical vapor deposition (CVD), physical vapor deposition (PVD), pulsed laser deposition (PLD) and spin coating are also used to create micro structures.

Among several micro fabrication methods that have been discussed, every method has own advantages and disadvantages. Therefore, proper method(s) should be

selected with careful consideration based on the target size, geometry and material type. In the next sub-chapter, laser based fabrication methods have been evaluated.

2.2 Laser Machining Technology

Laser systems are being used increasingly in many distinct micro-systems technology application areas such as biomedical, automotive industry, telecommunication sector, display devices, printing technologies and semiconductors [6]. In all of these application areas, lasers are being used for various purposes starting from cutting metals, drilling holes on PCBs, ink-jet printer nozzles [7], and reaching to direct fabrication of micro/nano structures [8]; with areas ranging from scientific research and development stages to full industrial production environments. Below figure 2.1 lists laser types, target application areas and related materials:

Laser	Applications	Material
Micro-electronics packaging		
Excimer	Via drilling and interconnect drilling	Plastics, ceramics, silicon
Lamp-pumped solid-state	Via drilling and interconnect drilling	Plastics, metal, ceramics, silicon
Diode-pumped solid-state	High volume via drilling, tuning quartz oscillators	Plastics, metal, inorganic
CO_2 sealed or TEA	Excising and scribing of circuit devices, large panel via drilling	Ceramics, plastics
Semiconductor manufacturing		
Excimer	UV-lithography IC repair, thin films, wafer cleaning	Resist, plastics, metals, oxides silicon
Solid-state	IC repair, thin films, bulk machining resistor and capacitor trimming	Plastics, silicon, metals, oxides silicon, thick film
CO_2 or TEA	Excising, trimming	Silicon
Data-storage devices		
Excimer	Wire stripping air bearings, heads micro via drilling	Plastics, glass silicon ceramics plastics
Diode-pumped solid-state	Disk texturing servo etching micro via drilling	Metal, ceramics metals, plastic
CO_2 or TEA	Wire stripping	Plastics
Medical devices		
Excimer	Drilling catheters balloons, angioplasty devices. Micro-orifice drilling	Plastics, metals ceramics, inorganics
Solid-state	Stents, diagnostic tools	Metals
CO_2 or TEA	Orifice drilling	Plastics
Communication and computer peripherals		
Excimer	Cellular phone, fiber gratings, flat panel annealing, ink jet heads	Plastics, silicon, glass, metals, inorganics
Solid-state	Via interconnect coating removal tape devices	Plastics, metals, oxides, ceramics
CO_2 or TEA	Optical circuits	Glass, silicon

Fig. 2.1 Laser micro-machining applications [9]

Increasing requirements, related with the production of high-specification products that are usually being considered nowadays, are often quite stringent and this has led to many refinements and enhancements in the laser systems and laser techniques that have been used. The combination of enhanced capabilities for tailoring the optical

energy density with new femto, picosecond laser systems improved processing strategies leading to further improvement [10].

These advances, have promoted laser-based technologies by providing technical, manufacturing and economical benefits. Two laser systems which are at the forefront of industrial integration, and whose applications have reached a high level of production quality, are excimer lasers and Nd:YAG lasers are in use world-wide in many configurations and the use of high repetition rate Nd: YAG lasers to pattern large areas is very common. Pulsed Nd: YAG as well as excimer lasers are applied to adjust (and bend) various materials as stainless steel, copper alloys or lead frame materials [11] or to machine difficult materials such as diamond (it is transparent in a wide wavelength range diamond machining is currently done by microsecond pulse Nd: YAG and nanosecond pulse excimer lasers [12]). Pulsed Nd: YAG lasers are also used in the cleaning and recycling of surfaces [13].

Light has different wavelengths ranging from 1nm to 1000µm as shown in Figure 2.2. Behind DUV, the X-ray has very short wavelength (0.01nm to 10nm), which is the light source for X-ray lithography.
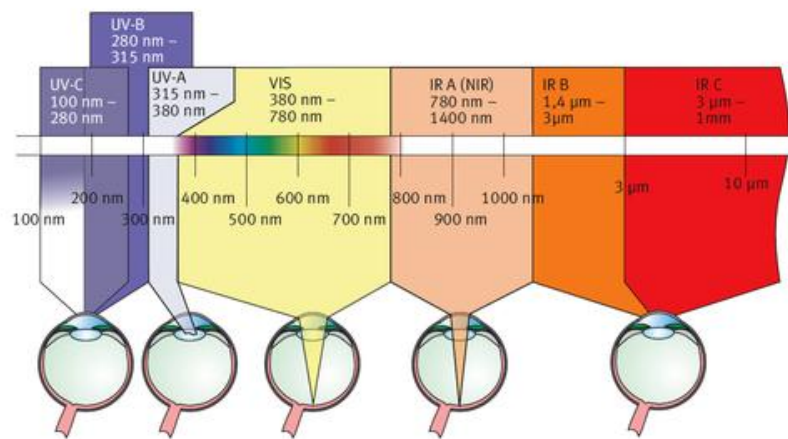
Fig. 2.2 Range of wavelength of light

Lasers have wavelengths changing from 150nm to 10um. Lasers can be classified according to the type of laser source used – solid, gas and semiconductor. The gas lasers can be classified according to the wavelength. Excimer lasers have the wavelength between 157nm and 351nm. On the other hand, Nd: YAG laser (together

8

with fiber-lasers they form the solid-state laser category) has wavelength ranging from 266nm to 1.065µm and CO2 has 10.6µm wavelength. Table 2.1 lists commonly used laser types and fundamental parameters.

Table 2.1 Pulsed Lasers

Laser	Wavelength (nm)	Pulse Length	Frequency (kHz)
TEA CO2	10600	200 µs	5
Nd: YAG	1060, 532, 355, 266	200 ns 10 ns	50
Excimer	*157-351*	20 ns	0.1-1
Copper Vapor	611-578	30 ns	4-20
Ti-Sapphire	775	100 fs	1-250

In general, shorter wavelength provides higher resolution to create structures. Furthermore, ultra short wavelength lasers utilize laser ablation instead of thermal effect to remove material (see Fig. 2.3).

time 0.2 ps   1 ps   3 ps
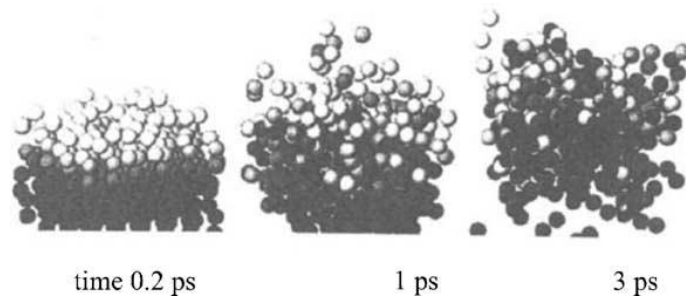
Fig. 2.3 Ablation of silicon by a 200 fs, 5×10^{10} W/cm^2 laser pulse [14].

On the other hand, longer wavelength laser, including Nd: YAG and CO2 use a thermal effect to create structures. Laser machining generally provides following advantages compared to other methods. (a) less number of processing steps (especially compared to chemical methods), (b) higher flexibility, (c) capable of mass and batch-mode production processing, (d) no major infrastructure investment required, (e) applicable to a wide range of materials such as polymers, glasses and metals [8].

9

2.2.1 Laser Operational Principles

The "LASER" acronym stands for Light Amplification by Stimulated Emission of Radiation because for the generation of the laser beam, the principle of stimulated emission is used [15]. Stimulated emission occurs when an electron is in an excited state. When a high energy state electron is dropped to a low energy state electron by passing a photon, the photon with a same wavelength is emitted in the same direction. The laser medium is necessary to emit a photon by stimulated emission. There are four different laser mediums such as gas, solid, semiconductor and liquid. Fiber laser is one of solid-state lasers. On the other hand, CO2 and excimer lasers are the gas lasers. In general, shorter wavelength of light can generate more energy as shown in the following equation.

$$E = \frac{hc}{\lambda}$$

"E" indicates single photon energy, "h" Planck's constant, "c" the speed of light and "λ" wavelength of light. Table below shows wavelengths of different lasers and corresponding photon energies. Decreasing wavelength results with an increasing energy level as given in the following table.

Table 2.2 Photon energies obtained from different laser sources [16]

Laser	Wavelength (nm)	Photon Energy (eV)
XeF	351	3.53
XeCl	308	4.03
KrF	248	5.00
KrCl	222	5.50
ArF	193	6.42
F_2	157	7.43

There are two main operation modes for lasers, which are continuous wave mode and pulsed mode. The continuous mode provides continuous energy flow but the pulsed laser transfers changing output energy depending on pulse duration. On the other

hand, pulsed laser mode can reduce the thermal effect during the laser process. A general laser machine is consisted of three main components which are laser medium, excitation (pumping) source and reflectors. A laser medium can be various materials, including gas, solid and semiconductor as mentioned before. Pumping makes the medium to be in excited state which has high electron energy and the reflectors keep stimulating the excited electron to emit photons. Figure 2.4 describes the concept and components of laser machine.
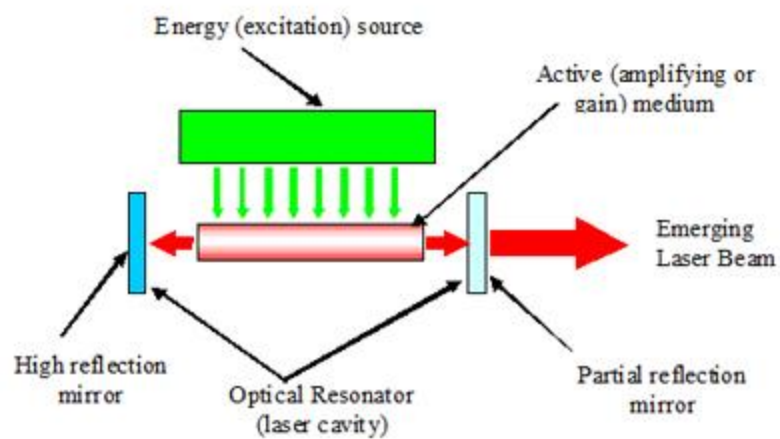
Fig. 2.4 Laser Operation

An important phenomenon for laser technology is ablation. It is characterized by pulsed removal of small amount of materials from the illuminated region of the target with minimal damage to the surrounding area [17]. Once the target material absorbs the laser energy, the material goes through photo thermal (heat induced bond breaking) and photochemical (bond breaking by photon absorption) processes [18]. Evaluation of photo thermal (pyrolytic) and (photochemical) photolytic processes has been demonstrated in the following figure 2.5.
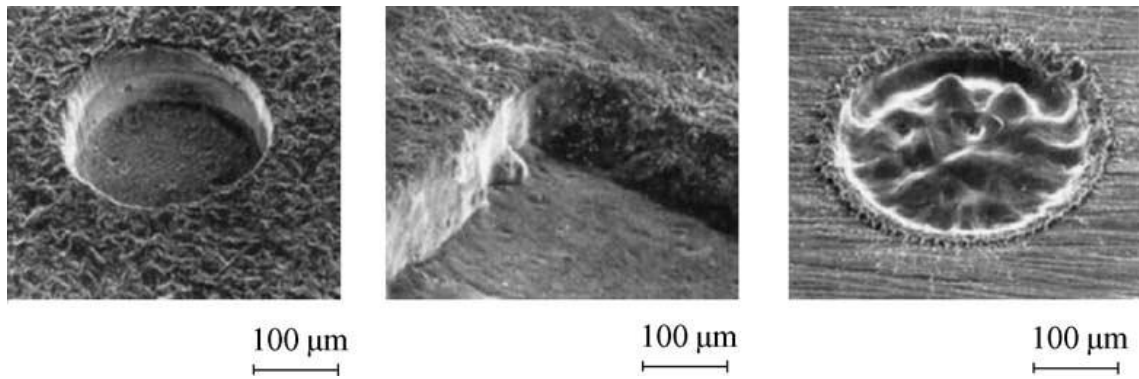
Fig. 2.5 Interaction of excimer laser radiation with solids. Right: PVC, photolytic ablation. Left: metal, melt. Middle: Al2O3 ceramic, combined photolytic and pyrolytic process [19].

Laser absorption varies depending on the material and the wavelength of laser. Generally, higher wavelength decreases the laser absorption. Ablation rate is measured based on Beer's law. Ablation rate (Ar) can be expressed by absorption coefficient (αeff), laser fluence (F) and threshold fluence (Fth). When F is larger than Fth, the laser ablation occurs. Absorption coefficient and threshold fluence rely on the material type and laser wavelength.

$$A_r = \ln\left[\frac{F}{F_{th}}\right]\frac{1}{a_{eff}}$$

Following table shows the ablation depth according to laser fluence for several different materials. It indicates that the ablation depth can vary with the different fluence and the laser wavelength. Table 2.3 lists ablation depths and fluences of common materials.

Table 2.3 Ablation depths and fluences of materials [15]

Material	Wavelength [nm]	Fluence [J/cm2]	Ablation Depth / Pulse [µm]
Polycarbonate (PC)	248	4.0	0.4
Polyester (PES)	248	4.0	0.8
Polyethylene (PE)	193	6.0	4.0
Polyimide (PI)	308	0.3	0.1
Zirkonia	248	10	0.12
Boron nitride	193	20	0.15

Piezoelectric ceramics	248	5.0	0.05
Alumina	193	45	0.06
Silicon carbide	248	10	0.13

The pulse duration is another important factor. Ultra short laser pulses can minimize photo thermal process during the laser machining so that the higher quality structures can be obtained with the expense of a higher cost. Comparing different pulse widths concludes that shorter pulses produce better quality but at higher cost [20].

Especially, melting effects (debris or recast) around the machining areas can be minimized by short laser pulses. The question what is short and what is ultra short can be discussed from the viewpoint of the material. The material is subjected to a beam of photons coming from outside and absorbed in a *skin layer*. The photons are absorbed in that skin layer by the free electrons, in about 1 f (10^{-15}) s. The relaxation time of the electrons is about 1 p (10^{-12}) s. During that time the energy is stored in the electrons, and after the relaxation time it is converted into heat. Expressing the intensity of the incoming beam by I_0, the decrease of the laser intensity depending on the depth can be found by $I_x = I_0 \, e^{-\alpha x}$ where α is the optical absorptivity of the material and x the depth into the material. An important quantity is the penetration depth δ ($\delta = 2/\alpha$) in which almost all laser energy is absorbed. This optical penetration depth is for metals in the order of 10 nm. It means that the laser energy heats a 10 nm thick layer of metal in 1 ps. This heat will diffuse from the skin layer to the rest of the material. The diffusion depth is expressed by $d = \sqrt{4at}$ with a as the thermal diffusivity and t the diffusion time. In case of steel we obtain in 10 fs a diffusion depth of 1 nm while during a 1 ps pulse the heat diffuses over 10 nm. Moving from these results one consider a pulse as ultra short when the (thermal) diffusion depth during the pulse is in the same order or less than the skin layer depth (optical penetration depth). The optical penetration depth depends on the material and the laser wavelength [21]. In general pulses shorter than 1 ps can be considered as ultra short.

By using laser micromachining technique, one can create structures not only by directly fabricating without mask patterns but also by using them [22]. Direct fabrication process usually provides high flexibility and simple implementation which

can be considered as the most valuable advantage of laser machining compared to other methods. Typically, micro fabrication methods consist of several consecutive processes. However, laser machining requires only one single process. On the other hand, supporting high production rate and high resolution structures has been dependent on whether a mask pattern is used while machining or not; because mask pattern usually provides high production rate and creates structures with high resolution. However, more efforts are needed to prepare such equipments. Following figure 2.6 clearly illustrates both "Direct-Write" & "Mask-Projection" methods.
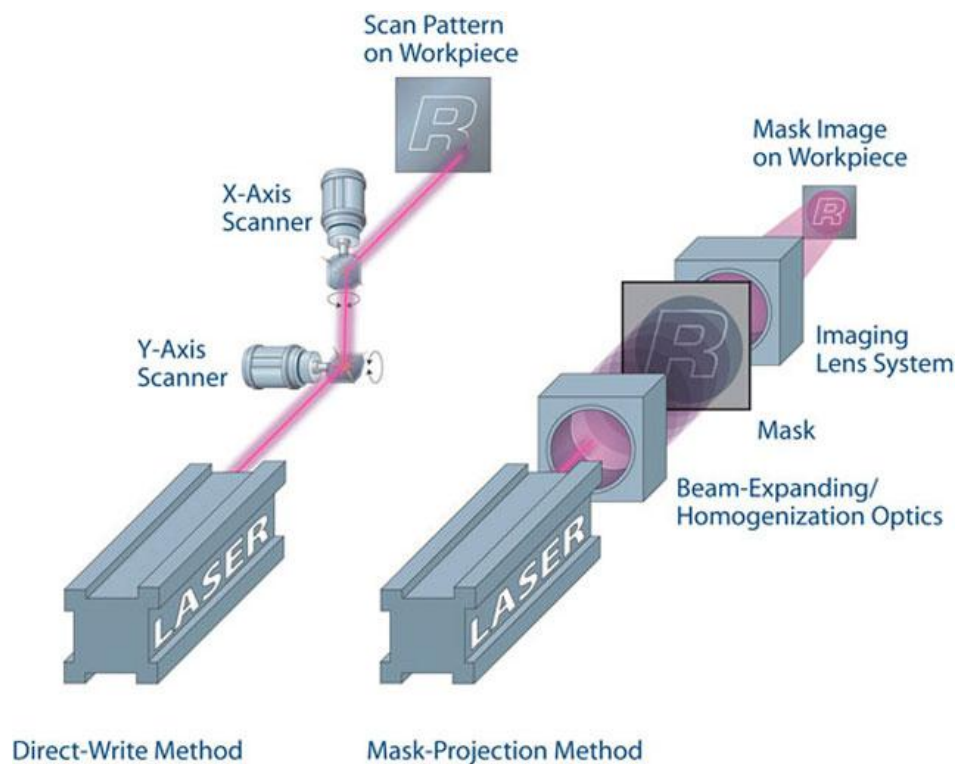
Fig. 2.6 Illustration of Direct-Write & Mask Projection Methods

2.2.2 More on Mask-Projection and Direct-Write Methods

Vast majority of laser machining systems using the technique of mask projection, have been based on excimer lasers [23]. This technique is especially suitable for excimer lasers since their optical properties mean that direct beam focusing may not be a feasible option and projection methods can be more efficient in the machining of various micro structures. Such features, which are depicted in for the machining of

polyimide, have led to excimer laser systems being used, for example, in the mass production of ink-jet printer nozzles [24] as previously stated (see Fig. 2.7).

(a)

(b)
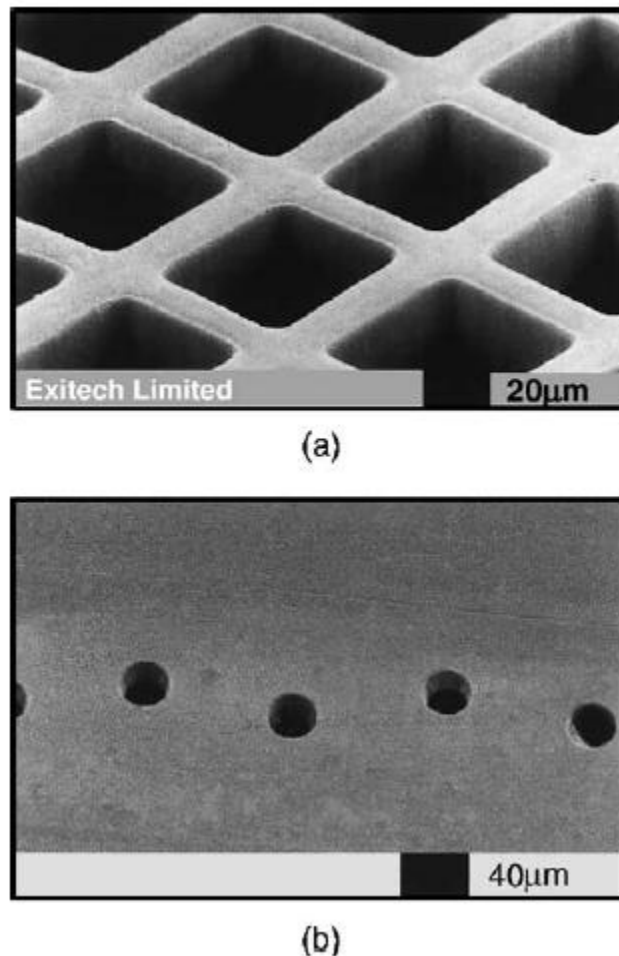
Fig. 2.7 Micro-machining of polyimide to produce ink-jet printer nozzles using excimer laser mask projection.

In standard mask projection systems, the depth of a micro-structure is controlled by the number of laser pulses that have been fired and the resolutions of the features are determined by the mask and the optical projection system. Machining of relatively large areas (i.e. hundreds of centimeter square) under the same laser beam conditions may be of concern such that all the micro-structures are engraved to the same depth. This is something which might be highly desirable in most applications; but in some areas (e.g. applications including micro-fluidic systems, bio-medical analytical chips and rapid prototyping [25]) there can be a need to modify the depth of the micro-machined structures across the sample area.

Standard mask projection techniques are very versatile and depth information can be imparted into micro-machined samples by an appropriate synchronization of the sample position and the laser firing sequence [26]. The level of control of the depth profile required in the above-mentioned applications, however, means that these standard methods do not extend far enough. To overcome this limitation, new techniques such as synchronized overlay scanning (SOS), has been developed. SOS Technique has been illustrated in the following figure 2.8.
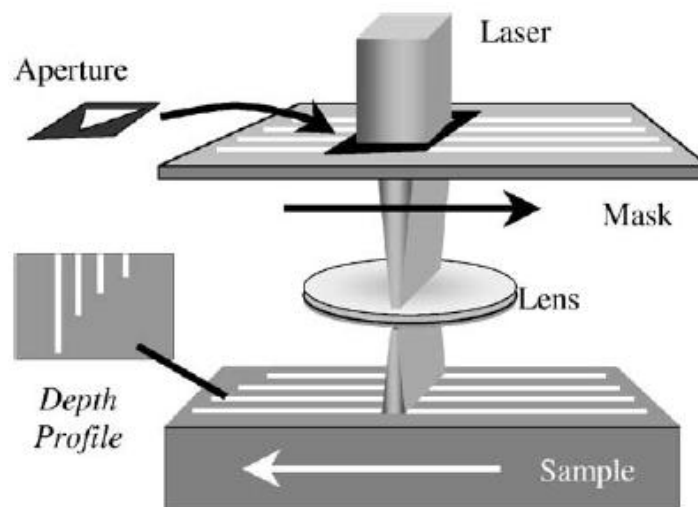
Fig. 2.8 SOS Technique.

To add depth information, the SOS method additionally shapes the laser beam which is used and it is the chosen beam shape which determines the depth profile that is imparted to the micro-structures [27]. The shape of the aperture (i.e. the shape of the beam) determines the profile of the sample and other features of the SOS method is that the choice of mask (which determines the features to be made). Below figure 2.9 represents the typical results obtained.
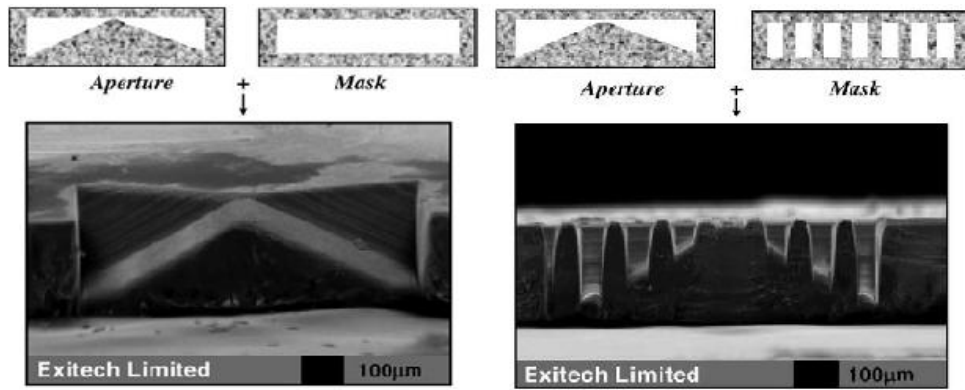
Fig. 2.9 Micro-channels on double ramp.

Solid-state lasers have usually been the preferred light sources in direct writing type of laser machining applications, mainly due to their high repetition rates (hundreds of kilohertz), adjustable pulse durations, and variable output power. Since the mechanism for generating laser pulses lies in the nature of the active laser medium and the corresponding lifetimes of the atomic energy levels. In that context by using different pulse generation techniques [28] the pulse duration, pulse energy and reproducibility can be modified over wide ranges. So that, many applications such as via hole drilling, solar panel scribing, display panel production and marking and cutting of devices or products use these lasers. In almost all cases, the technique of direct writing is used.

In direct write systems, the laser beam is focused to a small spot using a lens and either the beam or the sample (or both) are moved around to produce the desired pattern. In some cases, additional galvanometer-controlled scanning mirrors are also included. If scanning mirrors are used, then a flat-field lens is required as this keeps the focal plane position constant irrespective of the angle of the beam being deflected from the scanning mirrors (see Fig. 2.10).
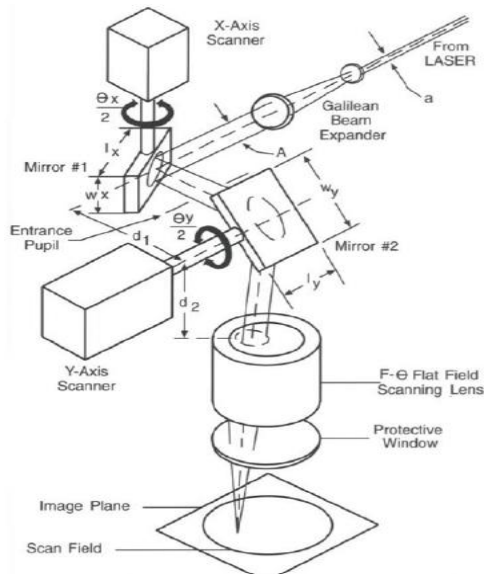
Fig. 2.10 Flat-field lens in direct-write scanning

Beam spot sizes of a few tens of microns can be achieved with such systems and the combination of fast scanner mirrors and high repetition rate lasers means that very high processing speeds can be reached.

Due to the non-availability of a micron level machining mask and related optics in hand; during the experimental part of this thesis, attention has been concentrated only on "Direct-Write" method.

2.3   Summary

In this chapter, laser micromachining together with other micromachining techniques have been introduced, including the basic principles and area of applications. Between the evaluated methods laser micromachining using direct writing offers a lot of advantages compared to other fabrication methods. It is an easy to implement, simple approach and easy to change a process according to different designs.

3 ANALYSIS & SIMULATION

3.1 Electromechanics

3.1.1 Galvos

The name "Galvo" stems from the historical Galvanometer, a moving coil instrument where a mirror was attached to the torsion band of the coil. Such instruments where used to demonstrate slow varying electric currents. The Galvo scanner use the same principle however, they are designed for rapid movement of the attached mirror. Instead of using a torsion band, electromagnetic forces are applied.

Galvo Scanners in modern sense have been widely used in applications such as laser etching, confocal microscopy, and laser imaging. A galvanometer can be defined as a precision motor with a limited travel, usually less than 360 degrees, whose acceleration is directly proportional to the current applied to the motor coils. When current is applied, the motor shaft rotates through an arc. Motion is stopped by applying a current of reverse polarity. If the current is removed, the motor comes to rest under friction. Typically, the term 'Galvo' refers only to the motor assembly, whereas a 'Galvo Scanner' includes the motor, together with a mirror, mirror mount and driver electronics.

Galvanometer:

The galvanometer consists of two main components: a motor that moves the mirror and a detector that feeds back mirror position information to the system. Commercial galvanometers have been supplied also with closed loop circuits to make sure that the desired position will be reached with high precision.

3.1.1.1 Galvo Types and Dynamic Behaviour:

The two main galvo types in terms of the electromechanical structure can be ordered as "moving coil" and "moving magnet" type. Following part covers these configurations and their dynamic behaviour.

Moving Coil:

The basic idea in that configuration is to exploit electromagnetic forces to generate an angular motion. For this purpose a moving coil is placed inside a permanent magnet. By means of a spiral spring which is fixed to the axis the electrical current is supplied to the moving coil. The same arrangement is attached to the bottom side of the coil. Beside the transport of the electrical current to the coil the spiral springs are also used to balance the electromagnetic forces that appear when the current is flowing through the coil against its restoring force. Conventional moving coil arrangement has been depicted in Fig. 3.2.

From the basics of electromagnetically phenomena we know that a current flux j always generates a magnetic field H like:

$$\nabla \times \vec{\mathbf{H}} = \frac{\partial \vec{\mathbf{D}}}{\partial t} + j$$

Since we consider here only conductors we can neglect the displacement field D. From the equation above we conclude that a linear current flux density which is present in a straight conducting wire generates a curled magnetic field as shown in Fig. 3.1 However if the currents flow in a curled conductor as it is the case for the coil then the generated magnetic field becomes linear.
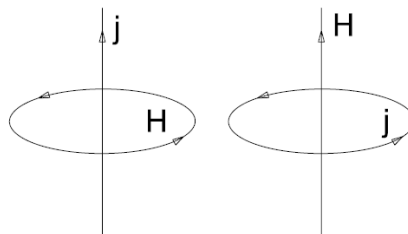
Fig. 3.1 Linear current flux generates a curled magnetic field and a curled flux generates a linear one

In the moving coil instrument the current flows in a curled manner thus generating a linear magnetic field H or magnetic flux density B. The superposition of the magnetic fields generated by the current flux and the permanent field results in a torque T of the moving coil:

$$T = N \cdot A \cdot I \cdot B$$

whereby N is the number of turns in the coil, A the area of the cross section of the coil, I the current flowing through it and B the magnetic flux density inside the gap. The torque T tries to turns the coil in such a way that the overall magnetic flux density becomes a maximum. However the spiral springs are generating a restoring torque (see Fig 3.2) T_r which goes linear with the angular deflection α, i.e.

$$T_r = c \cdot \alpha$$

Whereby c is the spring constant or a material property of it. The equilibrium is reached when both torques have the same value:

$$T = T_r \rightarrow \alpha = \frac{N \cdot A \cdot B}{c} \cdot I$$

From the equation above it can be seen that the deflection angle α is proportional to the current I flowing through the coil.
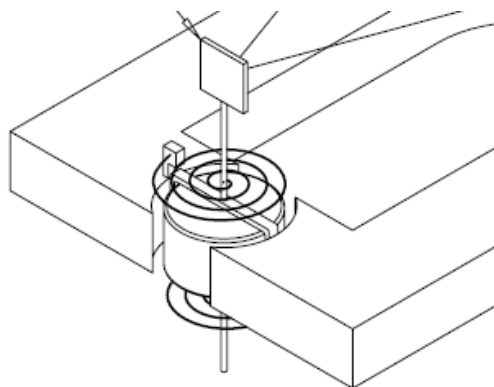
Fig. 3.2 Conventional Moving coil arrangement

To demand that the mirror follow fast variations of the current one has to consider the dynamics of the system. In a first approximation the system consists of a mass and a spring which is driven by an external force.

$$\Theta \cdot \frac{d^2\alpha}{t^2} + k \cdot \frac{d\alpha}{dt} + c \cdot \alpha = K_0 \cdot \cos(\omega \cdot t)$$

inertial + friction + restoring = driving torque

The equation above represents the differential equation for forced oscillation. Depending on the individual parameters as inertial moment, frictional (k) and restoring constants (spring constant c) such a system operates in four different modes:

1. Resonant mode
2. Damped oscillation
3. Maintained oscillation
3. A periodic mode

Depending on the value of the relative damping factor γ:

$$\gamma = \frac{k}{\sqrt{\Theta \cdot c}}$$

From a proper scanner, what is usually expected is that, it follows the variation of current **I** with highest possible speed. This can be achieved in the beginning of the periodic domain (critical damping), which means a short and small over shooting of the desired mirror position occurs. For this case the following equation must be true:

$$k = 2 \cdot \sqrt{\Theta \cdot c} \ \text{ or } \ \gamma = 2$$

However, in this mode the amplitude decreases with increasing frequency. To extend the range - while also preventing the amplitude to drop too much at high frequencies - the resonance frequency ωR of the system:

$$\omega_R = \sqrt{\frac{C}{\Theta}} - \sqrt{\frac{k^2}{\Theta^2}}$$

should be designed as high as possible. This can be achieved by reducing the friction (k) or the inertia moment of the rotating coil. That actually means the mass of the coil must be reduced. But here we are faced with the problem that reducing the mass finally means reducing the mass of the used conductor. For this reason instead of copper, aluminium can be used. Therefore in more advanced systems, moving magnets are used. This has the advantage that no electrical connections to the moving part are required and furthermore it lifts the limit of maximum power that can be introduced into a moving coil.

One has to consider that the current flowing through the coil - besides the magnetic field - produces heat due to power $P = I^2R$ where R is the resistance of the coil. The coil is moving inside an air gap and after vacuum; air is the worst thermal conductor. The only real heat sink for the coil is the pick-off structure. Therefore the heat is mainly dissipated by convection to the pole pieces. Consequently the main failures of moving coil scanners become prominent as the coil burn out and degradation of the permanent magnet. The two major problems that the performance of such scanners suffer from:

1. The thermal limit defined by the heat transfer capabilities of coils and the Curie temperature of the magnet
2. The coil creep and deformation of the coil under centrifugal acceleration

A moving magnet system can solve the problems of both burn out and magnet degradation. The principle of such a system is shown in Fig. 3.3.

Moving Magnet:

Galvos in that configuration contains a moving magnet, which means that the magnet is part of the rotor and the coil is part of the stator. This configuration provides faster response and higher system-resonant frequencies when compared to moving coil configurations. Mirror position information is provided by an optical position detector, which consists of two pairs of photodiodes and a light source. As the galvo and mirrors

are moved, differing amounts of light are detected by the photodiodes and the current produced is relative to the galvo actuator position.
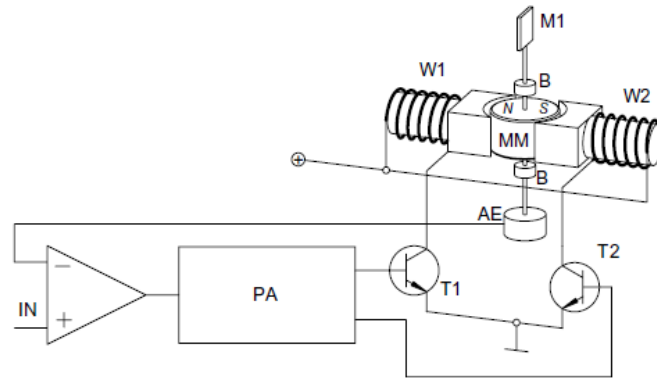
Fig. 3.3 Moving magnet arrangement

A permanent magnet (MM) is placed in the centre of two pole pieces which are supplied with two coils W1 and W2 which are thermally connected to the housing. High torque and high duty cycles, however, still require proper heat sinking to avoid thermal overload. A proper design of the magnet guarantees consistent properties beyond 135 °C (see Fig. 3.4). Compared to moving coil systems this arrangement can accommodate three times the power dissipation of equivalent inertia and torque constant. A spindle is attached to the magnet which is fixed in position by means of two ball bearings (B). Instead of using a mechanical spring a servo loop with a position sensor (AE) and controller is used.
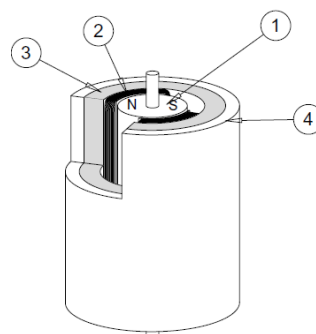
Fig. 3.4 Technical realization of a moving magnet scanner

In the arrangement of Fig. 3.5, a cylindrical permanent magnet (1) is used. Since the inertia of a solid cylinder is given by:

$$\Theta_{\text{cyl}} = \frac{1}{2} mr^2 = \frac{1}{2} \rho \cdot \pi \cdot L \cdot r^4$$

Usually a cylinder which has a length that is larger than the radius has been used to obtain the smallest possible inertia.

r₁ = 5
L₁ = 10
Θ₁= 6.25 Θ₂

r₂ = 2
L₂ = 62.5
Θ₂= 0.16 Θ₁
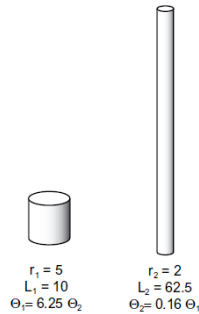
Fig. 3.5 Inertias of cylinders

Permanent rotor magnets for scanners are manufactured from an alloy of Neodymium, Iron and Boron. This compound allows the manufacturing of very strong magnets. A small air gap is between the magnet and the coils (2) which are wound around the pole pieces of the flux return piece (3). The housing (4) is also used as heat sink.

3.1.1.2   Critical Parameters in Selection of Galvos:

That part tries to cover the evaluation of some parameters that has been handled as critical in the selection of galvo modules.

In laser machining applications, optical energy level that is required to implement a certain type of processing job may vary depending on the work piece's material properties and other factors such as physical size and geometry as well as the application itself. Laser on time and optical output power both together, determine the amount of energy affecting on the work piece hence also the overall processing time. So an increase in the number of work pieces or amount of material to be machined might cause a growth in overall processing time which might be costly in some cases (i.e.: mass production). Considering the latest developments and technological tendencies of high-end industrial solutions in the market, lasers that offer nanosecond or picosecond level of pulse operation times have been of concern. Shortening the pulse on time typically provides the ability to use higher peak power levels and that also contributes to

25

faster operation. In that context other elements -such as beam guiding elements- related with those kind of systems should also be of a fast response type having actuators that can move relatively fast. So electromechanical systems integrated in such systems should also have high enough operational bandwidth. Since reaching to high accelerations and velocities might be necessary most of the time, galvanometric scanner modules which have widely been used in those applications have typical bandwidths around hundred hertz for full scale, large angle ($\pm20°$) and can reach up to 1kHz for small angle ($\pm0.2°$) motion. In most electromechanical systems, maximum achievable acceleration and velocity values for the motion has usually been limited by actuators' inertia. In that sense, inertia can be seen as an obstacle or kind of a disturbance that influences the system for high acceleration values and velocities. Due to the nature of the optical based scanning applications, used electromechanical actuators and other moving elements (i.e.: reflective surfaces/mirrors mounted on galvo rotors) should have low inertias to eliminate the undesired disturbances on the system motion and have fast scanning action and dynamic response. In addition to those, most of the industrial control applications require the use of a closed loop control techniques obtain the desired operational performance.

Most laser machining applications such as laser drilling, cutting, scribing and specifically applications such as laser micromachining, micro engraving, silicon wafer processing, medical equipment processing (i.e.: stent fabrication) requires relatively higher accuracy, compared to the conventional industrial control applications therefore accuracy of motion and precision levels has been critical issues.

Resolution has been another important parameter in identifying the performance of the material processing application systems. Assuming a target motion of micron levels; resolution of few hundred nanometers or higher has usually been considered as acceptable. Resolution level has mainly been decided depending on the step resolution of the used position detection systems (i.e.: rotary or linear optical encoders).

Stated SPI Laser platform has a beam diameter around 10mm, so the selected galvo system should have mirrors with appropriate size to be able to properly guide the laser beam on the projection surface. Also these reflective surfaces should have desired level of reflectivity (usually provided with special coatings) for target wavelengths and should absorb as little optical power as possible.

In most of the control applications, it has been expected that the driver/controller block for the actuators should have control input signal compatibility to provide adaptability with existing control interfaces/systems.

Due to the relatively high levels of precision aimed in micromachining applications, non-switching linear control signals have been more preferable rather than high speed switching, modulated signals; because non-switching drive techniques usually provides lower electrical noise therefore allowing higher control accuracies.

Under the guidelines of the above stated parameters; Thor Labs' GVS012 2-axis Galvanometric Scanner modules have been chosen for the studies.

GVS012 Modules:

Thorlabs' GVS Series of Scanning Galvanometer Mirror Systems can be classified as high-speed mirror positioning systems designed for integration into OEM or custom laser beam steering applications. GVS012 modules have been depicted in the following figure 3.6.

Fig. 3.6 Dual-axis Galvo Modules

Modules have the following fundamental features:

- Moving Magnet Motor Design for Faster Response
- High-Precision Optical Mirror Position Detection
- Analog PD Control Electronics with Current Damping
  and Error Limiter
- Protected Silver Mirror Coating
- Dual-Axis System for <Ø10 mm Beams

The system includes a dual-axis galvo motor and mirror assembly, together with associated driver cards and driver cards' heat sinks. GVS012 systems also include a base plate, which is a combined post adapter and tilt platform adapter. Use of a low noise, linear PSU has been recommended by the manufacturer to get the full performance from the modules.

GVS012 galvo consists of a galvanometer-based scanning motor with an optical mirror mounted on the shaft and a detector that provides positional feedback to the control board. The moving magnet design for the GVS series of galvanometer motors has been chosen over a stationary magnet and rotating coil designs in order to provide the faster response times and the higher system resonant frequency. The position of the mirror is encoded using an optical sensing system located inside of the motor housing. As previously mentioned, due to the large angular acceleration of the rotation shaft; size, shape and inertia of the mirrors become significant factors in the design of high performance galvo systems. Furthermore, the mirror must remain rigid (flat) even when subjected to large accelerations. All these factors have been evaluated in the selection of galvo system in order to match the desired characteristics and maximize performance.

3.2   Optics

3.2.1   High Power Laser

3.2.1.1   *Understanding Laser Features & Parameters:*

Besides power or energy level of a laser source, there are other parameters that are still critical in terms of operational performance of the module. Among them, beam

diameter (or radius), spatial intensity distribution (or profile), divergence and the beam quality factor (or beam parameter product) can be handled as the most prominent ones. In many applications, these parameters may define success or failure and, therefore, their optimization seems to be crucial.

Beam Diameter (Radius, Width):

The beam diameter can be thought as the most important propagation-related property of a laser beam. In case of a perfect flat-top profile the beam diameter is clear but most laser beams have other transverse shapes or profiles (for example, Gaussian) in which case the definition and measurement of the beam diameter is not trivial.

The boundary of arbitrary optical beams is not clearly defined and, in theory at least, extends to infinity so that a commonly used definition of the beam diameter is the width at which the beam intensity has fallen to $1/e^2$ (13.5%) of its peak value. Other common definitions of the beam diameter are the full width at half-maximum (FWHM) diameter or the diameter that includes 86% of the beam energy. Many lasers exhibit a significant amount of beam structure, and applying these simple definitions leads to problems. Therefore, the ISO 11146 standard specifies the beam width as the $1/e^2$ point of the second moment of intensity, a value that is calculated from the raw intensity data and which, for a perfect Gaussian Beam, reduces to the common definition.

Spatial Intensity Distribution (Beam Profile):

The spatial intensity distribution of a laser beam combines all the mechanical, thermal and electromagnetic variables that created the beam. The way that the power has been distributed across a laser beam depends on both the mode or combination of modes running in the laser cavity and on how those modes are distorted by the presence of apertures, refractive index of optical elements used, imperfect optical surfaces and other perturbing effects. Therefore, spatial intensity distribution is one of the fundamental parameters which indicate how a laser beam will behave in an application.

Divergence:

The beam divergence of a laser beam is a measure for how fast the beam expands as it propagates in space. According to a common definition, the beam divergence is the derivative of the beam radius with respect to the axial position in the Far Field. This definition yields a divergence half-angle, and further depends on the definition of the beam radius (or, diameter). Sometimes, full angles are used which results in twice as high angles. Beams with a very small divergence, i.e. with an almost constant beam diameter over a significant propagation distance are generally called "collimated beams".

Beam Quality Factor M² (Beam Parameter Product):

The beam quality factor M² is derived from the uncertainty principle. The factor is shown to describe the propagation of an arbitrary beam. M² is a measureable quantity in order to characterize real mixed-mode beams. For example, the angular size of a non-Gaussian laser beam in the Far Field will be M² times larger than calculated for a perfect Gaussian beam. In other words, M² describes how close to "perfect-Gaussian" a laser beam is. For a perfect Gaussian beam, M² is 1. For a non-prefect Gaussian beam, M² is >1. See following figure 3.7.
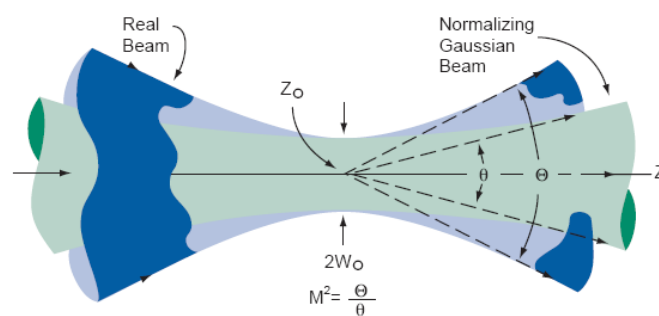
$$\Theta = M^2 \times 2\lambda / (\pi W_0), \text{ FOR A BEAM WAIST DIAMETER } 2W_0.$$

Fig. 3.7 Laser Beam Quality

3.2.1.2 Technical Details:

Main laser module that has been used during the experimental studies is red ENERGY™ G3 HS Series 20W, 1065nm wavelength pulsed fiber laser from SPI Company. Laser module has been shown in below figure 3.8.

Fig. 3.8 High Power Laser Module

Features:

- 12kW nominal peak power with up to 20W average output power
- Up to 500 kHz pulse repetition frequency
- Pulsed and CW (Continuous Wave) operation
- $M^2 < 2$
- High speed marking compatible (2000 cps)
- Bitmap marking compatible
- Pulse width variable (across 25 pre-set waveforms)
- Maximized peak power over full operational repetition rate
- Isolated optical output
- Analogue power control input, pulse gate, and pulse trigger
- Hardware-only interface or simple RS-232 software control

Selected laser module has been classified by the manufacturer as: suitable for applications like; marking of plastics/metals/poly-compounds, scribing, ablation, silicon processing, solar cell processing, thin film cutting, fine foil drilling.

The device is technically described as a DC-powered laser module built around a dual-stage Yb doped fiber amplifier system with an optical seed pulse generated by a single-mode semiconductor laser diode. These amplifiers are pumped by multi-mode laser diodes with wavelengths around 900nm. Fiber beam delivery is done from a fiber-optic beam delivery cable that is terminated with a beam collimator, optical isolator, and beam expander. The module contains drive electronics for the diodes, amplifiers and synchronization of the optics with the user set parameters (see Fig 3.9).
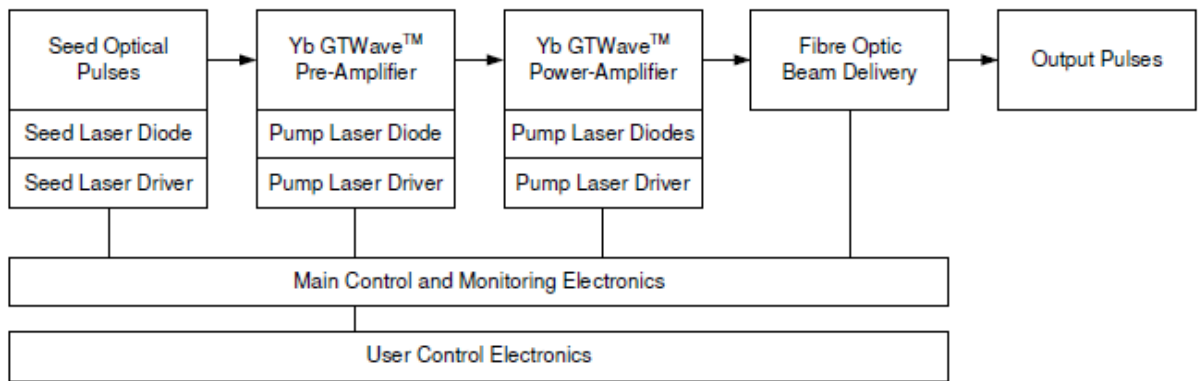
Fig. 3.9 Functional block-diagram of the Laser Module

Laser module can be controlled by using either one of three different methods:

-Basic Hardware Control

-Extended Hardware Control

-Software Control

3.2.1.3 Laser Control:

The main philosophy behind the designed controller board was targeting a highly functional but also compact design that will make the system integration easy; serving to that purpose instead of using parallel communication methods which usually includes many data lines hence also many other potential that might occur due to the high number of wirings-connections; it uses serial communication methods to communicate with most of the peripherals.

So that with the exception of a few control features, software communication method has been used for the control of high power laser. That mode supports many functions that can be accepted as fundamental for the target experimental work and most future work.

Following figure 3.10 summarizes the main functions supported by different modes.

Control	Basic Hardware Control	Extended Hardware Control	Software Control
Global Enable	DIGITAL INPUT	DIGITAL INPUT	RS-232
Laser Emission Gate	DIGITAL INPUT	DIGITAL INPUT	DIGITAL INPUT
Pulse Trigger	EXTERNAL TRIGGER DIGITAL INPUT	EXTERNAL TRIGGER DIGITAL INPUT	RS-232 CONTROL OF INTERNAL FREQUENCY GENERATOR PRF
Power-amp Active-State Set-Point	ANALOGUE INPUT	ANALOGUE INPUT	RS-232 [ANALOGUE INPUT]
Laser Ready	DIGITAL OUTPUT	DIGITAL OUTPUT	RS-232 [DIGITAL OUTPUT]
Laser Disable	DIGITAL INPUT	DIGITAL INPUT	DIGITAL INPUT
Alignment Laser Enable	[DIGITAL INPUT]	[DIGITAL INPUT]	RS-232 [DIGITAL INPUT]
Power-amp Simmer Current Set-Point	N/A	ANALOGUE INPUT	RS-232 [ANALOGUE INPUT]
State Select	N/A	DIGITAL INPUTS	RS-232
Pulsed / CW Mode select	N/A (PULSED ONLY)	DIGITAL INPUT	RS-232
Current Feedback Monitor	N/A	ANALOGUE OUTPUT [RS-232]	RS-232 [ANALOGUE OUTPUT]
Base-plate temperature monitor	N/A	ANALOGUE OUTPUT [RS-232]	RS-232 [DIGITAL OUTPUT]
Fault Reporting	DIGITAL OUTPUTS	DIGITAL OUTPUTS [RS-232]	RS-232 [DIGITAL OUTPUT]

Fig. 3.10 Control Availability and Implementation

As can be observed from the table, some features such as "Laser Emission Gate Control", "Laser Disable" must be controlled by using digital connections. In addition to that, optional hardware control of the global enable pin may provide convenience in some cases. So as a solution, some pins in the PWM output port of the controller board has been reserved for the control of those lines. Using dedicated PWM outputs ports has advantages in the cases where duty cycle based control might be necessary (e.g. modulation of the laser emission gate to be able to adjust the output power in an alternative manner).

Different applications or working with different materials might require setting of laser output parameters such as output power level, pulse burst length, pulse repetition rate,

pulse duty factor). These parameters can be adjusted by using the related commands (*see Appendix D*). For example below figure 3.11 exhibits the change in output pulse shapes depending on the selected waveform and pulse repetition frequency.
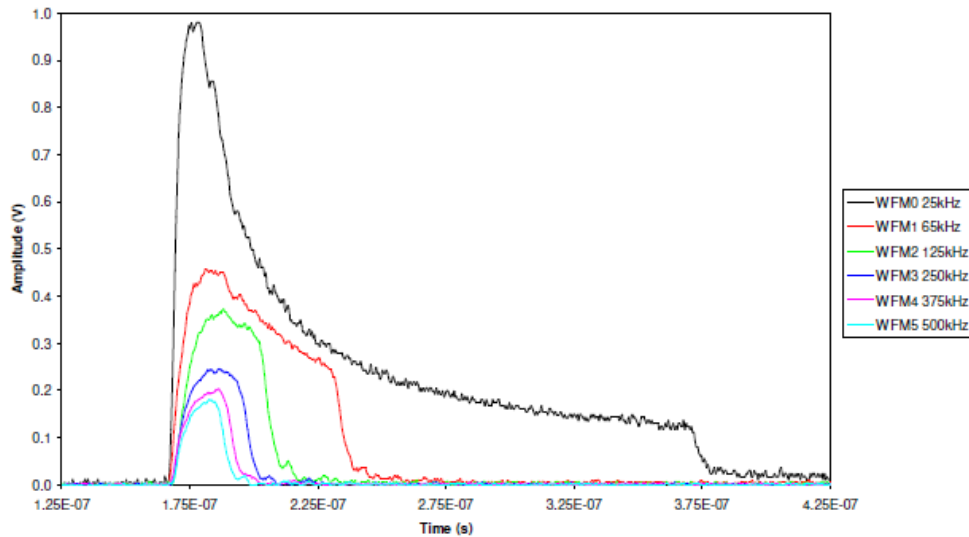

Fig. 3.11 Examples of Optical Pulse Shapes

One can observe that the relation exhibited in the above plot between pulse time and pulse energy level is as seen in the following figure 3.12.
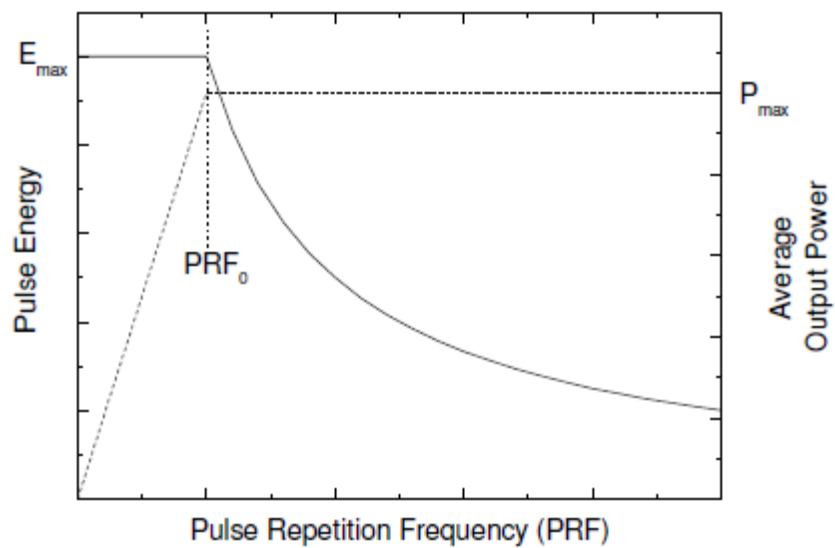

Fig. 3.12 Illustration of average power / pulse energy variation with PRF

3.2.2 Mirrors

The mirror assembly is attached to the end of the actuator, and deflects the light beam over the angular range of the motor shaft. Scanning galvo applications demand high speeds and frequencies of the shaft rotation, so that the inertia of the actuator and mirror assembly can have a profound effect on the performance of the system. High resonant frequencies and enhanced stiffness in the mirror assembly also add to system performance by increasing bandwidth and positively affecting response times. The mirrors that have been used, have protective silver-coating (*see Appendix C*) and are suitable for applications from 400nm up to near infra red (2000nm), and can tolerate powers around 100 to 150W/cm2.

3.2.3 Scanning Lens

Galvanometric scanning based laser machining applications require the use of special optics to improve the processing quality and performance by decreasing the image distortion due to scanning action and increasing the resolution. This type of objective lens is usually called a scan lens because a laser beam is scanned across the back aperture of the objective lens in order to form the image of the sample. Each position that the laser is scanned over corresponds to one point in the image formed. This approach results in a focal spot on the sample that is not, in general, coincident with the optical axis of the scan lens. In traditional lenses, this would result in the introduction of severe aberrations that would significantly degrade quality of the resulting image. However scan lenses were designed to create a uniform spot size and optical path length for the laser for every scan position, which allows a uniform, high-quality, image of the sample to be formed.

When designing an imaging system that uses a scan lens, it is important to accommodate the Design Wavelength, Parfocal Distance, Scanning Distance, Entrance Pupil, and Scan Angle specifications in order to maximize the image quality (see Fig. 3.13). For imaging systems with a single galvo mirror the center of the objective's entrance pupil must be coincident with the center of the galvo mirror. If the imaging system uses two galvo mirrors (as in our case) then the entrance pupil should be located between the two galvo mirrors. It is important to minimize the distance between the two

galvo mirrors, because when the entrance pupil and beam steering pivot point are not coincident, the quality of the image is degraded. This is principally due to the variation in the optical path length as the beam is scanned over the sample. Drawings for an imaging system containing two galvo mirrors have been given in following figure 3.13.
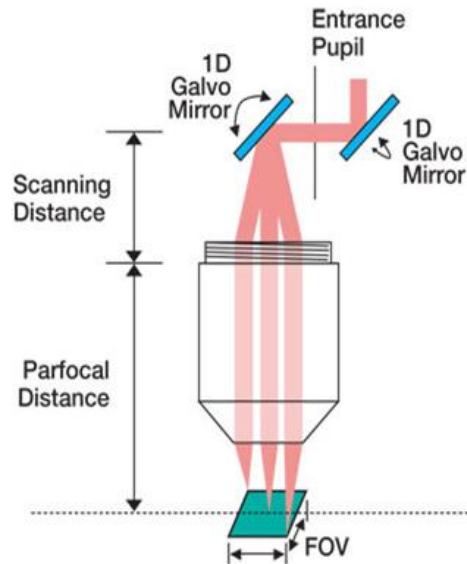
Fig. 3.13 Entrance Pupil in 2-axis Scanning System

Considering the requirements of the application, LSM02-BB (Broad Band) telecentric scan lens have been selected from Thor Labs Company.

3.2.3.1 *LSM02-BB Lens Technical Features:*

Features

- Constant Magnification Over Entire Field of View (FOV)
- Constant Spot Size
- Flat Image Plane
- Excellent Coupling Efficiency
- Large Field of View
- EFL (Effective Focal Length)= 18mm
- WD (Working Distance)= 7.5mm

- Scan Lens Thread: M25 x 0.75

The LSM series of scan lenses are telecentric objectives that have been classified as ideal –by the manufacturer- for use in laser scanning applications. Those telecentric objectives are used in laser imaging systems because of the advantages of a flat imaging plane when used in applications that scan the laser across the sample being processed. A flat imaging plane minimizes image distortion, which in turn allows for the creation of geometrically correct images without the need for extensive post image processing. In addition, the spot size in the image plane is nearly constant over the entire FOV (see figure 3.14 Scan Lens Plot) so that resolution of the image is constant.
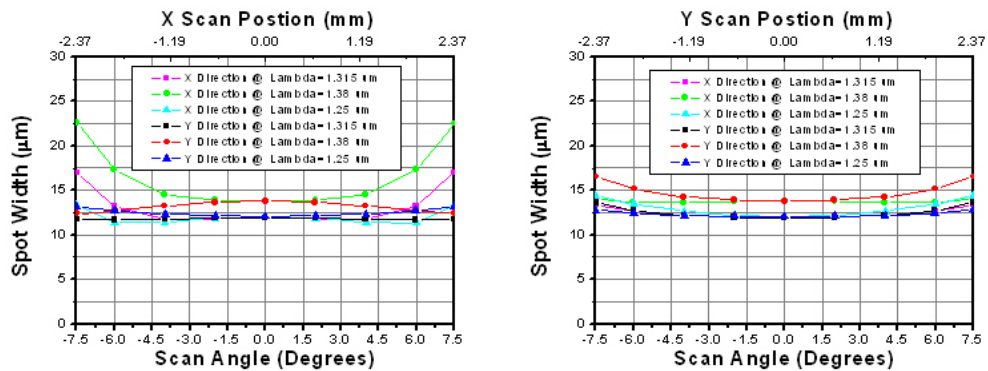
Fig. 3.14 Scan Lens Plot

A very important factor in micromachining applications is the final spot size after focusing. Following equation can be used to estimate theoretically allowable diffraction limited minimum spot size:

$$D_{min} = \frac{4\lambda f M^2}{\pi D_o}$$

Ex: Getting $\lambda (wavelength) = 1064\ nm$, $f\ (effective\ focal\ length) = 17.97\ mm$, D_o (input beam diameter) = 9.1mm, M^2(beam quality factor) = 2 ➜ D_{min} = 5.35 μm

For the telecentric lens used, due to the minimum level wavelength and scan angle dependency of the spot size and lens specs, it is around 15 um for most values of the scan angle and wavelength.

Selected LSM02-BB scan lens also have an AR (Anti Reflection) coating designed to minimize back reflections from broadband light sources so that minimizing the optical power loss (see plot below). The lens have an AR coating that is effective over a wavelength range from 800 nm to 1100 nm, which makes it compatible with the used SPI laser having 1064 nm wavelength. This can be observed from the following figure 3.15.
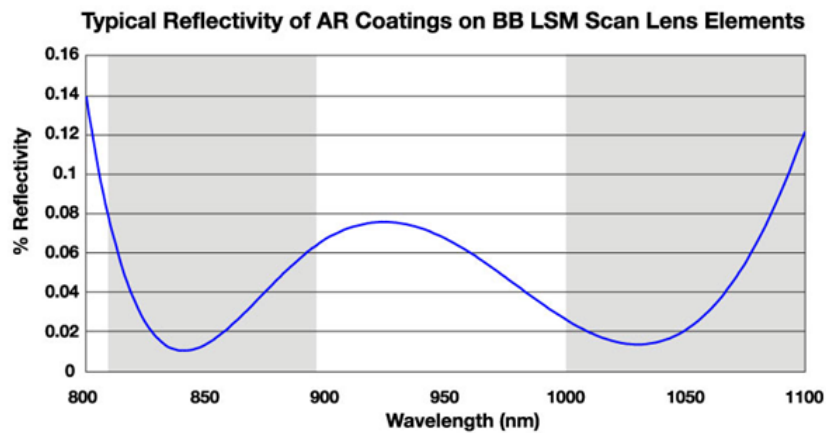
Fig. 3.15 LSM02-BB Scan Lens Reflectivity

3.2.3.2 Using Scan Lens Parameters:

Some of the lengths/distances critical for the operation of the lens can be seen in the following figure 3.16:
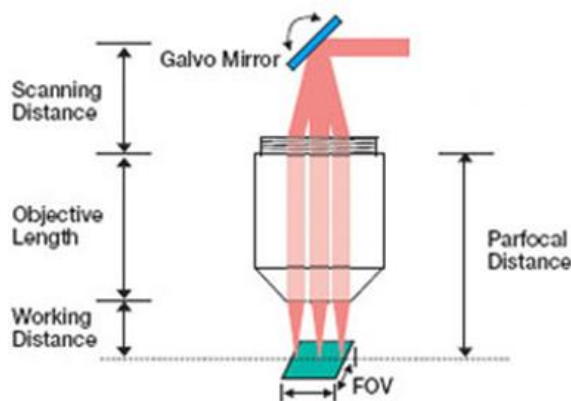
Fig. 3.16 Scan Lens

As previously mentioned; for ordinary lenses, beam position in the FOV (Field of View) depends on the "tangent of the scan angle"; whereas on the other hand telecentric lenses and F-theta lenses have no tangent of the angle dependency; but instead beam position directly depends on the angle.

Following figure 3.17 represents output pattern of an F-theta lens with telecentric behaviour for a typical dual-axis galvo system:
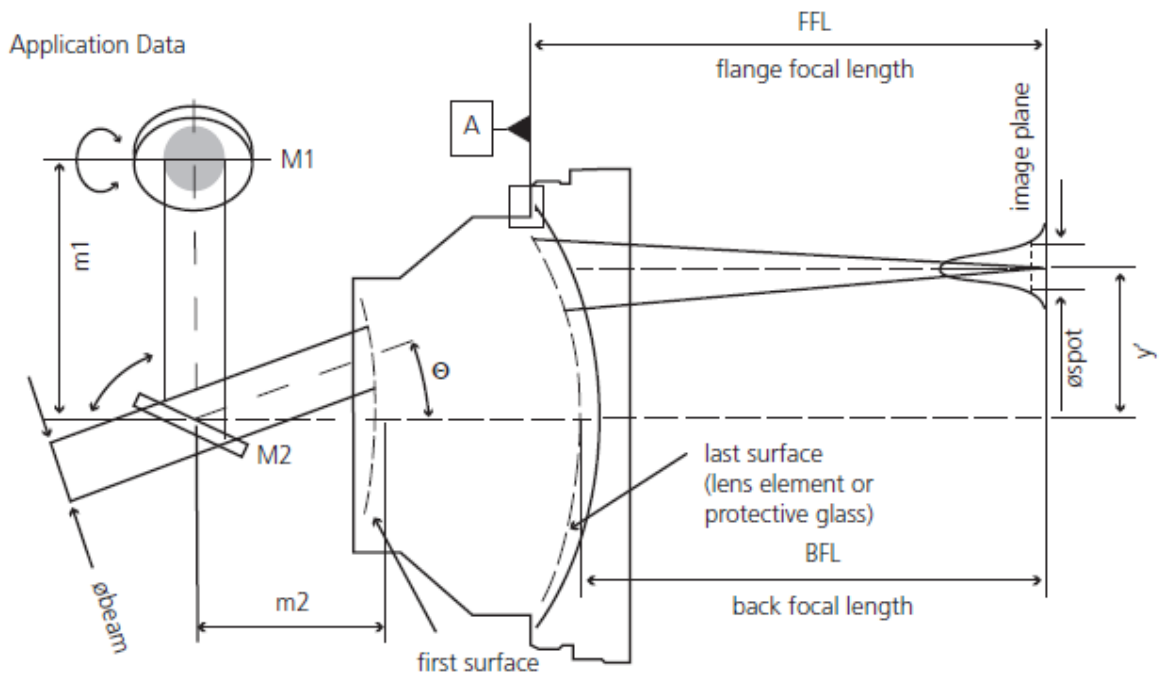
Fig. 3.17 Scan Lens

(*) "Partial" F-theta nature of the selected lens can be understood by using the following relations:

-Overall scan angle θmax refers to the maximum diagonal scan angle

-The scan length can be calculated with the formula:

$$2\gamma = EFL \times 2 \times \theta \times \pi/180$$

Example: For LSM02–BB scan lens specs given in table *(see Appendix A)* "θ" scan angle= 7.5 degree; "EFL" (Effective Focal Length) = 17.97 mm (around 1050 nm wavelength)

FOV= 17.97*2*7.5* π /180 ➔   solving the equality

FOV= 4.704534 mm   ➔   also matches with the given 4.7 mm x 4.7mm FOV
parameter

Note: π/180 is conversion factor from degrees to radians

Assuming full utilization of the given 4.7 mm x 4.7 mm area and a focused beam spot
size of 23.5 um (worst case scenario) ➔ 4.7mm/23.5um = 200 spot workspace are in
each axis, which is equivalent to 200 x 200 spot based resolution. That value can be
considered as acceptable for most machining purposes.

(*): The word "Partial" is due to slight differences between focusing behaviour of
telecentric and F-theta lenses in terms of focused beam's angle of incidence. This can be
observed from the following figure 3.18:
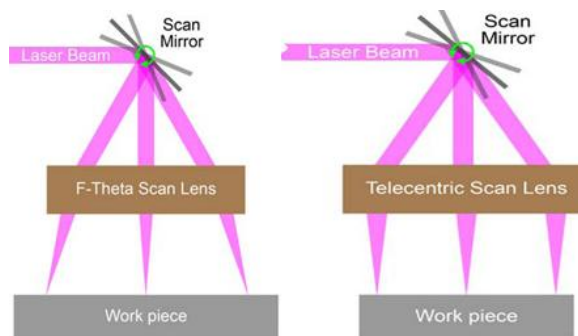
Fig. 3.18 F-Theta & Telecentric

The problem with the simplest type of F-theta lens is that the focused beam hits the
work piece at an angle, causing an elliptically shaped focused spot which may have to
be taken into consideration in some applications. For surface treatment applications,
such as marking, this may not be a problem; however for material removal applications,
such as hole drilling, this can be an issue (unless a hole slanted with respect to the
surface is desired). In a telecentric lens, the exit beam from the optical system is
perpendicular to the work surface over the entire field of view. This solves the problem
just described. However, it necessitates having a lens which is at least as large
physically as the scan field that can increase optical system costs.

3.3   Electronics

3.3.1   Servo Driver Board

As previously stated, galvos have their dedicated driver&controller stages based on servo drive structure. The servo circuit interprets the signals from the position detector, then uses positional error, speed and integral of current terms to output control voltages to drive the actuator to the demanded position. The scanner uses a non-integrating, Class 0 servo, which enables higher system speeds compared to integrating servo systems, and can be thought as ideal for use in applications that require vector positioning (e.g. laser marking) or raster positioning (printing or scanning laser microscopy). It can also be used in some step and hold applications. The proportional derivative circuit gives acceptable dynamic performance and includes an additional current term to ensure stability at high accelerations. The figure 3.19 below shows the architecture of the driver in more detail.
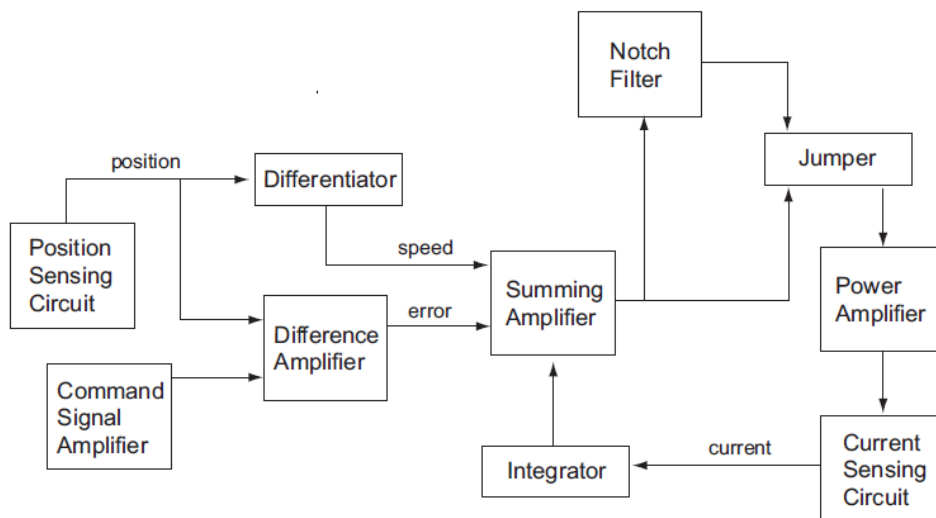
Fig. 3.19 Servo Driver Board Schematic Diagram

Here considering the additional current term integrated and fed to the system, that block in a sense behaves like a disturbance observer structure. Further information will be given in "**3.4 Simulations**" Section.

Fig. 3.20 Servo Driver Board

In the figure 3.20 above, it can be seen the general view of a driver board for a single axis. Both X-axis and Y-axis galvos have their dedicated servo drivers. Depending on the measurements made on the X and Y galvos, their electrical characteristics can be considered almost as identical:

Table. 3.1 Galvo Module Electrical Characteristics

	X Galvo	Y Galvo
Rc (Coil Resistance)	2.49 Ohm	2.50 Ohm
Lc (Coil Inductance)	166uH	168uH

Note: Measurements have been done with an Agilent U1731A LCR meter.

So one can expect the drivers can be used interchangeably; but due to the differences in size, geometry and the inertias of the mirrors mounted on the rotors, each galvo should be used with its matching, calibrated driver. Galvos have been used with the factory default settings, without making additional adjustments or tuning; with the exception of

enabling of the onboard notch filter located at the input of the power amplifier stage, to eliminate the hissing type high frequency noise.

Each driver board requires the use of a split power supply. Power supply output voltage can be between ±15V - ±18V. Drivers have on board signal connections for position sensor currents (e.g. Position Sensor A Current, Position Sensor B Current, motor coil drive signals). Driver boards support either single-ended or differential mode operation; first one providing ease of use while the latter one making higher common mode rejection ratios achievable. Driver boards can be enabled by using an external control signal but there is no such option for disabling or bypassing the on board controller which might be considered as a handicap for control applications. Low output impedance +12V, -12V output

In addition to all those a separate on board connector provides diagnostic information for:

    -Scanner Position
    -Internal Command Signal (*)
    -Positioning Error x 5
    -Motor Drive Current
    -Test Input (NC)
    -Motor + Coil Voltage / 2

(*)= Internal command signals produced by the controller stages can be observed externally; but that control signals can not be modified (e.g. changed or added or subtracted) without making additional modifications on the board physically; that is why flexibility of control has been limited with the drivers' built-in control features.

3.4   Simulations

Main focus of the simulation studies can be summarized as: to get familiar with the dynamic behaviour of the galvo modules and better understand the effect of the internal/external disturbance(s) on the position tracking performance of the galvos.

3.4.1   Definition of the Problem

  In terms of the relative motion of the laser beam and work piece during the laser micromachining process; procedure can be classified in three main categories:

a) Laser beam moving, work piece stationary

b) Laser beam stationary, work piece moving

c) Laser beam moving, work piece moving

Simulation work, tries to concentrate on the case "a)", in which only laser beam moving and work piece assumed as stationary. Main reason for choosing this approach is that, it reflects the existing scenario in the real world experiments, best. In that context synchronization between galvos might be an important control challenge to better observe how differences in galvo characteristics act on the dynamic behaviour of the modules especially when acceleration values are high as it might be the case in raster type of scanning applications. So this part focuses on the synchronized control model of a dual-axis galvo system, and elimination of differences such as inertial differences (e.g. due to the different mirror geometry, electrical characteristics) using related control structures.

Methodology:

Overall methodology can be summarized as first understanding the structure of the reference hardware (galvos, controller board), than mathematically modeling and simulating the proposed synchronization approach in Simulink environment.

3.4.2   Hardware Overview & Analysis

Plant:

As stated previously, galvos of the GVS012 system have moving magnet DC motor structure, thus can be driven either in a voltage controlled or a current controlled manner. When the electronic hardware overviewed, an onboard audio class power amplifier that uses the current output driving configuration and related current

measurement features have been observed. Since the control input to the driver board is taken as voltage reference; additional mathematical transformation - scaling factors can be used to convert voltage reference input to desired position reference value.

Driver & Controller Block:

The evaluation of that block is as it has been given in the *Servo Driver Board* subsection of the **Electronic Elements** section.

Under the guidelines of those analyses, a corresponding plant and controller model have been implemented in Simulink.

Math Model:

Here instead of directly concentrating on synchronization we begin with single axis galvo control. Proposed control scheme has been given in the following figure 3.21:
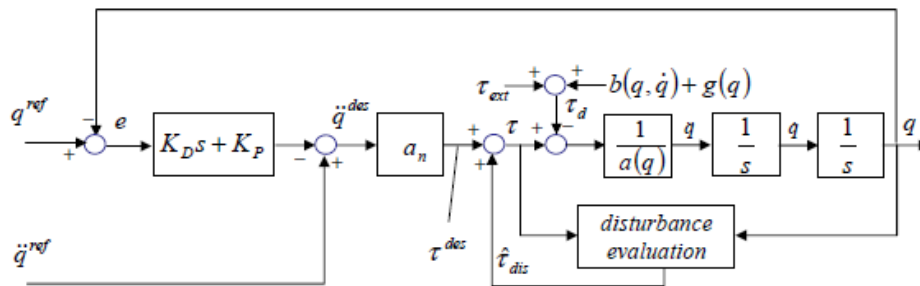
Fig. 3.21 Proposed Scheme

Double integrator plant part can be thought a suitable mechanical representation for a brushed DC galvo motor; τ_{ext} showing the external disturbances (such as load inertia); τ_{dis} as total disturbance effect due to both internal (rotor inertia, friction, coil-armature resistance…) and external effects.

Controller part is formed of a "feedback term" ➔ PD Controller and a "feed forward term" ➔ $\ddot{q}^{ref}$. $\ddot{q}^{ref}$ term is expected to decrease transient times so that dynamic response of the system (i.e.: to a step input) can be further enhanced.

45

The part named "*disturbance evaluation*" can be thought as the block that provides the previously stated "additional current term" which might be required to suppress reaction torque (i.e. caused by rotating mirrors) that may occur due to the inertia at high acceleration values. It also helps minimizing the effects of the disturbances on the system.

Plant:

$$\tau_{ext} \overset{+}{\longrightarrow} \bigcirc \overset{+}{\longleftarrow} b(q,\dot{q}) + g(q) + \Delta a\ddot{q}$$
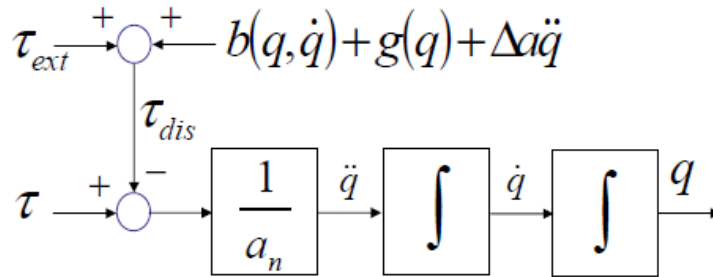
Fig. 3.22 Plant Model

After analyzing the related hardware, plant internal structure has been selected as a double integrator configuration (see Fig. 3.22), which later by control internal dynamics have been canceled out so that desired position reference tracking operation can be implemented. When formed as below; given a current input, a position output is produced by the plant. To realize a more realistic plant model, disturbance effects (e.g. inertia values calculated previously) can be applied to the system through the "LoadInertia_Effective" input. See following figure 3.23.
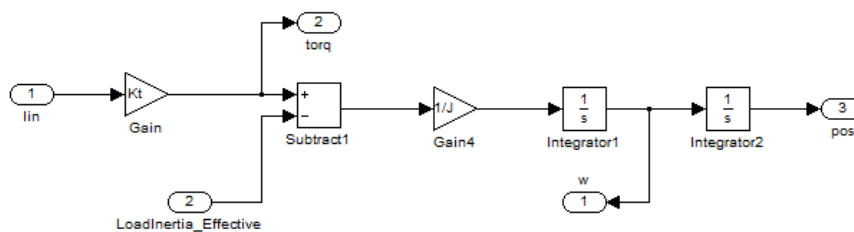
Fig. 3.23 Plant Simulink Model

3.4.3   PD Controller

Considering the proposed control scheme above, PD controller (see Fig 3.24) can be thought as the "feedback based" convergence term of the control so that error dynamics have been enforced to zero in a closed loop.
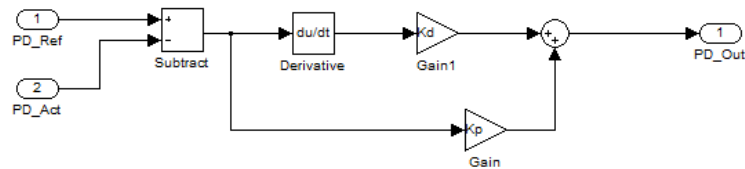
Fig. 3.24 PD Controller

Basic functionality of the PD block, for different "kp" and "kd" values can be seen from the following figures:
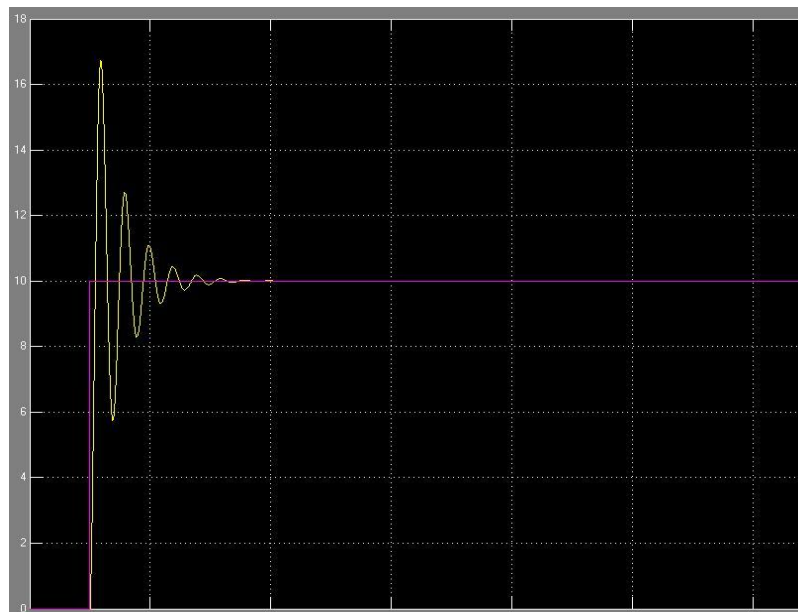
Fig. 3.25 -Step Response for "10" (PD Control kp=100 kd=10)

(Horizontal axis: *time* ; each slot represents **1** second)
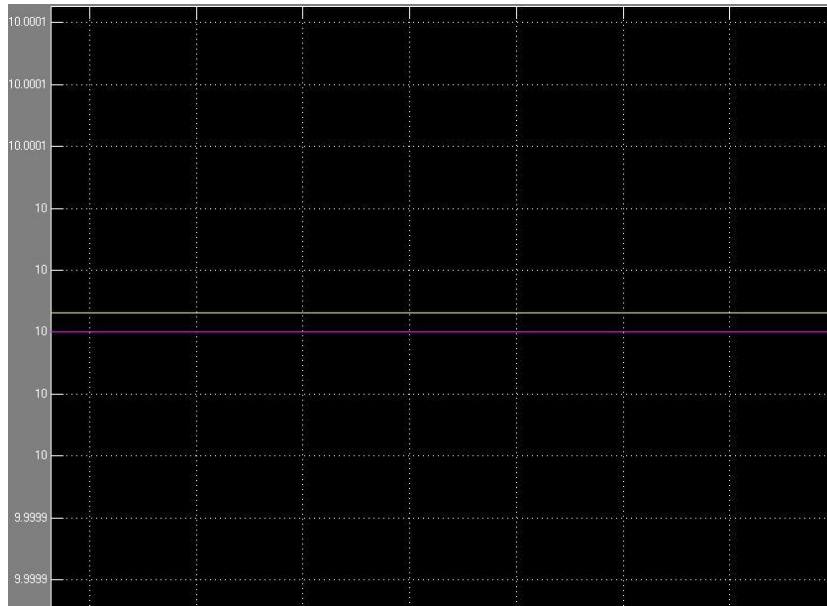
Fig. 3.26-Step Response for "10" (PD Control kp=160 kd=140)

(Horizontal axis: *time* ; each slot represents **1** second)

3.4.4 DOB

To be able to represent the controller features of the hardware better, a DOB having a first order low pass filter structure have been used. Below can be seen the DOB structure used in simulations. It takes the torque applied to the system (labeled as "DOB_torq_in") and measured angular velocity (DOB_w_in) as known inputs. Output of the observer is the estimated disturbance torque (DOB_torq_out) which has later been fed in to the plant after being transformed to an additional current term to minimize the effect of the disturbances on the system. Considering the measured variables on the electronic hardware, each known input used in the observer block can be derived from a related measurement on the controller board, so that proposed observer can be thought as an appropriate alternative to the specific part of the existing hardware. Proposed DOB structure and operational performance has been depicted in the following figures.

48
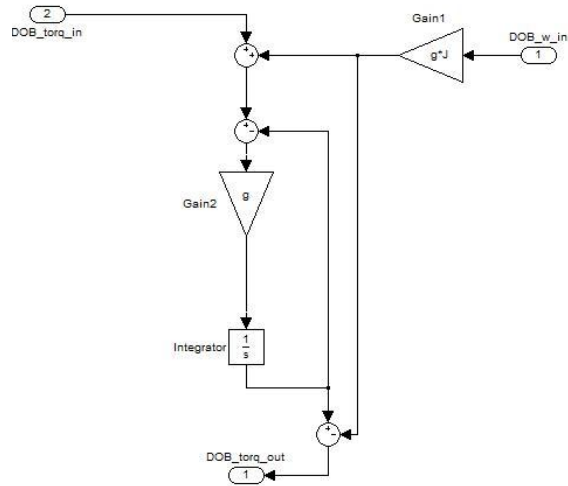
Fig. 3.27 DOB Structure
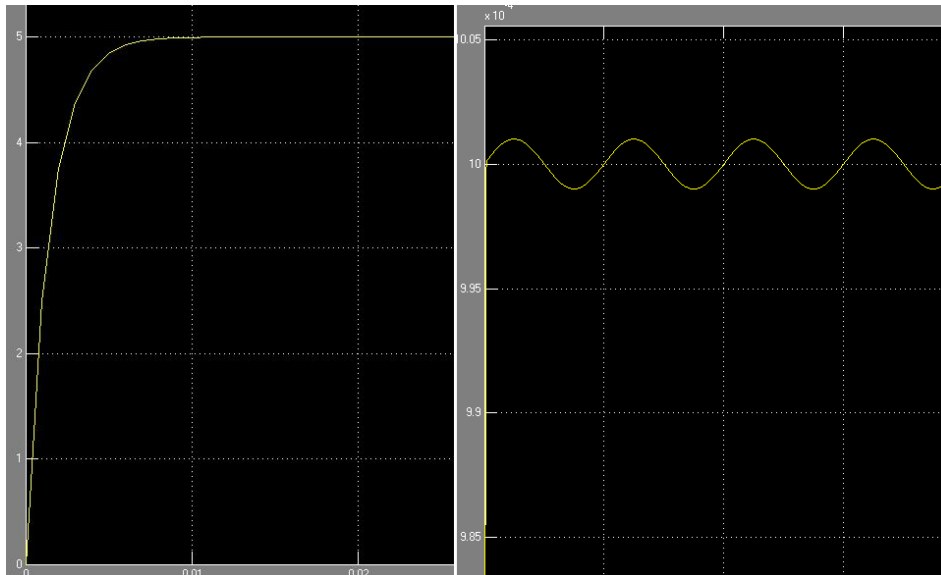
Fig. 3.28 Sample DOB outputs for "5" and "0.001+ 0.000001*sin(2*pi)"

(Horizontal axis: *time* ; each slot represents **0.01** second)

For given disturbances at plant input, proposed DOB structure gives the expected estimation values for constant or slowly varying inputs, independent of the amplitudes. The transient delay observed at the beginning of the estimation is due to the filter structure of the observer. That corresponds to less than 10 samples for a simulation step of 0.001s.

Feed forward Term:

Following figure clearly shows that transient time is decreased after additional $\ddot{q}^{ref}$ term which is obtained by double differentiation of the position reference input.
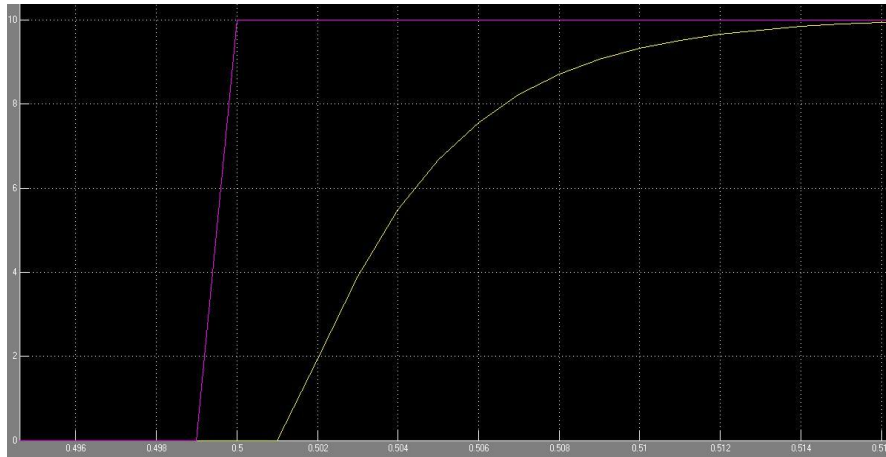
Fig. 3.29 Transient Response for "10" (PD Control kp=125 kd=20)

(Horizontal axis: *time* ; each slot represents **0.002** second)

Initially no disturbance has been applied to the plant, to better observe the difference in the transient response time (see Fig. 3.30):
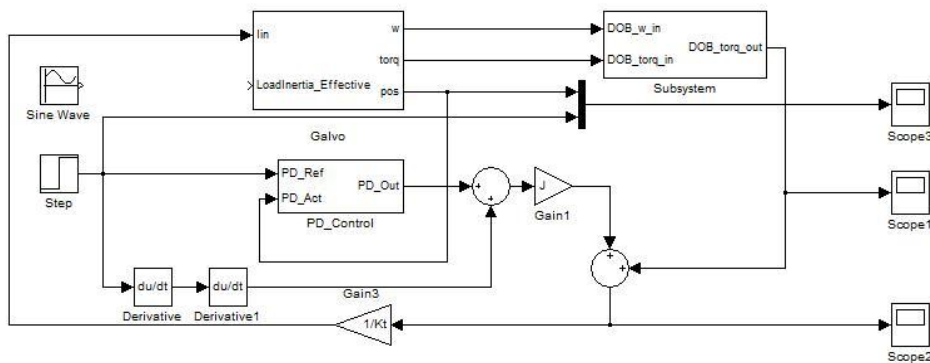
Fig. 3.30 PD Controller and Observer (no disturbance)

Fig. 3.31 Transient Response for "10" (Feed Forward + PD Control kp=125 kd=20)

(Horizontal axis: *time* ; each slot represents **0.001** second)

3.4.5 Synchronization Problem (Functionally Related Systems Approach)

In terms of control synchronization problem of two galvos can be handled as two systems tracking the same reference. We can start by making error definitions such that the control problem has been transformed into a new one in which it will be implemented using sum and difference of the initial terms. If both plants succeeds to track the given reference than at the end we should have two systems tracking the same reference such that their sum should be qref+qref=2*qref and difference is qref-qref=0 and when back transformed to the initial terms, the desired unique controls can be found [32].

Error definitions:

$$e_c = q_c - q_c^{ref} = q_c - 2q^{ref}$$

$$e_d = q_d - q_d^{ref} = q_d - 0$$

Generalized errors can be written as:

$$\sigma_c = cq_c + c_1\dot{q}_c - 2(cq_c^{ref} + c_1\dot{q}_c^{ref})$$

$$\sigma_d = cq_d + c_1\dot{q}_d - 0$$

By using the generalized error definitions above exponential convergence can be found using

$$\ddot{q}\,_i^{con} = -k|\sigma_i|^{2\alpha-1}\mathrm{sign}(\sigma_i), \qquad \frac{1}{2} < \alpha < 1$$

The derivative of the generalized errors when evaluated at 0 gives equivalent control terms

$$\ddot{q}\,_c^{eq} = 2\big(c\dot{q}\,_c^{ref} + \ddot{q}\,_c^{ref}\big) - c\dot{q}_c$$

$$\ddot{q}\,_d^{eq} = 0 - c\dot{q}_d$$

Sum of convergence and equivalent control terms gives the desired control:

$$\ddot{q}\,_c^{des} = sat\big(\hat{\ddot{q}}\,_c^{eq} + \ddot{q}\,_c^{con}\big)$$

$$\ddot{q}\,_d^{des} = sat\big(\hat{\ddot{q}}\,_d^{eq} + \ddot{q}\,_d^{con}\big)$$

And after the final transformations:

$$\ddot{q}\,_m^{des} = \frac{\ddot{q}\,_c^{des} + \ddot{q}\,_d^{des}}{2}$$

$$\ddot{q}\,_s^{des} = \frac{\ddot{q}\,_c^{des} - \ddot{q}\,_d^{des}}{2}$$

3.4.6 Synchronization Blocks

a) General view of the synchronization model:
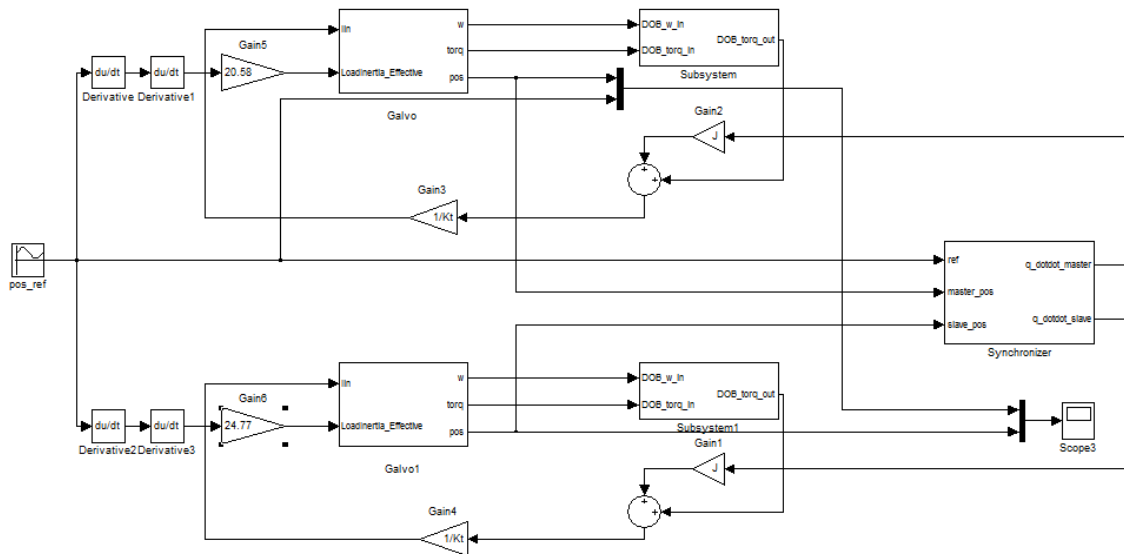
Fig. 3.32 Synchronizer

b) Internal structure of the *sigma_common* and *sigma_difference* blocks (including equivalent control term calculations) can be shown as:
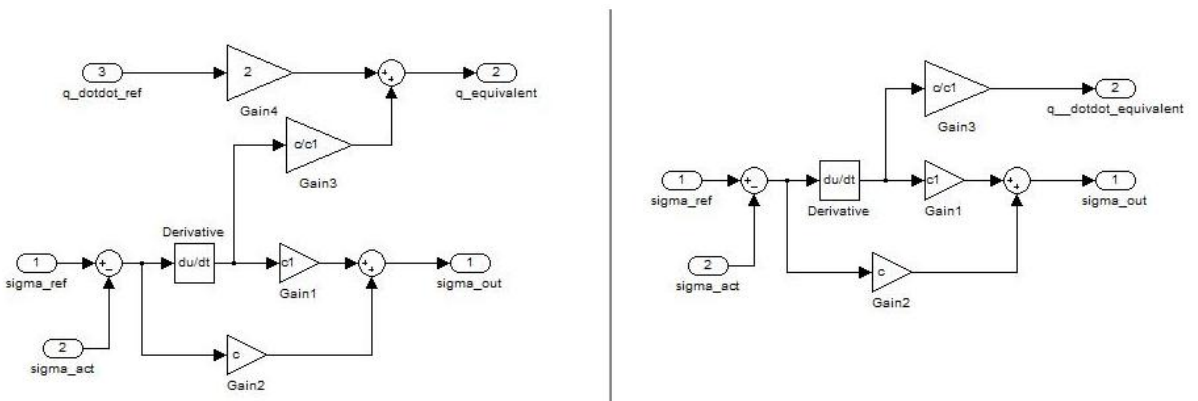
Fig. 3.33 Synchronizer

c) Inside the *Synchronizer* block:

53
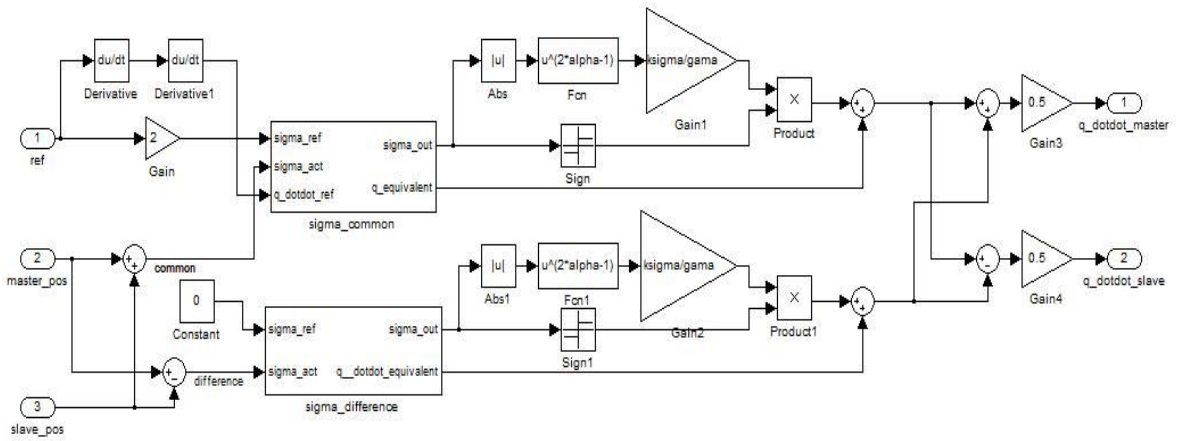
Fig. 3.34 Inside Synchronizer

Synchronization Result:
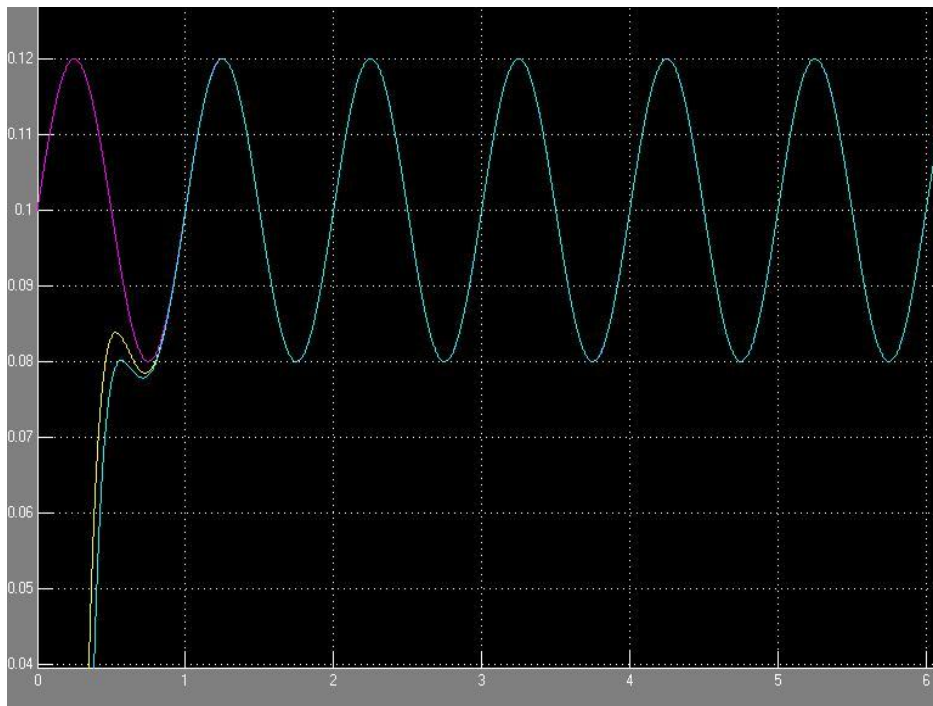
Fig. 3.35 Tracking 0.1+0.02*sin(2*pi) for c=100, c1=1, ksigma=100, alpha=0.75

(Horizontal axis: *time* ; each slot represents **1** second)

3.5 Galvanometric Scanning Principle & Image formation

The idea of forming a certain image or a pattern by scanning action is based on the combined movement of the laser beam on two axis and simple ON/OFF control or modulation of the laser beam.

Incoming laser beam initially hits on a reflective surface - so called "X-axis mirror" - mounted on the rotor shaft of a galvo, then resulting reflected beam has the ability to move in one axis due to the angular motion of the X-axis mirror. Later that beam has been transferred to the Y-axis mirror and which gives the additional beam steering capability in second axis so that final reflected beam has combined, two axis scanning property and can move both in X and Y axis simultaneously. Contrary to the X-axis mirror case; beam acting on the Y-axis mirror does not form a single spot on the mirror surface; but instead - due to the effect of the rotational motion of the X-axis mirror - it forms a line in longitudinal direction of Y-axis mirror. That's also why Y mirrors have usually been designed slightly larger compared to the X-axis mirrors in length. Then either by controlling the intensity of the laser beam or by completely turning it ON and OFF; desired images & patterns can be obtained on a target surface.

For a dual-axis beam steering system, without the use of an additional focusing mechanism or just using an ordinary lens; the motion of the beam along each individual axis can be represented with the equation: $I = 2d \tan \theta$.

This relation is shown in the Fig. 3.36
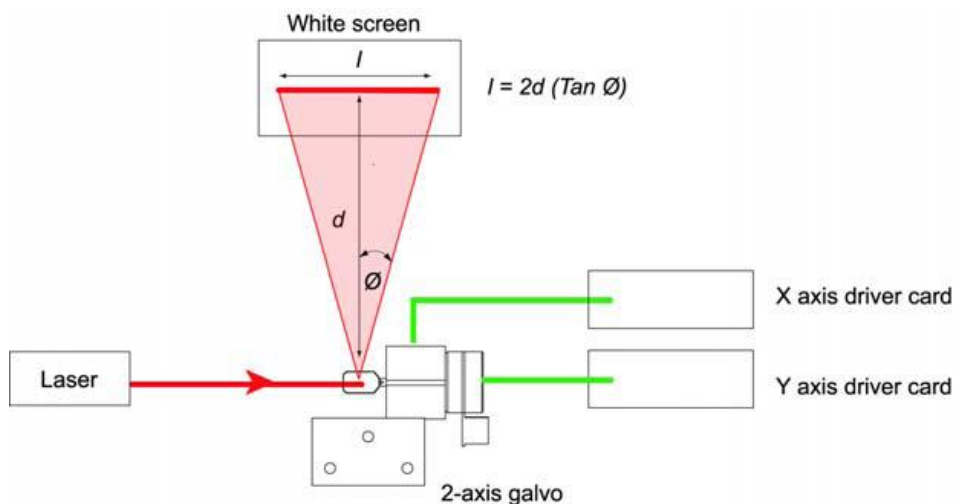
Fig. 3.36 Typical Beam Steering System

Typical example: $I = 2d \tan 20.0°$

or with a more detailed representation which includes the combined action of the mirrors and assuming that the X and Y scanners have been located orthogonally in Cartesian coordinates, the equations derived from Fig. 3.37 are as follows:
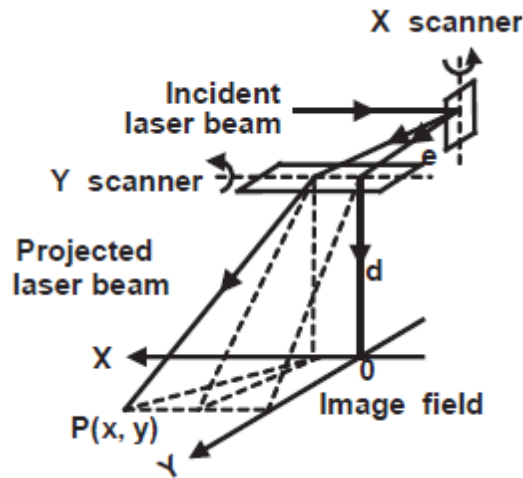
Fig. 3.37 Cartesian Scanning System

$$x = e \tan \theta_x + \sqrt{d^2 + y^2} \tan \theta_x = \left(e + \frac{d}{\cos \theta_y}\right) \tan \theta_x$$

$$y = d \tan \theta_y$$

$$fr = \sqrt{x^2 + \left(e + \sqrt{d^2 + y^2}\right)^2}$$

$$\Delta fr = \sqrt{x^2 + \left(e + \sqrt{d^2 + y^2}\right)^2} - (e + d)$$

$$\alpha_x = \frac{1}{2}\theta_x = \frac{1}{2} arctan \left(\frac{x}{e + \sqrt{d^2 + y^2}}\right)$$

$$\alpha_y = \frac{1}{2}\theta_y = \frac{1}{2}arctan\left(\frac{y}{d}\right)$$

where:

(x, y) ➔ the coordinate of a scanning point on the image field

d ➔ the perpendicular distance from the center of the Y scanner to the image field

e ➔ the distance between the center of the X and Y scanners

fr ➔ the travel length of the beam from the center of the X scanner to the coordinate in question

Δfr ➔ defocus error

θ_x ➔ the optical scanning angle of the X scanner, corresponding to the coordinate in question

θ_y ➔ the optical scanning angle of the Y scanner, corresponding to the coordinate in question

α_x ➔ the mechanical scanning angle of the X scanner, corresponding to the coordinate in question

α_y ➔ the mechanical scanning angle of the Y scanner, corresponding to the coordinate in question

3.5.1 Types of Scanning Systems

According to the different locations of the X and Y scanners in the scanning system, there are two kinds of dual-galvanometric scanning systems in practical applications. One is called a pre-objective scanning system, in which the X and Y scanners are located before an F-Theta objective lens. The other is called a post-objective scanning system, in which the X and Y scanners are located behind an ordinary objective lens (Fig. 3.38). In the pre-objective scanning system, the F-Theta objective focuses a parallel beam on the image field, without defocus error according to any coordinate on the image field. The disadvantage of the pre-objective scanning

system is that the size and cost of the F-Theta objective lens rise exponentially with the scanning field size or as the scanning aperture is increased. The merit of the post-objective scanning system is that it eliminates the need for the F-Theta objective lens through the use of a high-speed dynamic focusing module (DFM). The dynamic expansion lens that is located in the DFM travels up and down along the optical axis to adjust the focus on the image field. The length of movement of the DFM corresponds to the defocus error of every coordinate on the image field [28].
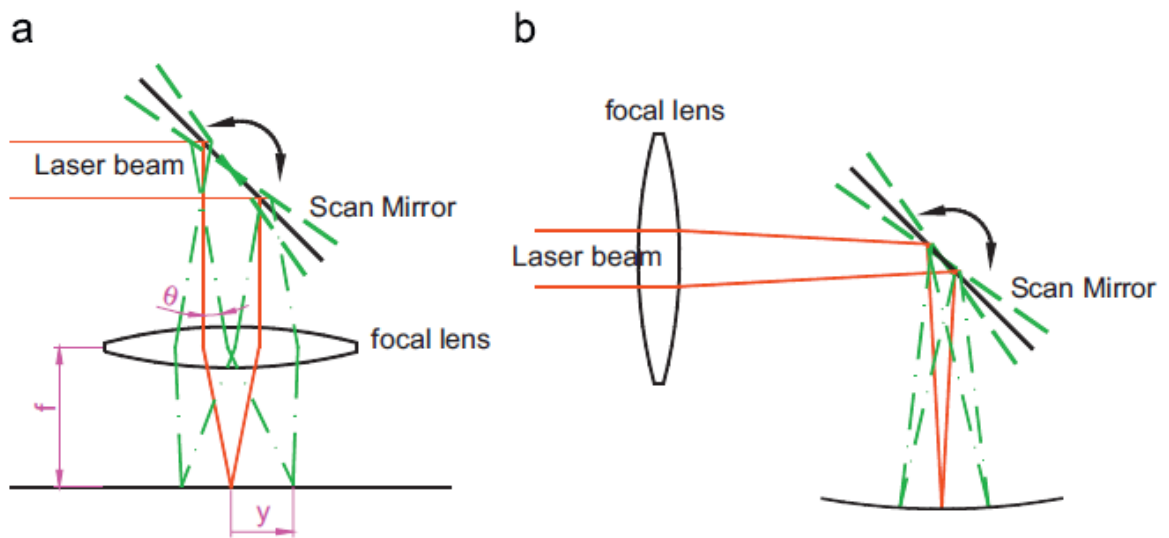
Fig. 3.38 Scanning System Types [30]. (a) Pre-objective scanning and (b) Post-objective scanning

3.5.2 Image Distortion

Laser scanning systems have been extensively used in laser marking, laser printers, laser projection, and laser coding. They represent a very reliable technique in the marking industry, and the galvanometric scanning systems are usually adopted in the laser marking systems. Although the galvanometric scanning system usually increases the marking speed, that is usually accompanied by field distortion (*see Appendix B*).

3.5.2.1   Error analysis of the galvanometric scanning system:

The field distortion of the laser marking systems is generated by the laser beam drift error and optical path error. These various sources of errors that influence the scanning system will be discussed.

Optical path errors

The distortion error does not result in a blurred projection image. In the absence of any other aberration, distortion appears as the misshaping of the image as a whole, even though each point is sharply focused. Fig. 3.39 shows a scanning system with F-theta lenses, and it indicates the origin of distortion. The laser beam incident at an angle on the F-theta lens, passes through it, such that a reasonable difference arises between the paraxial angle of refraction and the real ray angle of refraction. Restated, distortion arises because different areas of the lens have different focal lengths and different magnifications. In this case, this caused the real image to be pulled inward from the paraxial image thus causing negative or barrel distortion. The amount of distortion is expressed either as a lateral displacement in units of length units or as a percentage of the paraxial image height in an image plane. It is defined as [31]

$$\text{Distortion} = \left(\frac{y - yp}{yp}\right) \text{ x } 100\%$$

where y is the height of image plane and yp is the paraxial height
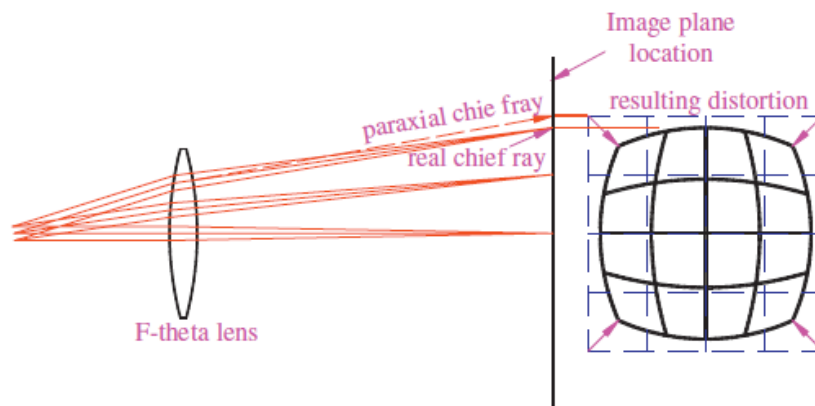
Fig. 3.39 Illustration of field distortion in the laser scanning system with an F-theta lens [31].

The extent of distortion may be positive or negative. A few distortions in the galvanometric scanning system, including pillow-shaped, barrel-shaped and pillow-barrel-shaped image, are because of optical path error, as illustrated in Fig. 3.40. Although the scanning system is supposed to draw a square, the actual image is not a square. A scanning system suffering from positive distortion deforms a square grid array, as shown in Fig. 3.40 (b). In such a situation, each image point is displaced radially outward from the center, and the most distant points move farthest. For negative distortion, each point on the image moves radially inward toward the center, as shown in Fig. 3.40 (c). Positive distortion typically results in a pillow-shaped image in the image plane; negative distortion results in a barrel shape.
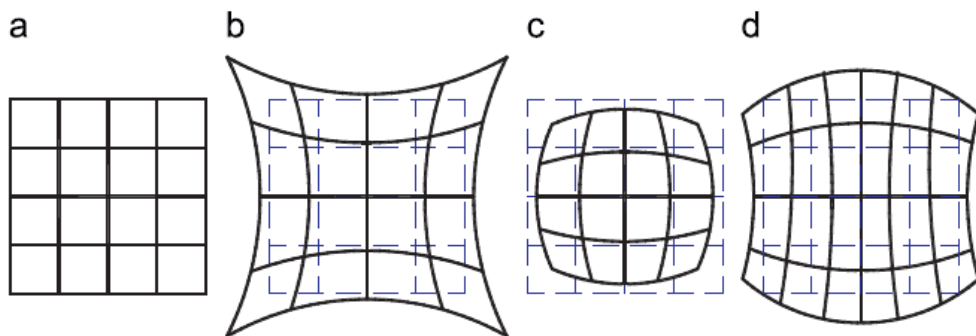
Fig. 3.40 Illustration of different distortions in an optical system [31]. (a) *No distortion*, (b) *Pillow shape*, (c) *Ballew shape and* (d) *Pillow-Barrel shape*

Laser beam drift errors

These errors usually include the mechanical misalignment, thermal influence, and the assembly errors **[28].** Several mechanical misalignments are produced by fixing of the scanning head, which results in the laser beam drift. Thermal effect can also be the source of the beam drift errors in the laser marking system. Moreover, the position transducer of the scanning system is usually sensitive to the change in temperature.

4 HARDWARE & SOFTWARE DESIGN

4.1 Electronics

4.1.1 DSP Based Supervisory Platform

Digital controller platforms such as industrial PC's, programmable logic devices like FPGA's, or embedded hardware solutions like microcontrollers, have widely been used in most of today's applications since increased mobility and modularity of the electronic hardware have been important issues most of the time. Considering the electronic hardware requirements for the laser micromachining systems (such as galvanometric scanner/general purpose DC motor drive & control) a relatively mobile and compact control platform with computer interface becomes a necessity. To meet those requirements a digital signal controller based supervisory board has been designed and implemented (see Fig 4.1).
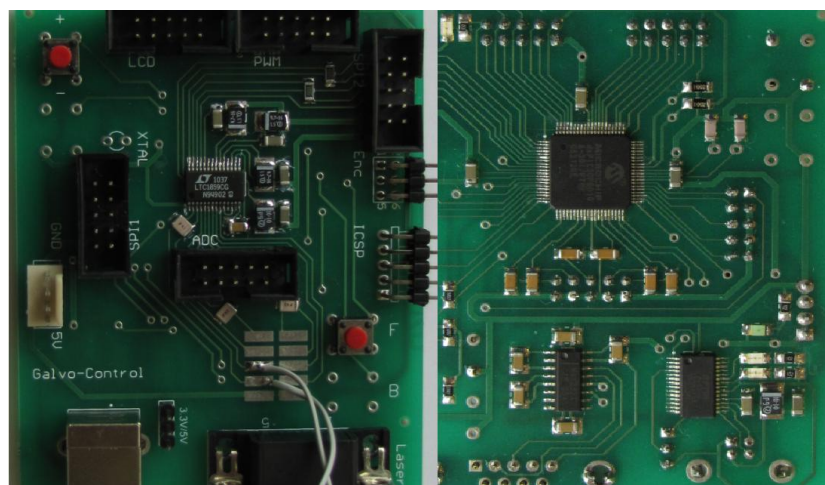
Fig. 4.1 Front and Bottom View of Designed Controller Board

Following parts explain the main components and functionalities of the designed controller.

4.1.1.1 *DSC (Digital Signal Controller):*

Preferred dsPIC30F6010A is a 80-pin 16-bit microcontroller, that has high-performance modified RISC (reduced instruction set computing) CPU core, leading to faster code development compared to CISC (complex instruction set computing) CPUs. 144 Kbytes on-chip Flash program space (instruction words) can be seen as enough for most control applications. In cases, where existing flash may not be enough for the target application, with the aid of external storage connectivity, using the SPI (Serial Peripheral Interface) communication features of the microcontroller, it is also possible to connect an SD (Secure Digital) Card for larger external data storage; thus also giving the ability of standalone operation without having the need for an additional controller PC or laptop. Below can be seen the main hardware features of some of the controllers in dsPIC30F family and physical view of selected controller.

dsPIC30F Motor Control and Power Conversion Family*

| Device	Pins	Program Mem. Bytes/ Instructions	SRAM Bytes	EEPROM Bytes	Timer 16-bit	Input Cap	Output Comp/Std PWM	Motor Control PWM	A/D 10-bit 1 Msps	Quad Enc	UART	SPI™	I²C™	CAN
dsPIC30F2010	28	12K/4K	512	1024	3	4	2	6 ch	6 ch	Yes	1	1	1	-
dsPIC30F3010	28	24K/8K	1024	1024	5	4	2	6 ch	6 ch	Yes	1	1	1	-
dsPIC30F4012	28	48K/16K	2048	1024	5	4	2	6 ch	6 ch	Yes	1	1	1	1
dsPIC30F3011	40/ 44	24K/8K	1024	1024	5	4	4	6 ch	9 ch	Yes	2	1	1	-
dsPIC30F4011	40/ 44	48K/16K	2048	1024	5	4	4	6 ch	9 ch	Yes	2	1	1	1
dsPIC30F5015	64	66K/22K	2048	1024	5	4	4	8 ch	16 ch	Yes	1	2	1	1
dsPIC30F5016	80	66K/22K	2048	1024	5	4	4	8 ch	16 ch	Yes	1	2	1	1
dsPIC30F6010A	80	144K/48K	8192	4096	5	8	8	8 ch	16 ch	Yes	2	2	1	2
dsPIC30F6015	64	144K/48K	8192	4096	5	8	8	8 ch	16 ch	Yes	2	2	1	1

Fig. 4.2 dsPIC30F Family Chart and Component View

In terms of operational speed, CPU can be clocked around 120MHz so that instruction cycle can reach up to 30 MIPS operation. Integrated PWM module provides dedicated features optimized for motor control applications. 8 PWM output channels can either be controlled by automated PWM features or manual override, it is possible to drive multiple DC motors (i.e.: motors for macro motion of motion stages) or a 3

phase synchronous motor. Positional feedback information necessary for control applications can be obtained by using QEI (Quadrature Encoder Interface) based on a 16-bit up/down position counter. In addition to the standard Phase A, Phase B and Index pulse measurement inputs, count direction status and x2 or x4 position measurement mode; it also has programmable digital noise filters on inputs that can be used to eliminate the encoder output noise. Between the other peripheral features: five 16-bit timers/counters, 3-wire SPI modules, 2 UART modules with FIFO Buffers, 2 CAN modules that are 2.0B compliant (for industry standard CAN communication).

The controller have to handle possible complex control algorithms and implement reliable data acquisition and process the incoming data and control the actuators, so additional signal processing capabilities might be required. For such purposes integrated 17-bit x 17-bit single-cycle hardware fractional/integer multiplier, ±16-bit single-cycle shift (higher performance for integer multiplication and division operations), single-cycle multiply-add operation functions can provide ease of calculation.

4.1.1.2 Analog Data Acquisition:

To be able to interface with the analog environment, controller needs analog features such as an ADC (Analog-to-Digital Converter). Built-in integrated ADC (Analog to Digital Converter) module of dsPIC30F6010A can provide sampling rates up to 1Msps, with a 10bit resolution. Considering the electromechanical systems, specified sampling rate can perform well for most control loops; but the resolution might not be enough for micro precision control applications where drive signal resolution is usually critical for accurate positioning of beam steering mechanisms such as galvanometric scanner modules. As a solution, an on board 16-bit ADC IC - LTC1859 - suitable for industrial process control with SPI communication interface - have been used on the controller board (see Fig 4.3).
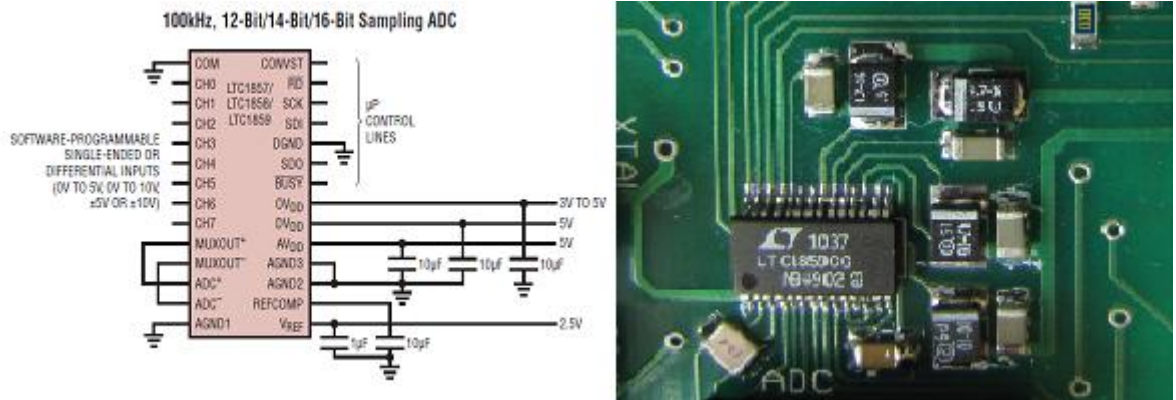
Fig. 4.3 Schematic and Component View of LTC1859 ADC

Although off-the-shelf ADC modules, using the conventional parallel line interface exists on the market; considering the number of bits hence also the number of required digital I/O s required for parallel communication; bus like architecture of SPI communication (see Fig 4.4) can provide multiple device operation using less number of physical connections.
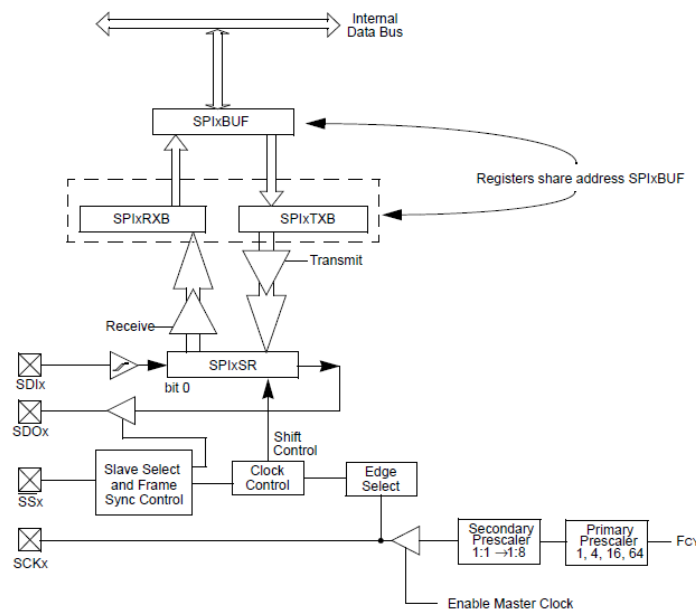
Fig. 4.4 Internal Structure of Integrated SPI Module

According to the datasheet values LTC1859, having a 5us maximum conversion time, can guarantee 100ksps sampling rate. It has 8 ADC channels (CH0-CH7), each can be configured by software, either for single ended or differential mode operation (see Fig 4.5).
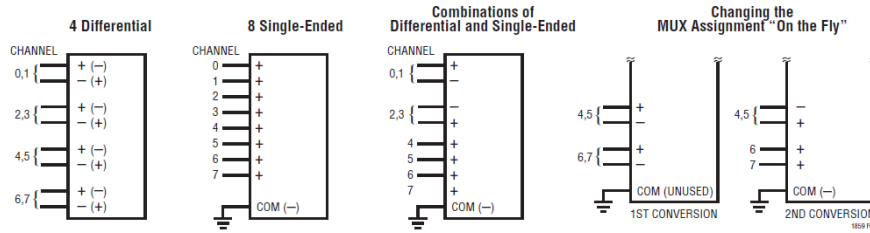
Fig. 4.5 Different Configurations of ADC Inputs

In both configurations, ADC+ and ADC- inputs of all channels are sampled at the same time so that input common mode noise can be rejected up to 96db. One other important feature is the flexibility to select the suitable input range required by the target application. Following figure shows an example configuration.
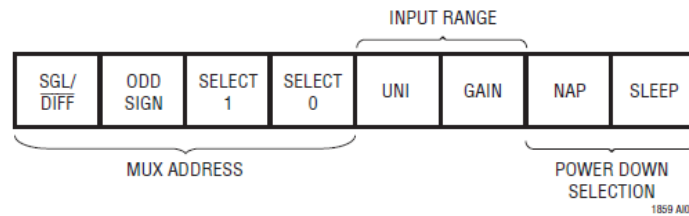
Fig. 4.6 ADC Configuration Byte

Available input ranges are 0V to 5V, 0V to 10V, ±5V or ±10V (see Fig 4.7). Considering the output signal levels of the sensors, photo sensitive devices, positioners that have been widely used in control applications; having such a range adjustability can increase system adaptability.

UNI	GAIN	INPUT RANGE
0	0	±5V
1	0	0V to 5V
0	1	±10V
1	1	0V to 10V

Fig 4.7 Selectable Input Voltage Modes

4.1.1.3 Computer Interface:

Considering the fundamental needs of the micromachining application, a high speed computer interface might be required to be able to transfer the preprocessed vector/raster machining data to the controller board, which will later guide the galvos or

65

other motor control hardware to achieve the desired motion. For those purposes, a communication method based on USB (Universal Serial Bus) - which has been standard almost in any computer platform and has enough communication bandwidth- has been selected. Since, dsPIC30F6010A IC does not have a built-in USB feature, an external USB communication IC, FT232RL from FTDI Company have been used. For interfacing the external USB IC to the microcontroller, an on board UART (Universal Asynchronous Receiver Transmitter) module has been used (see Fig 4.8).
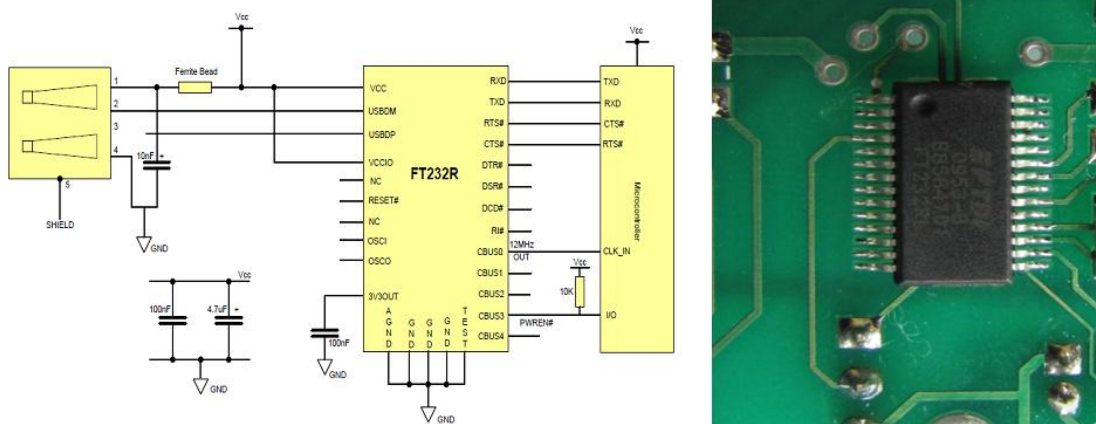
Fig. 4.8 USB to MCU UART Interface

4.1.1.4 Laser Control Interface:

Laser hardware offers three options for external control of the laser, one of which is the software control option throughout RS-232 connection. To be able to connect the internal UART of the microcontroller to the RS-232 interface an external level shifter IC➔ MAX232 has been used (see Fig 4.9).
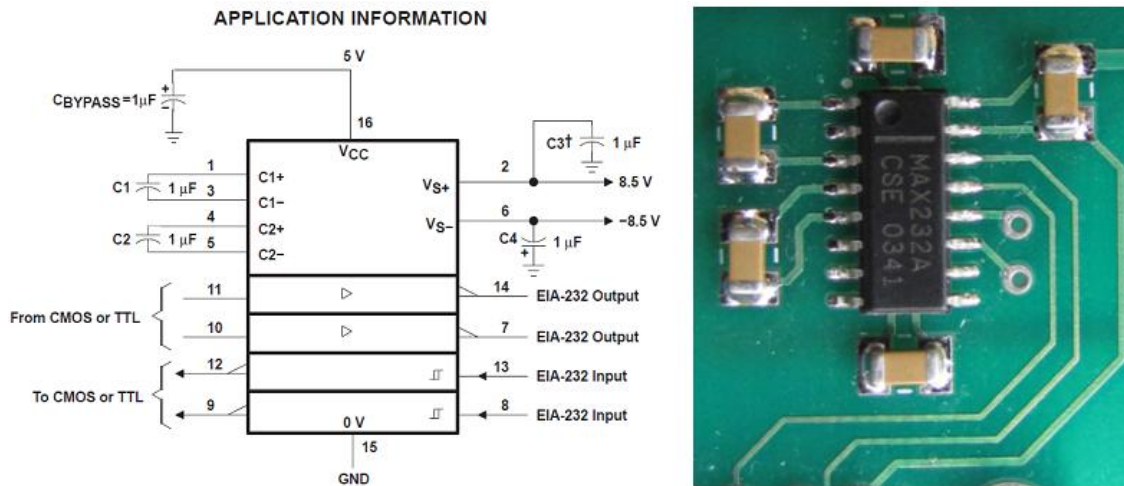
Fig. 4.9 MCU to Laser Interface

For safety purposes, not all of the commands are available by software control (i.e.: Global Enable). To produce those signals, external digital I/O pins on "PWM" connector can be used.

4.1.1.5 Operational Status Tracking Elements:

For viewing the operational state of the board, there is also an on board connector, which can be used for driving a either a 2 or 4 line character LCD (Liquid Crystal Display). 3 on board LEDs can be adjusted to provide information about the operational state of the PWM outputs. When the related motor control PWM output have been configured as a standard digital I/O pin; they can also be used for any other type of visual feedback (status tracking). Another led provides information about the power input status of the board (see Fig 4.10).
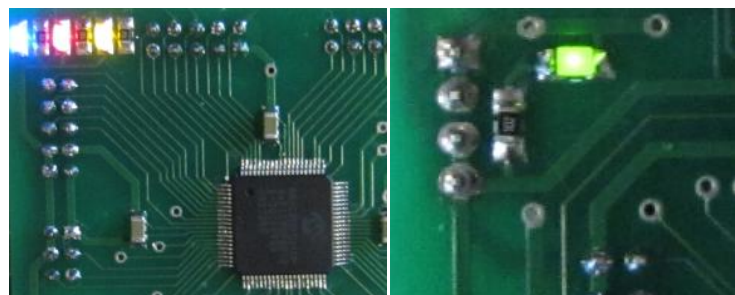
Fig. 4.10 Status LEDs

4.1.1.6   External User Intervention:

User can externally modify the operation of the controller board, through the on board push buttons that are observed in an event driven (interrupt based) manner by the software. Buttons have been labeled as "+", "-", "F", "B" to provide ease of use (see Fig 4.11).
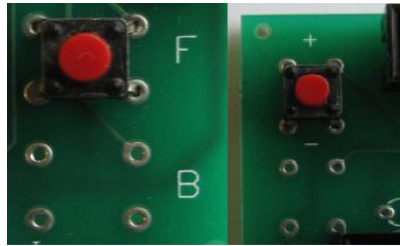
Fig. 4.11 Push Buttons

4.1.1.7   Programming & Debugging Interface:

Controller board also have an ICSP(In Circuit Serial Programming) feature that provides faster software development using an external programmer/debugger hardware such as Pickit2 / ICD3. Below can be seen the example pin out for Pickit2.
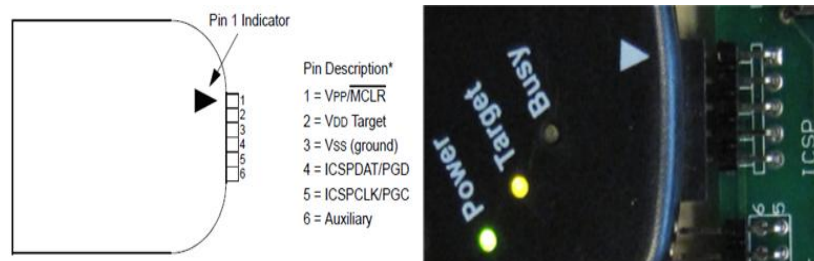
Fig. 4.12 ICSP Connectivity and Programming

4.1.2   Design of DAC Board

Driver & controller platform for galvanometric scanners requires bi-polar, low noise, clean, relatively large bandwidth control signals to precisely position the laser beam on

the work piece as desired. Selected 16bit LTC2642 DAC modules can provide low 0.5nV•sec glitch impulse and can support up to 50MHz SPI communication. Designed PCB uses low noise split supply op-amps as output buffers to obtain the desired low output impedance, bi-polar voltage output. Split supply bias voltage generation (i.e. ±5V) for DAC output drivers is done by an onboard capacitive charge pump IC (MAX660). DAC module also has an on board precise voltage reference component so that with the aid of voltage selection jumper, it is possible to switch between 4.096V and 5V reference voltage options (see Fig 4.13).
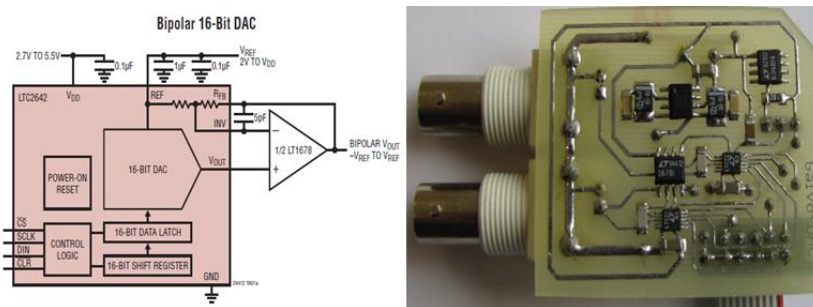
Fig. 4.13 Schematic and Component View of DAC Module

4.2   Software

4.2.1   Embedded Software Design for Controller Board

After designing the controller board, next step was the selection of software development environment that will be used in coding. Since C programming language - compared to assemble language based tools - usually provides relatively faster code development, CCS PICC C Compiler has been used as the embedded software development platform for the dsPIC30F6010A. Compiler has also advantages like inline asm code integration to C code for increased coding compatibility.

Code for the microcontroller platform has been implemented such that it's working algorithm is mainly based on interrupts; in other words done in an event driven fashion, thus leading to a more conflict-free, time-efficient operation, especially considering the various number of operations such as data acquisition, transferring of position data to

DACs through SPI bus; UART communication with PC and laser, external user intervention and control.

The form for storing the machining data in controller environment has been chosen as array based. Every single array contains "image" elements saved as struct data type. Each "image" struct contains part of machining data that will later be sent to DACs and laser in {X,Y,D} format such that ➔ 16-bit unsigned integer X, representing beam position in X axis; 16-bit Y, representing position in Y axis; 8-bit D value either for laser beam ON/OFF control (in B/W mode) or duty cycle value (in Grayscale Mode) corresponding to power level adjustment parameter for software controlled high power laser or small power visible test laser.

During the initial experiments; a standalone 5mWatt visible red laser, having the wavelength of 640nm has been used, to test the reliability of DAC-Galvo operation and proposed image formation approach, without excessively interacting with a 20Watt high power laser, at least for the initial tryouts. The brightness level of used 5mW laser can be adjusted using a TTL logic level 20kHz PWM signal. For that purpose high resolution PWM features of the selected microcontroller have been used. The PWM resolution (for edge-aligned mode) while controller operated at 120MHz clock frequency can be found using:

$$Resolution = \frac{\log\left(2 \bullet \frac{f_{CY}}{f_{PWM}}\right)}{\log(2)}$$

$$\frac{\log\left(2 \bullet \frac{29,48\,MHz}{20kHz}\right)}{\log(2)} = 11.5255 \qquad (\text{where: } f_{CY} \text{ is the instruction clock})$$

It is around 11bit, which can be taken as acceptable for laser intensity adjustments.

4.2.2   GUI Design

Nowadays, most systems – whether an industrial solution or scientific research is the main concern - have a built-in embedded intelligence that may require the transfer of operational commands or data from a digital control platform (i.e.: industrial PC) to the system, so an "intermediate step" software might be convenient in terms of both device

control, data transfer between digital platforms (i.e.: pc/laptop & controller board) also making the system integration easier due to partial elimination of complex intermediate hardware stages.

Considering most of today's professional laser machining solutions, use user friendly graphics based control environments so called GUIs (graphical user interface); a windows form application based C# GUI has been implemented to meet similar requirements.

Designed application simply gets an image file, than converts that file to a new image in suitable format and size, and then extracts the pixel based image data and writes it to a text file; content of which, later be transferred to the controller board and laser module through serial (USB/RS-232) connections.

4.2.2.1   Design Method:

Chosen approach was using the .NET based C# software component available in Microsoft Visual Studio. The program can export executable outputs with ".exe" extension, removing the necessity for additional software installation; so that any computer with appropriate RS-232 and USB can be used to operate the system. Other advantages can be ordered as: communication through serial ports can be done easily in an object based manner using the windows form application toolbox; many desired time dependant features can be added to modify the operation of the system like counting down, having time limited operation. Built-in toolboxes have visual elements that can be used to view the levels of data acquisition signals, leading to nearly full status tracking of the controller and interconnected hardware.

For ease of understanding the operation of GUI window, it can be evaluated in three main parts in terms of functionality.

Part A:

That part includes controls for main actions and features related with image preparation:

- Importing source image to extract the target machining data

- Specifying width and height in pixels

- Scaling of the final machining data output

- Keeping aspect ratio might be enabled/disabled

- Choosing between Gray Scale & Black-White modes

- Exporting machining data to a text file

Part B:

That part includes controls for main actions and features related with device configurations (laser, controller board), communication to realize machining data transfer:

-Data transfer tracking windows for communication with laser through RS-232 and with PC/Laptop through USB

-Manual control of digital I/O s where forced HW control is needed

-Laser Control Features:

HW Controlled (using digital I/O s):

Laser Disable, Laser Emission Gate Control

SW Controlled:

Laser Global Enable, Alignment Laser Disable/Enable, Laser Duty Factor, Laser Burst Length, Laser Pulse Repetition Rate Selection, Laser Pulsed/CWM mode selection, Laser Waveform Selection/Setting, Laser Power Adjustment, Task Start, and Turn ON/OFF

Part C :

That part includes controls for main actions and features related with galvo output control and output machining data:

-Galvanometric scanner enable/disable

-Selecting the output data to be machined (extracted from a file or stored in the memory)

4.2.2.2   Operation of the GUI:

Part A - To obtain the machining data from an image, imported source image file should have one of the ".jpg" ".jpeg" ".bmp" ".gif" file extensions. Once successfully imported the image file can be viewed from the picture box. Then in the next step user should decide width and height parameters in pixels for the machining data output that will be extracted from the source image. Calculated pixel count of the new image is shown in pixels tab. One should note that ordinary image resizing operations can lead to distortion in image quality so that in our case the technique that has been used for image conversion is interpolation based so resizing causes less image distortion. While resizing, it is user's choice whether to keep the aspect ratio between width and height of the image or to resize it with a new desired ratio. Other parameter to be adjusted is the final scaling factor value that can be used to make ordinary scaling of the output image so that it can directly be used by the controller to drive the DACs, hence also the galvos for more or full utilization of the galvo's scanning range. As previously stated each machining data output contains x,y coordinates for the related pixel and a light intensity value. The method for obtaining the intensity value is based on reading the RGB values of a certain pixel each represented with a byte. Since this machining application and reference images has a monochromatic nature, it has only been focused on the G value (R or B also can be used since they all give same result in existing case) and that has been compared with 128; such that values higher than 128 produces "1" corresponding to "ON" state of the laser and values smaller than 128 produces "0" which means laser beam "OFF". If gray-scale mode is active then this comparison is not made and G value is directly sent to be later used for intensity information of the laser beam.

Part B - In the device communication and control part of the GUI: after activating the desired devices and choosing the COM ports related with each device (controller board, laser) and desired communication Baud rates; in the next step, parameters such as laser burst length, laser pulse repetition rate, laser output power (controlled based on stby and active state current levels), laser duty factor and laser

waveform can be adjusted by entering numeric inputs. Other features related with laser operational modes and controlled by checkboxes can be ordered as: Pulsed/CWM mode selection and alignment laser ON/OFF control. Remaining functions such as task start, shutdown can be implemented by using buttons.

Part C - Machining data can either be based on data obtained from an imported image or available patterns such as dots, lines, circle, varying sine wave figures stored in controller board's program memory. The source for that data can be specified by using the data source selection menu. After enabling the galvos from the GUI control panel, selected data can be diverted to drive to the DACs on the controller board to actuate the galvos and form the target pattern on the work piece.
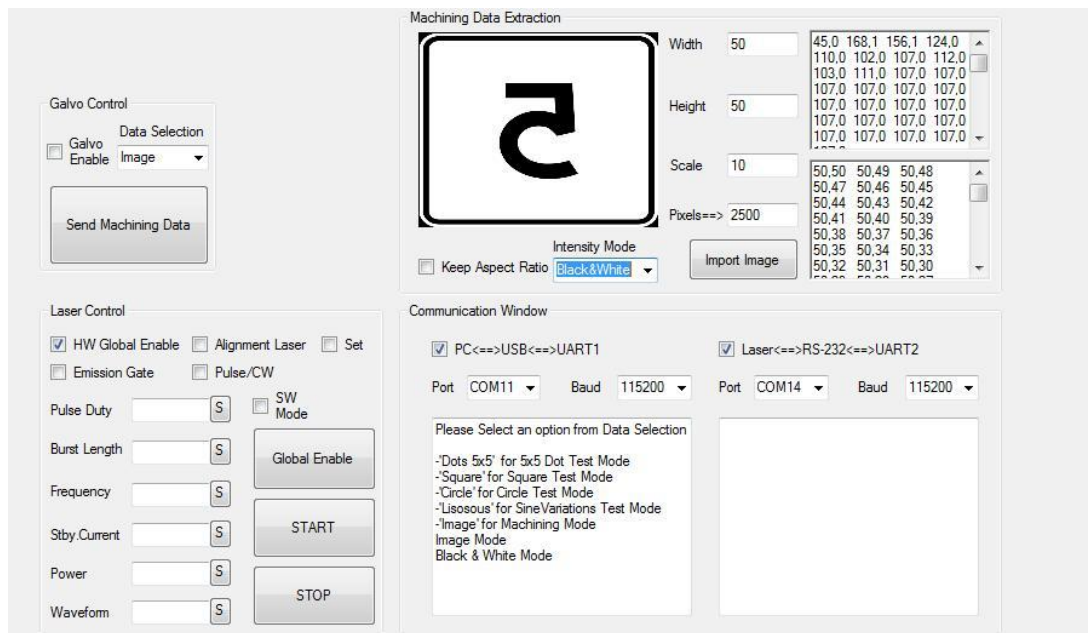
Fig. 4.14 GUI on a sample run

4.3 Mechanical Design

The experimental studies require the accurate positioning of the optics, as well as their proper connection with the electromechanic systems. For such purposes, additional mechanical parts have been designed in Solid Works environment, machined and used during the experimental studies. That part tries to cover the design procedure of the mechanic parts and working principles.

74

4.3.1   Fine Focusing Mechanism

Most of the distances-lengths corresponding to optical parameters have been decided by the telecentric scanning lens design specifications so that correct placement of the scanning lens becomes crucial. Due to the system tolerances related with the mechanical parts, and their positioning relative to each other, fine adjustment of the telecentric scanning lens for proper focusing is essential. So under the guidelines of these requirements, a fine focusing mechanism has been developed (see Fig 4.15).
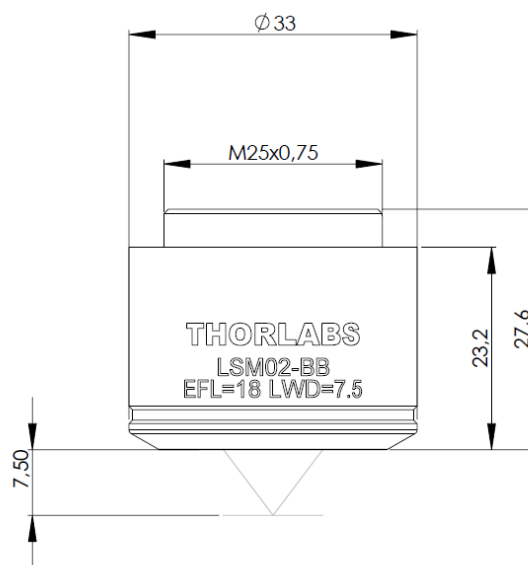
Fig. 4.15 LSM02 Technical Drawing

Operational principle of the designed manual focusing mechanism can be summarized as: the rotational motion results a lens movement along the focusing axis (e.g. CW rotation moves the lens "up"➔ away from the work piece; whereas CCW rotation moves the lens "down"➔towards the work piece. As can be understood from the figure above, the pitch size for the lens threads is 0.75mm. Considering the pitch size and number of threads (which is 5 for the LSM02 lens); using the lens threads directly might have degrade the mounting stiffness after a few turns in CCW rotation; so an outer ring with a single-start thread structure and finer pitch value has been designed and machined to be able to reach higher focusing adjustment resolution.

The inner side of the designed ring has female thread directly matching to the lens (again 0.75mm); but the outer side of the ring has a male thread with a finer pitch of 0.5 mm and lower thread angle, thus together leading to more precise adjustment of the lens position through the focusing axis. One other advantage of the ring mechanism is that, due to the higher total threaded length (9.96 mm), the ring makes it possible to go at a closer distance towards Y-axis mirror. That value is higher compared to the case in which overall focusing action is limited with the vertical distance of 0.75mm*5 turns ➔ approximately 3.75mm total threaded length of the lens itself.

Finally that ring sits in a counterpart having a female thread and 0.5mm pitch. The counter part is tight-fixed to a rectangular plate that is mounted on the galvo assembly. CAD drawing and photo of the produced part mounted on the galvo assembly is given in the following figure 4.16 ("blue" shows the ring and "green" shows the plate):
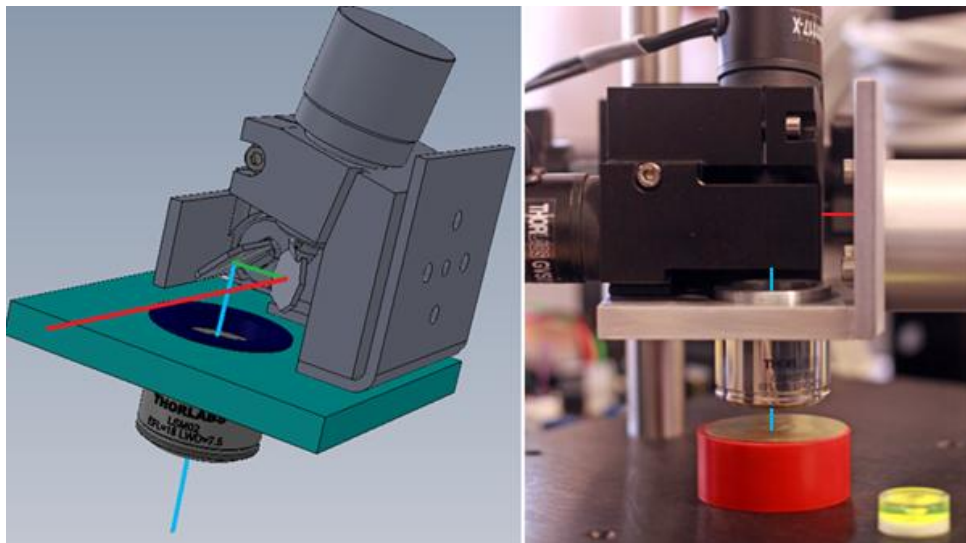
Fig. 4.16 Focusing Mechanism

Note: Incoming beam is shown by RED; reflecting beam shown by GREEN; outgoing beam shown by CYAN

4.3.2 Beam Expander Mounting Part

Laser beam transferred with the fiber optical guide finally comes out through a beam expander unit so that the outcoming beam can be focused more effectively by the final focusing mechanism. Laser beam expander unit should be fixed firmly to the galvo assembly to be able to properly feed the incoming laser beam to the X-axis mirror. Mentioned beam expander unit is shown in the figure 4.17 below:

Fig. 4.17 Beam Expander

Considering the size and geometry of the expander unit (*see Appendix E*) and also taking into account that the centre of the laser beam should be coincident with the center of the target X-axis mirror; an appropriate part, satisfying these demands, has been designed and produced. CAD drawing and photo of the machined part is given in the following figure 4.18:
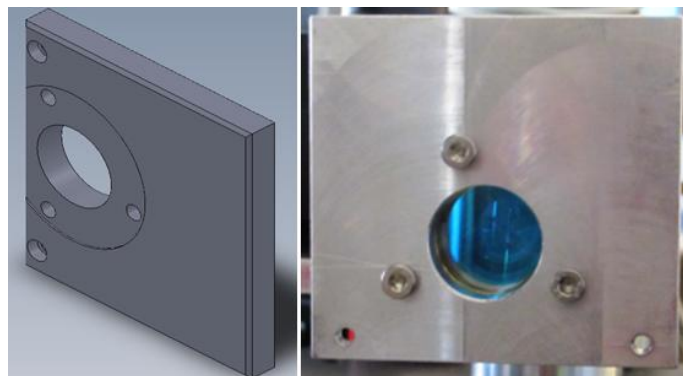
Fig. 4.18 Beam Expander Mount

For safety issues and to prevent damage to surrounding environment another requirement is that the regions where active laser radiation exists should be in an isolated closed form as much as possible; but due to the design geometry of the galvo assembly a fully-closed enclosure does not seem to be feasible. So those parts also form a semi-closed enclosure that minimizes the laser radiation to emit out of the allowable region.

4.3.3   Mirror Inertia Calculations (for simulations)

In this part inertias of the mirrors have been calculated using software tools, to use that information later in the simulation model of the galvo models. During the simulations, the inertia values have been applied to the system as disturbance terms to improve the reliability of the simulation model.

This procedure can be summarized as: creating the mirrors in Solid Works design environment and calculating the inertias of the mirrors using the built-in inertia calculation tool of the Solid Works. Below shown the 3D drawings of the mirrors in Solid Works:
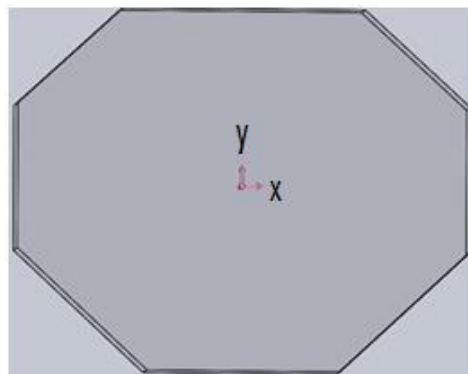
Fig. 4.19 X-axis mirror   Fig. 4.20 Y-axis mirror
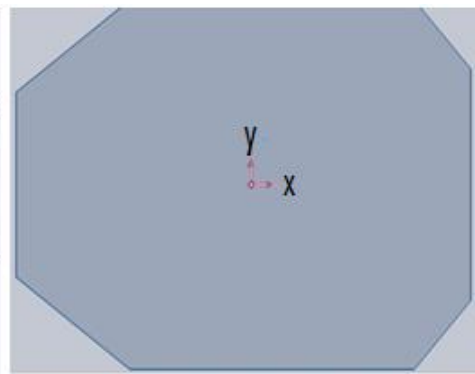
The inertia values obtained using the tools are like the following:
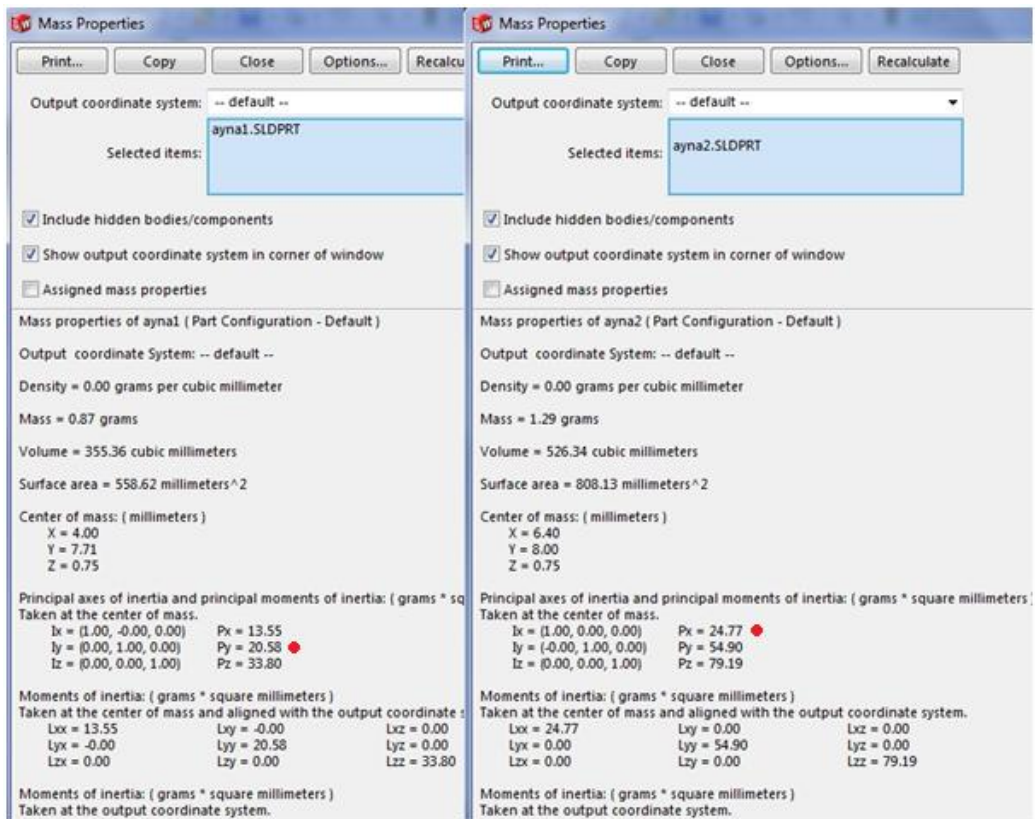
Fig. 4.21 Calculated Inertia Values

Considering the coordinate plane specified in the figures, one should note that rotary action is along "Y" axis for "X-mirror" and along "X" axis for "Y-mirror". The inertia values related with rotation is marked with red dots: Ix=24.77 gr $*$ mm^2=24.77 x 10^{-9} kg $*$ m^2 & Iy=20.58 gr $*$ mm^2=20.58 x 10^{-9} kg $*$ m^2

5 EXPERIMENTS & CONCLUSION

5.1   Experiments

Experimental studies of the thesis work can be handled in two main parts:

- **Macro level image formation experiments**

- **Micro level machining experiments**

A) Macro level image formation experiments using a visible spectrum laser:

During that part of experiments the main aim has been the proof of image projection concept to ensure the reliable operation of galvanometric scanner system hardware as well as control software.

Equipments: (in addition to default scanning hardware and electronics)

- Laser Pointer

Fig 5.1 Laser Pointer

- PDQ80A PSD (Position Sensing Detector)

Fig 5.2 PSD Device

Laser Pointer:

It is a visible spectrum 5mWatt laser with 640nm wavelength and a modulation input that can be driven using a TTL level 20kHz modulation signal so that beam intensity control can be done. The focusing has been adjusted by using the built in collimator of the laser.

PDQ80A PSD:

A PSD device from Thor Labs Company having a segmented-quadrant (*see Appendix F*) device structure and separate analog voltage outputs for each axis.

Method:

Image data to be projected on the surface, have been stored in program memory of the designed supervisory board. Analog drive signals for the galvo servo driver boards have been produced by using the designed DAC board which has been controlled according to the image data coming from the supervisory board through 20MHz SPI communication interface. Galvos have been used to steer the laser beam on the target surface. No additional focusing mechanism has been used.

Continuous line images: (laser continuously ON)

Using that method phase and frequency varying sine wave variation curves (Lissajous Curves) have been formed. See following figures.
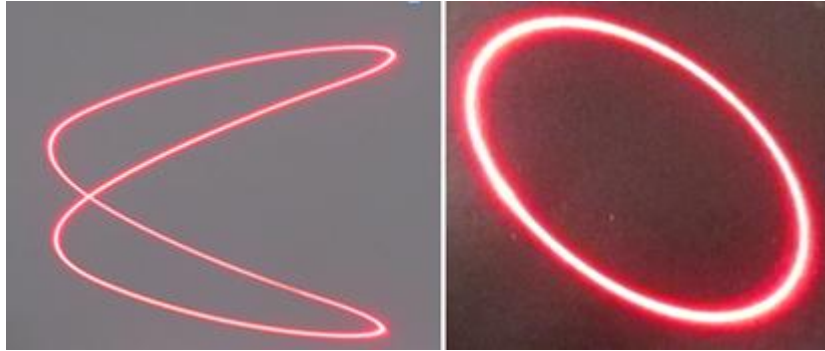
Fig. 5.3 Snapshots from a rotating Lissajous Curves

Another stage in experiments can be thought as "intermediate" transition between macro and micro level experiments. Above stated PDQ80A PSD device has been used to test the micro level scanning operation and closed loop data acquisition capability (i.e. 16-bit external ADC) of the supervisory board (especially for possible future closed loop power tracking). To eliminate the noise in obtained signals, 10 Hz low pass filter has been considered as a remedy but that causes the side affect of decreasing bandwith so for high speed scanning tests that method has been left aside and rest of the experiments have been established by high power laser module and machining on materials.
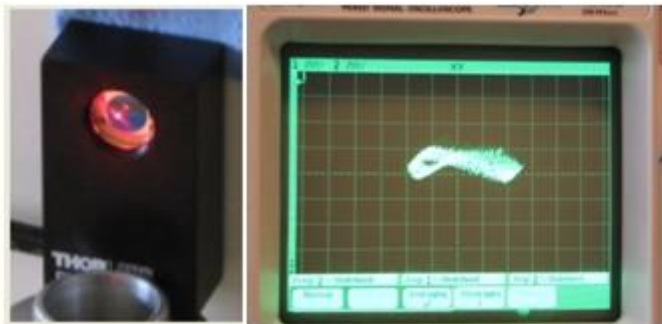
Fig. 5.4 PSD output for micro scale curve

Discontinuous line images (with laser ON/OFF modulation):

In that type of image creation the laser is ON between any two consecutive points where the smallest unit curve (i.e. line) exists; and OFF during a blank transition. Using this method vector images such as geometric shapes, logos have been formed (see Fig. 5.5).

Fig. 5.5 Laser Radiation Logo

B) Micro level machining experiments with high power laser

During that part of experiments the main aim has been the laser micro scribing of a projected image on a target surface by using before mentioned direct-write method and raster scanning approach.

Equipments: (in addition to default scanning hardware and electronics)

- LSM02-BB telecentric scanning lens

- 20Watt 1064nm pulsed-fiber laser module

- 7.0X Beam Expander

Method:

Image data to be scribed on the surface, have been extracted using the designed GUI and transferred to the program memory of the designed supervisory board through USB interface. Analog drive signals for the galvo servo driver boards have again been produced by using the designed DAC board which has been controlled according to the image data coming from the supervisory board through serial communication interface. Galvos have been used to divert the laser beam on the lens surface and the focusing of the beam has been implemented by using the specified lens. Following figure 5.6 shows general view of experimental setup.
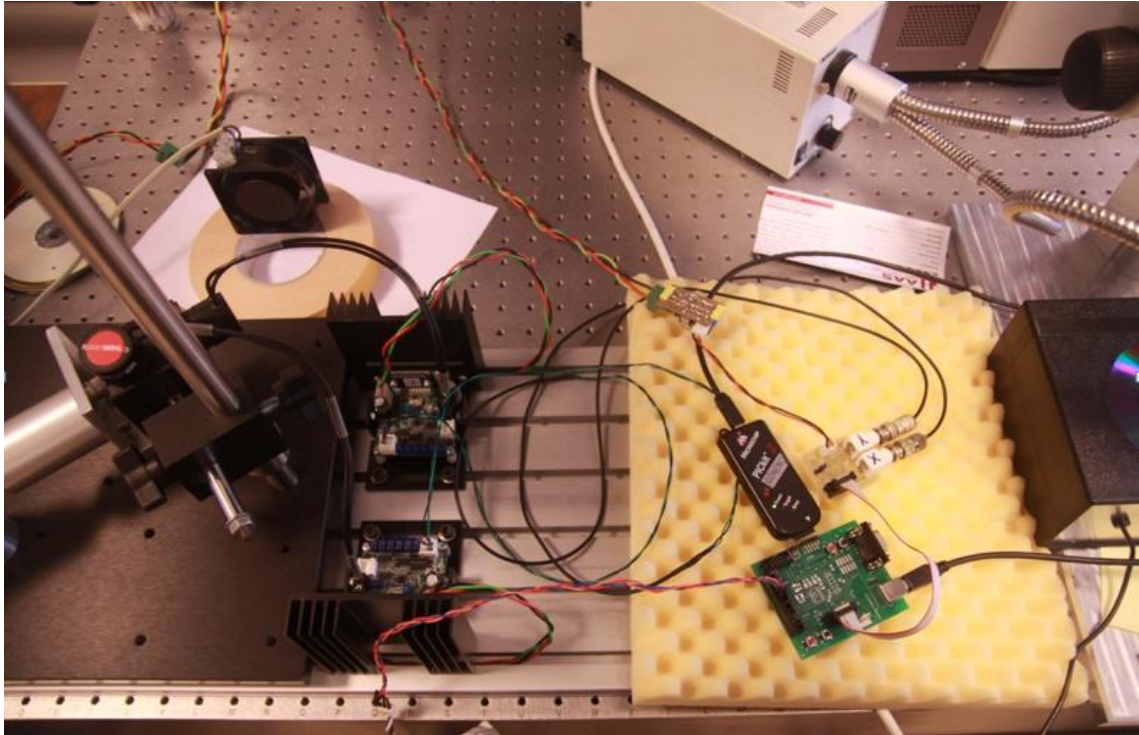
Fig. 5.6 Experimental Setup

Various scanning rates and output powers have been used. Materials such as special laser alignment paper, brass disc, and optical storage discs have been evaluated during the experiments. Scribed surfaces have been viewed using an optical microscope.

In the experiments additional variable scaling factors have been used which makes location of each spot has been decided by the "pixel coordinate x scaling factor", plus an additional centralizing offset value of 32768, that has been used to form an image normalized to the center of coordinate plane. There is also an internal multiplier which is set experimentally so that between each adjacent pixels the digital value send to DACs have been incremented by "internal multiplier x scaling factor" (over 655536). Since machining performance relies on fundamental parameters like spot size, initial experiments have been concentrated on focusing. Following are the results obtained for different materials and power levels:

Material: Bristol cartoon covered with cellophane coating, Thickness= 0.33 mm approximately.

Fig. 5.7 Bristol Cartoon Hole

Note: Each gap is 0.5mm

Average Power Level: 4 Watt approximately (linear power output assumption for ease of calculation) *Pulse Rate: 25kHz, Burst Length: 2seconds*

Comment: The region that photo thermal effect occurs is larger compared to drilled hole itself.

*Material: Black ABS plastic, thickness 2 mm approximately

Fig. 5.8 ABS Plastic

Average Power Level: 8 Watt approximately (linear power output assumption for ease of calculation) *Pulse Rate: 25kHz Burst Length: 1seconds.*

Comment: Shorter pulse length provides advantage in minimizing the thermal expansion even with higher power levels.

Experiments continued with the scribing of "5" figure on surface of target materials.

Material: Brass disc, thickness 0.18 mm approximately
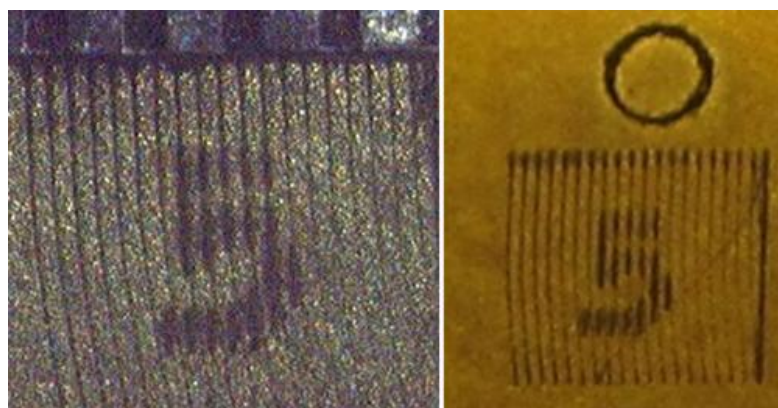
Fig. 5.9 Brass Disk Microscope & Super Macro Views

Note: Each gap is 0.5mm

Average Power Level: 20 Watt approximately (full power)

Pulse Rate: 25kHz, Burst Length: 10 seconds, Area: 2.5mm x 2.5mm, Scaling Factor: 50, Scanning Rate: 2.25 Hz

Comment: High power low frequency scanning causes undesired lines in regions that no scribing should occur. Distance between adjacent lines is around 166 μm.

Material: Compact disc, thickness 1.25 mm approximately

Note: Optical media used in experiments have a polycarbonate plastic substrate, added to this an organic dye recording layer (azo, cyanine, dipyrromethene or others) followed by a metal reflective layer, silver alloy.
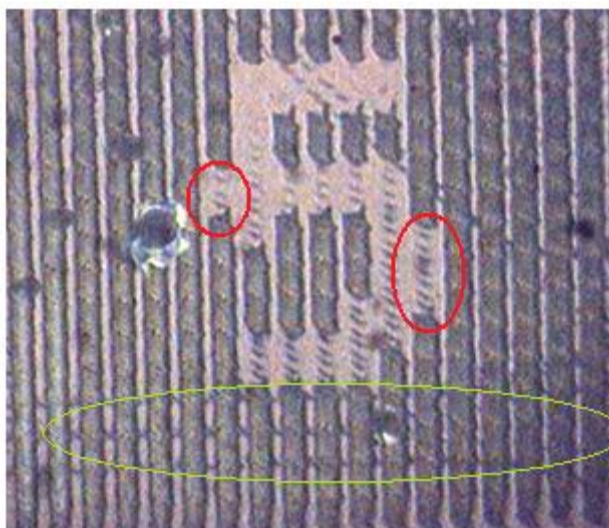
Fig. 5.10 CD

Average Power Level: 3 Watt approximately (linear power output assumption for ease of calculation), *Pulse Rate: 50kHz, Burst Length: 2 seconds, Area: 3mm x 3mm, Scaling Factor: 50, Scanning Rate: 2.25 Hz*

Comments: Undesired pixels circled are due to rounding-up of pixel intensity data and related with imaging data itself not a marking error. The lines parallel to horizontal axis (circled with green) occur because of turning back to initial scanning start point at the end of each full scanning of the image data array. So for the following experiments bi-directional scanning technique has been used.

*Material: Compact disc, thickness 1.25 mm approximately

Fig. 5.11 20x20 "5" on CD
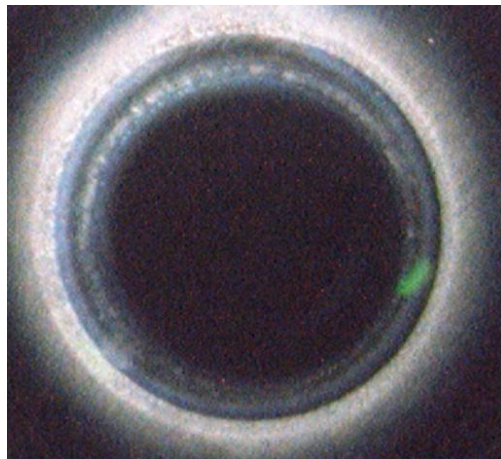
Average Power Level: 2 Watt approximately (linear power output assumption for ease of calculation) *Pulse Rate: 50kHz, Burst Length: 2 seconds, Area: <1mm x 1mm (20 x 20 pixels), Scanning Rate: 2.25 Hz*

Material: DVD+R disc, thickness 1.25 mm approximately
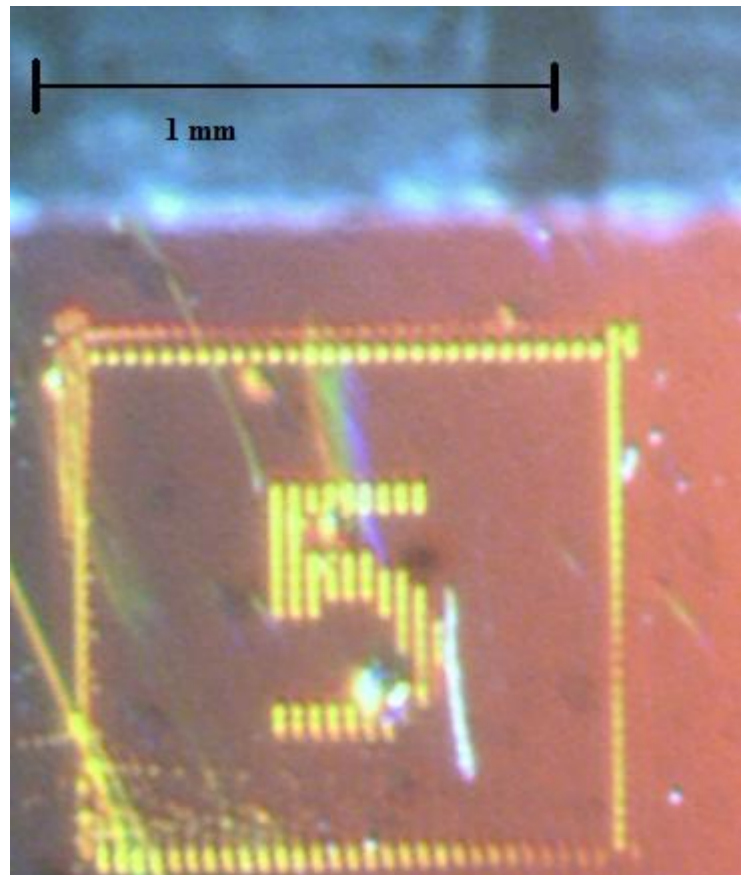
Fig. 5.12 32x32 "5" on DVD

Average Power Level: 2 Watt approximately (linear power output assumption for ease of calculation) *Pulse Rate: 25kHz, Burst Length: 2 seconds, Area: 1mm x 1mm (32 x 32 pixels), Scaling Factor: 10, Scanning Rate: 0.86Hz*

Comments: Inverted version of the extracted image data has been used so that "black pixels" on the reference image means laser ON while "white pixels" corresponds to laser OFF condition. Number of undesired pixels decreased clearly, leading to a finer marking. The distance between center of spots can be calculated as less than 1000 µm / 32= **31.25** µm (technical spec given for LSM02-BB points to a 13 µm minimum achievable spot size); because the gap between adjacent spots can still be distinguished in horizontal axis. Although the reference image resolution is the same for both vertical

and horizontal axis; marks along vertical axis are in a more "continuous" fashion compared to the general behaviour along horizontal axis. This effect might be occurring due to the horizontal scanning at low speeds, such that the fast scanning in vertical axis - this is actually what forms the equivalent "vertical scanning line effect"- results with many consecutive laser spots affecting short time after each other extracting more heat and leaving less time for cooling down thus leading to combining of transition regions between spots.

Internal multiplier has been selected as "18" experimentally, so that the digital value send to DACs have been incremented at least by 180 (10 x 18); which means galvo modules can still be forced for increasing resolution (of course considering the ±1LSB INL and DNL changes over temperature of the DACs).

5.2 Conclusion

The design and implementation of a laser micromachining system, mainly targeting micro scribing and marking operations have been explained in previous several chapters, together with the theoretical background and proof of overall system functionality. Following is the summary of the conclusions of this research work.

1) Laser micromachining parametric relations:
Before laser machining, parameters related to the material removal rate should be examined. Machining of different materials may require examination of different machining parameters, including laser intensity, number of laser pulses, scanning rate. It is obvious that a higher energy level and higher number of laser pulses provide a higher material removal rate. Higher scanning rates cause less thermal deformation in the regions where no machining should occur.

2) Scanning Techniques:
Raster scanning approach requires the use of bi-directional back and forth steering of the laser beam to maximize useful bandwidth of the galvo modules and minimizing undesired markings due to fast transitions between adjacent columns or rows. Bandwidth increase is due to small angle bandwidth being larger than large angle bandwidth so avoiding long trajectories provide such an advantage.

3) Machining Resolution

In machining operations, the focused spot size that can be achieved with fast pulsed operation is smaller than it's with slow continuous wave mode operation. Decreasing pulse repetition may contribute in similar way. These effects are mainly due to lack of thermal deformation in pulsed case.

4) Scanning Approach - Operational Performance Relation

Raster scanning approach usually provides better results in marking operations whereas vector scanning may be more convenient for drilling, cutting type of applications.

5) Modification of machining area requires the consideration of power level

To obtain better linearity in terms of optical power control, an external closed loop control system based on optical sensors can provide advantage in gray scale marking and scribing.

6) Machining Control Algorithm

A control algorithm that includes scanning speed rate adjustment feature or auto power tuning depending on machining area is necessary for reliable operation.

6 POSSIBLE FUTURE WORK

So far, the content and results of this research work have been summarized. It mainly focuses on laser micromachining by implementation of fast marking operations on certain type of materials. Behind this research, there are several possibilities for future work

1) Increasing the scanning resolution:

Staying within the limits of existing hardware, the image resolution might be increased further.

2) Extending machining area:

Machining to a larger area without sacrificing from the resolution might be possible with the synchronization of scanning elements and additional motion stages to move the work piece.

3) Parametric study of machining and measurement:

Forming tables to be able to observe the relation between machining parameters, material types and type of processing job might contribute to the performance and effectiveness of overall processing procedure. SEM (Scanning Electron Microscopy) technique can be used for more detailed measurements.

4) Improvement of machining quality and extending range of target materials:

The laser that has been used during this study is a nano-second pulse type. However, it may be difficult to produce high quality machining surfaces on most materials due to photo thermal heat effect being dominant in nano-second machining. A possible improvement might be promoting to a femto or picosecond pulse time laser.

5) Improving vector scanning compatibility:

For now, designed system can also be used for vector scanning purposes; but this capability is limited with the use of third party programs to obtain the necessary vector scanning information. In that context, vector data extraction feature might be integrated to the control software so that it can provide convenience in drilling, cutting type of applications.

6) Adding external data storage feature:

To increase the standalone behavior of the system (for example: fully eliminating the dependency on a controller PC), an external storage feature might be added by interfacing with a SD (Secure Digital) card through SPI communication.

7) Closed loop optical power tracking:

With the use of additional optics - such as beam splitter mechanism - tracking of beam power level can be implemented so that closed-loop optical power control can be realized.

REFERENCES

[1] Madou, M.J., "Fundamentals of microfabrication: the science of miniaturization (2nd ed)", CRC Press LLC, 2002.

[2] Xia, Y., Whitesides, G.M., "Soft lithography", Annu. Rev. Mater. Sci., 28, 1998, pp. 153-184.

[3] Park, J.W., S.S. Lee, B.S. So, Y.H. Jung, N.Kawasegi, N.Morit and D.W. Lee, "Characteristics of mask layer on (100) silicon induced by tribo-nanolithogrphy with diamond tip cantilevers based on AFM", Journal of Materials Processing Technology, Vol. 187-188, 2007, pp. 321-325.

[4] Stiévenard, D., and B. Legrand, "Silicon surface nano-oxidation using scanning probe microscopy", Progress in Surface Science, Vol. 81, 2006, pp. 112-140.

[5] Vieu, C., Carcenac, F., Pépin, A., Chen, Y., Mejias, M., Lebib, A., Manin- Ferlazzo, L., Couraud, L., and Launois, H., "Electron beam lithography: resolution limits and applications", Applied surface science, 164, 2000, pp. 111-117.

[6] Crafer, R.C., Oakley, P.J. (Eds.), Laser Processing in Manufacturing, Chapman & Hall, London (1993).

[7] Riccardi, G., M. Cantello, F. Mariotti, P. Giacosa, Micromachining with excimer laser, Ann. CIRP 47 (1) (1998) 145–148.

[8] Gower, M.C., "Industrial applications of laser micromachining", Optics express, 7(2), 2000, pp. 56-67.

[9] Ogura, G., Angell, J., Wall, D., Applications test potential of laser micromachining, Laser Focus World 34 (1998) 117–123.

[10] Klimentov, S.M., Garnov, S.V., Kononenko, T.V., Konov, V.I., Pivovarov, P.A., Dausinger, F., High rate deep channel ablative formation by picosecond–nanosecond combined laser pulses, Appl. Phys. A 69 (1999) 633–636.

[11] Hoving, W., Laser fine adjustment, in: Proceedings of the ICALEO, 2001.

[12] Windholz, R., P. Molian, Nanosecond pulsed excimer laser machining of CVD diamond and HOPG graphite, J. Mater. Sci. 32 (1997) 4295–4301.

[13] Spur, G., Industrial cleaning technologies for hard surfaces: dry ice blasting and laser, in: Proceedings of the 40th International detergency Conference IDC'01, 2001, pp. 156–165.

[14] Ishizaka, Y., Watanabe, K., Fukumoto, I., Ohmura, E., Miyamoto, I., Three-dimensional molecular dynamics simulation on laser materials processing of silicon, in: Proceedings of the ICALEO98, 1998, pp. A55–A63.

[15] Basting D., Marowsky, G., "Excimer laser technology", Springer-Verlag Berlin Heidelberg, 2005.

[16] Meijer, J., Du, K., Gillner, A., Hoffmann, D., Kovalenko, V.S., Matsunawa, T., Ostendorf, A., Poprawe, R., Schulz, W., Laser machining by short and ultra short pulses, state of the art and new opportunities in the age of the photons, Ann. CIRP 51 (2) (2002) 531–550.

[17] Paterson, C., Holmes, A.S., and Smith, R.W., "Excimer laser ablation of microstructures: A numerical model", Journal of applied physics, 86(11), 1999, pp. 6538-6546.

[18] Saxena, I., Agrawal, A., and Joshi, S.S., "Fabrication of microfilters using excimer laser micromachining and testing of pressure drop", J.Micromech. Microeng, 19, 2009, pp. 025025-1-025025-10.

[19] Basting, D., Excimer Laser Technology: Laser Sources, Optics, Systems and Applications, Lambda Physik AG, Göttingen (D), 2001.

[20] Chen, X., Liu, X., Short pulsed laser machining: how short is short enough? J. Laser Appl. 11 (6) (1999) 268–272.

[21] Bosman, J., Laser engraving processes, Ph.D. Thesis, University of Twente, in preparation.

[22] Zheng, H.Y., Liu, H., Wan, S., Lim, G.C., Nikumb, S., and Chen, Q., "Ultra short pulse laser micromachined microchannels and their application in an optical switch", Int. J. Adv. Manuf. Technol., 27, 2006, pp. 925-929.

[23] Dubreucq, G.M., Zahorsky, D., KrF excimer laser as a future deep UV source for projection printing, in: Proceedings of the InternationalConference on Microcircuits Engineering, 1982, pp. 73– 78.

[24] Rowan, C., Excimer lasers drill precise holes with higher yields, Laser Focus World August (1995).

[25] Ben, A. -Yakar et al., "Femtosecond laser machining of fluidic microchannels for miniaturized bioanalytical systems," Proceedings of SPIE, Vol. 4637, p. 212-217

[26] Harvey, E.C., Rumsby, P.T., Fabrication techniques and their application to produce novel micromachined structures and devices using excimer laser projection, in: Proceedings of the SPIE Conference on Micromachining and Microfabrication Process Technology III, Vol. 3223, 1997, pp. 26–33.

[27] Rizvi, N.H., Harvey, E.C., Rumsby, P.T., Burt, J.P.H., Talary, M.S., Tame, J.A., Pethig, R., An excimer laser micromachining system for the production of bioparticle electromanipulation devices, in: Proceedings of the SPIE Conference on Micromachined Devices and Components III, Vol. 3224, 1997, pp. 266–272.

[28] Meijer, J., in: J.A. McGeough (Ed.), Micromachining Materials, Marcel Dekker, 2002, pp. 203–237.

[29] Xie J., Huang S., Duan Z., Shi Y.,Wen S., Correction of the image distortion for laser galvanometric scanning system. Opt Laser Technol 2005; 37: 305–11.

[30] Chen M.F., Chen Y.P., Compensating technique of field-distorting error for the CO_2 laser galvanometric scanning drilling machines. IntJ Mach Tools Manuf 2007; 47: 1114–24.

[31] Fischer R.E., Tadic-Galeb B., Optical system design. New York: McGraw-Hill; 2000.

[32] Asif Sabanovic and Kouhei Ohnishi, *Motion Control Systems*, Wiley, Singapore, 2011, ISBN 978-0-470-82573-0.

Appendix A

Definitions of Scan Lens Parameters & Specs

- **Scanning Distance (SD)**: The SD is the distance between the galvo mirror pivot point and the back mounting plate of the objective. Since the LSM scan lens is telecentric, the galvo mirror pivot point must be located at the back focal plane of the objective in order to maximize image resolution.

- **Pupil Size (EP)**: The size of the EP determines the ideal $1/e^2$ collimated beam diameter that should be used for the beam of light used to image the sample in order to maximize the resolution of the imaging system. Used scan lenses have an EP 4 mm in diameter.

- **Working Distance (WD or LWD)**: The distance between the tip of the scan lens housing and the front focal plane of the scan lens is defined as the WD.

- **Depth of View (DOV)**: The DOV parameter reported for the scan lenses corresponds to the distance between the front focal plane and a parallel plane where the beam spot size has increased by a factor of the $\sqrt{2}$.

- **Field of View (FOV)**: The FOV is the maximum size of the area on the sample that can be imaged with a resolution equal to or better than the stated resolution of the LSM scan lenses. In order to meet this specification the imaging system must be designed to properly utilize the LSM scan lenses in the system.

- **Parafocal Distance (PD)**: The PD is the distance from the scan lens mounting plane to the front focal plane of the scan lens.

- **Curvature (C)**: The curvature is the maximum distance between the front focal surface and an ideal plane.

- **Scan Angle (SA)**: The SA is the maximum allowed angle (in the X or Y direction) between the beam and the optical axis of a scan lens after being reflected off of the galvo mirror

LSM Series Lens Specs Chart

Item #	LSM02-BB		LSM03-BB		LSM04-BB	
Magnification	10X		5X		3X	
Design Wavelengths	850 nm	1050 nm	850 nm	1050 nm	850 nm	1050 nm
Wavelength Range	±40 nm	±50 nm	±40 nm	±50 nm	±40 nm	±50 nm
Effective Focal Length (EFL)[1]	17.93 mm	17.97 mm	35.78 mm	35.88 mm	53.61 mm	53.79 mm
Lens Working Distance (LWD)	7.5 mm	7.5 mm	25.1 mm	25.0 mm	42.3 mm	42.2 mm
Scanning Distance (SD)(Distance from Pupil Position to Mounting Plane)	15 mm					
Pupil Size (1/e²) (EP)	4 mm					
Depth of View (DOV)	0.12 mm		0.58 mm		1.15 mm	
Variation of Spot Size Over FOV (dS)	8 μm	9 μm	3 μm	3.5 μm	8 μm	9 μm
Distance Between First Lens Surface and Mounting Plate	-4.0 mm		-3.1 mm		-3.0 mm	
Field of View (FOV)	4.7 x 4.7 mm		9.4 x 9.4 mm		14.1 x 14.1 mm	
Parfocal Distance (PD)	30.7 mm	30.7 mm	50.5 mm	50.5 mm	80.7 mm	80.7 mm
Mean Spot Size (S) (1/e² Beam Diameter in the Field of Focus)	9 μm	11 μm	17 μm	21 μm	24 μm	29 μm
Curvature (C)	48 μm	48 μm	280 μm	290 μm	220 μm	200 μm
Scan Angle (SA)	7.5°					
Max Var. in Optical Path Length (OPL)² from Center to Corner of Image	<1 μm	<1 μm	<3 μm	<5 μm	<10 μm	<5 μm
Transmission Efficiency[3] (Beam Energy into Spot Energy)	>93%					
Linearity of Conversion from Scan Angle into Spot Position	<2.0%	<2.0%	<1.3%	<1.3%	<2.4%	<2.2%
Lateral Color (Maximum Shift Permitted)	<1.6 μm	<3.2 μm	<9.7 μm	<8.1 μm	<16 μm	<17 μm
Vertical Color, Axial Color, or Chromatic Focal Shift (VC) (Maximum Shift Permitted)[1]	<2 μm	<9 μm	<14 μm	<8 μm	<29 μm	<9 μm
Lens Operating Temperature Range (TA)	10 - 50 °C					

Appendix B

Reasons of Image Distortion

The deflection of a laser beam with a two-mirror system results in three effects:

(1) The arrangement of the mirrors leads to a certain distortion of the image field –see Fig. B.1 below.
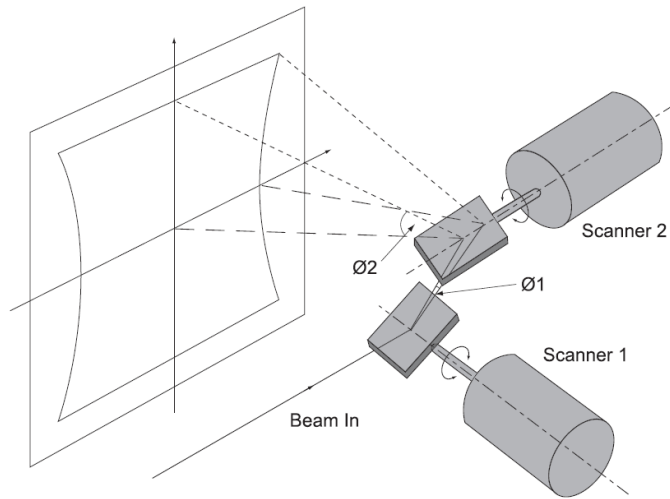
Fig. B.1 Field Distortion in a Two-way Mirror Deflection System

This distortion arises from the fact that the distance between mirror 1 and the image field depends on the size of the scan angles of mirror 1 and mirror 2. A larger scan angle leads to a longer distance.

(2) The distance in the image field is not proportional to the scan angle itself, but to the tangent of the scan angle. Therefore, the marking speed of the laser focus in the image field is not proportional to the angular velocity of the corresponding scanner.

(3) If an ordinary lens is used for focusing the laser beam, the focus lies on a sphere. In a flat image field, a varying spot size is the result.

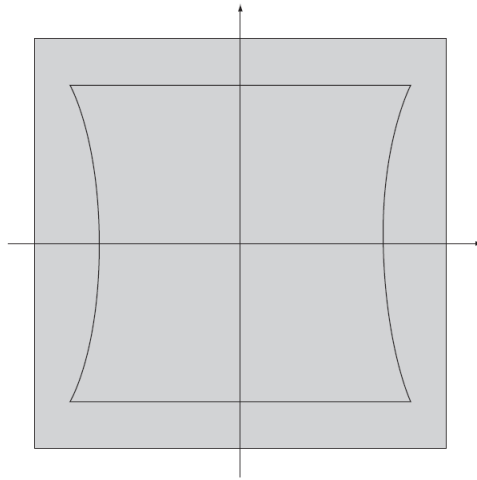As a result, the scanning field turn out to be a "pillow-shaped" image, see Fig. B.2 below.

Fig. B.2 Pillow-shaped Field Distortion Caused by the Arrangement of Mirrors

The F-Theta objective, however, causes a barrel-shaped distortion of the image field.
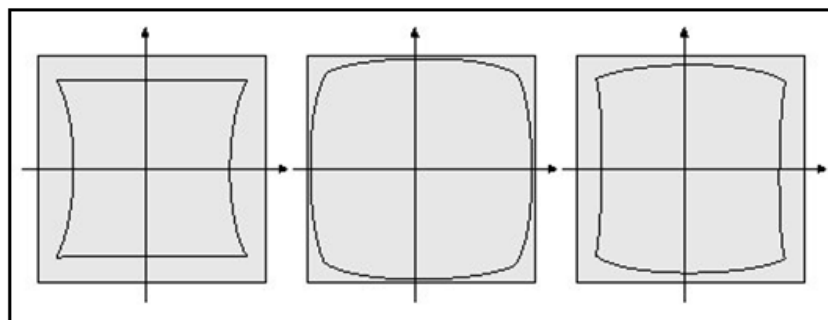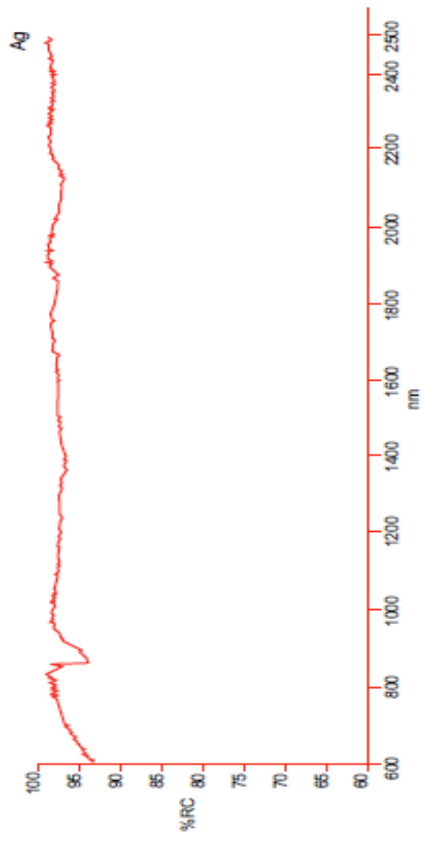
See Fig.B.3

Fig. B.3 Types of Field Distortion a) *Pillow Shaped* b) *Barrel-Shaped* c) *Barrel- Pillow Shaped*

Appendix C

Reflection Curve for Silver Coated Mirrors

Appendix D

Laser Control

Status Word Bit Values

STATUS word bit	Description	Type	Levels	QS Bit-Mask Value
15	Alarm Flag	Read-only	1 = ALARM 0 = NO ALARM	32768
14	System Alarm		1 = SYSTEM ALARM 0 = NO ALARM	16384
13	Beam Delivery Alarm		1 = BEAM DELIVERY ALARM 0 = NO ALARM	8192
12	Temperature Alarm		1 = TEMPERATURE ALARM 0 = NO ALARM	4096
11	Interlock Status		1 = INTERLOCK CLOSED 0 = INTERLOCK OPEN	2048
10	(Reserved for future use)			1024
9	Control Interface Mode (**)		1 = HARDWARE INTERFACE 0 = SOFTWARE INTERFACE	512
8	Alignment Laser Enable	Read/write	1 = ENABLE(D) 0 = DISABLE(D)	256
7	(Reserved for future use)			128
6	(Reserved for future use)			64
5	(Reserved for future use)			32
4	Current Control Mode (*)		1 = EXTERNAL (ANALOGUE INPUT) 0 = INTERNAL (SOFTWARE)	16
3	Pulsed/CWM mode select (*)		1 = CWM 0 = PULSED	8
2	(Reserved)			4
1	Task Start		1 = ENABLE (START)	2
0	Global Enable		1= LASER READY 0 = LASER NOT READY	1

(*)Changes of these bits require the Task Status Enable bit (STATUS word bit 1) to be asserted to affect the change.

(**)This bit is stored in non-volatile memory and is remembered by the laser after turning the laser power off

RS-232 Command Set

Description	Set	Get
Query Alarms This command queries alarm info. Active alarm codes are re-turned as a comma-delimited string. Calling this command also acknowledges the alarm condition and will reset the system Alarm flag if the error(s) conditions that raised the Alarm(s) have been removed.	N/A	**QA** Returns: nn, nn, nn [nn = 0 to 99]
Baud Rate Set/get the Baud rate used for communication The Baud rate (nnnnnn) is 3–6 ASCII decimal digits	**SB nnnnnn** [nnnnnn = 9600, 19200, 38400, 57600, 115200]	**GB** Returns: nnnnnn
Pump duty factor (*) Set/get duty factor of pre-amplifier and power-amplifier pump laser diode pulses. **CWM MODE ONLY**	**SF nnnn** [nnnn = 0 to 1000]	**GF** Returns: nnnn
Power-amp Simmer Current Set Point set/get the stand-by current set-point used for the power-amplifier pump laser diode. nn = 0 to 100 (%) of max current set-point voltage	**SH nn** [nnn = 0 to 100 (pulsed mode), nn = 0 to 85 (CW mode)]	**GH** Returns: nn
Operating Hours Returns the operating hours for this unit (time for which the con-troller has been powered)	N/A	**QH** Returns: nnnnn [nnnnn = 0 to 99999]
Power-amplifier Active State Current Set Point Set/get the active-state current set-point used for the power-amplifier pumps laser diode driver nnnn = 0 to 1000 (0 - 100%)	**SI nnnn** [nnnn = 0 to 1000]	**GI** Returns: nnnn

Query Actual currents Query pump diode driver current reported by pump laser diode driver boards. Returned as comma-delimited data (pre-amp mA, power-amp mA)	N/A	**QI** Retutns: nnnn,nnnn [nnnn = 0 to 1000]
Pulse Burst Length (*) Set/get the number of pulses triggered by laser enable command SL 0 specifies continuous pulsing (default).	**SL nnnnnnn** [nnnnnnn = 0 and 1 to 1000000]	**GL** Returns: nnnn
Pulse Repetition Frequency (*) Set/get pulse repetition frequency of internal trigger (Hz). (set command requires Task Enable bit (2) of STATUS word = 0)	**SR nnnnn** [nnnnn = 1000 to 500000 (pulsed mode), nnnnn = 100 to 100000 (CW mode)]	**GR** Returns: nnnnn
Set STATUS Word Bits Set/get asserted bits of the STATUS word	**SS n** [n = 0 to 8]	**GS** Returns: nn, nn, nn
Clear STATUS Word Bits Clear STAUTS word bits A string of comma-delimited integers in the range 0 – 8 specify which bits of the status word are to be cleared.	**SC nn,nn,nn…nn** [nn = 0 to 8]	
Query STATUS Word Returns the STATUS word as a sixteen bit integer. Bit masks can be used to determine the status of each bit	N/A	**QS** Returns: nnnnn [nnnnnn = 0 to 633535]
Query Temperatures Query temperature monitor on laser base. Returned value in ℃.	N/A	**QT** Returns: nn.n [nn.n = 0.0 to 99.9]
Pulse Waveform (*) Selects pulse waveform shape. Each pulse waveform has an associated pulse rate, pulse burst length and pump duty factor that can be set. For example, this means that calling SW 0 will recall the last pulse rate, pulse burst length and pump duty factor used with waveform 0	**SW nn** [nn = 0 to 63]	**GW** returns: nn
Query_Part Number	N/A	**RPN**
Query_Serial Number	N/A	**RTN**
Query Vendor Info Returns information regarding the controller	N/A	**QV**

Appendix E

Mechanical Parts

E.1 Beam Expander Technical Specs

|	Parameter		Value
Optical Parameters	Rated Operating Power (average)		30W
	Rated Operating Power (peak)		30kW (10ns Pulse) 10kW (100ns Pulse)
	Design Wavelength		1064nm
	Maximum Input Diameter (1/e2)		2.0mm
Optical Performance	Magnification (nominal)		2.6, 4.2, 5.0, 7.0, 8.7
	Magnification Tolerance		±6%
	Divergence		Internally Adjustable
	Pointing Error		≤2.0mrad
	Offset		≤ ($Offset_{in}$ * Magnification * 1.1)
	Transmission @ 1064nm		>95%
	Transmission @ 650nm		> 50%
Environmental Parameters	Housing Material		Aluminium
	Dimensional Tolerance		Refer to outline drawings
	Housing Length	2.6-5.0x	72.6mm
		7.0 & 8.7x	109.0mm
	Clamp Region Diameter		44.0 ± 0.3mm
	Clamp Region Length	2.6-5.0x	>30mm
		7.0 & 8.7x	>50mm
	Output Interface	2.6-5.0x	3 x M4 (34mm PCD)
		7.0 & 8.7x	3 x M4 (38mm PCD)
Environmental Conditions	Operating Temperature		0 to 50°C
	Storage Temperature		-10 to 60°C
	Operating Humidity		5-85%RH (non condensing)
	Storage Humidity		0-95%RH (non condensing)

E.2 Beam Expander Technical Drawing
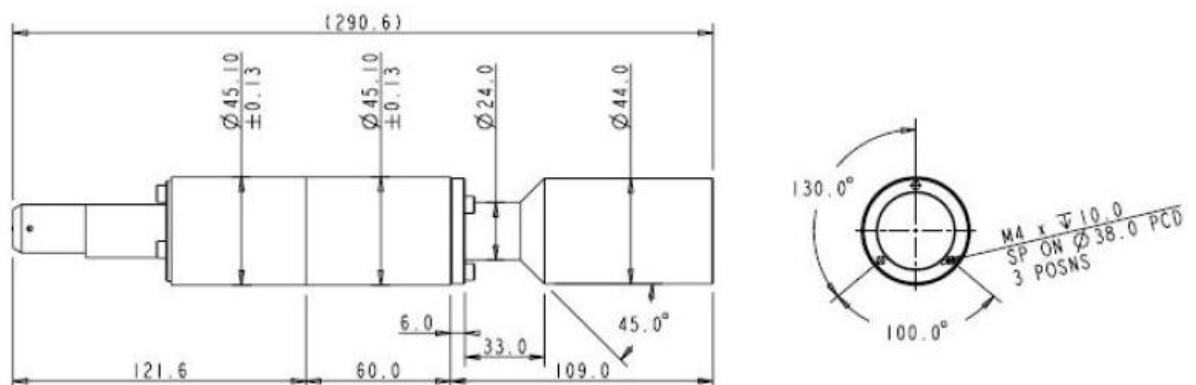
E.3 Focusing Adjustment Mechanism

Ring

Plate

E.4 Beam Expander Mount
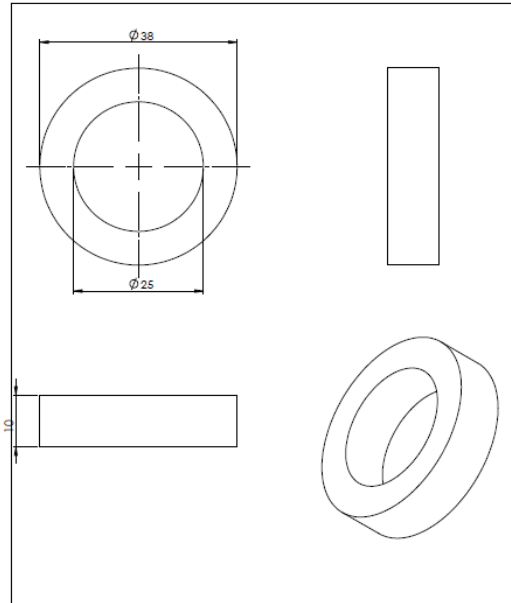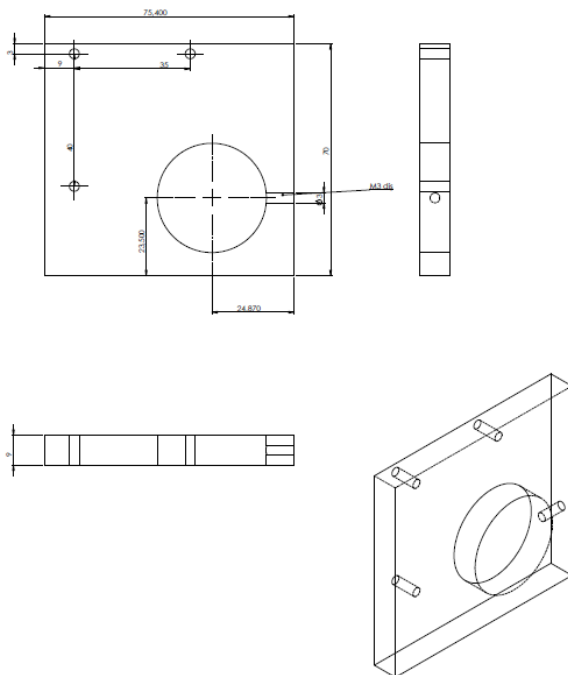
Appendix F

Segmented-Quadrant Sensing Detectors

F.1 Segmented-Quadrant Detectors

Segmented-Quadrant Position-Sensing Detectors

The segmented-quadrant position sensors consists of four distinct yet identical quadrant-shaped photodiodes that are separated by a ~0.1 mm gap and together form a circular detection area capable of providing a 2D measurement of the position of an incident beam. When light is incident on the sensor, a photocurrent is detected by each sector (labeled A, B, C, and D as shown in the figure to the right). From these signals difference signals can be determined using an appropriate A/D converter. The sum of all four signals is also determined for normalization purposes. The normalized coordinates (X, Y) for the beam's location are given by the following equations.
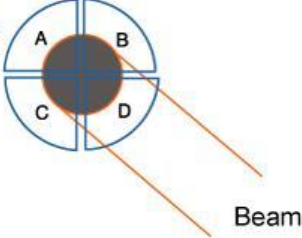
$$X = \frac{(A+C)-(B+D)}{(A+B+C+D)} = \frac{X_{Diff}}{SUM}$$

$$Y = \frac{(A+B)-(C+D)}{(A+B+C+D)} = \frac{Y_{Diff}}{SUM}$$

If a symmetrical beam is centered on the sensor, four equal photocurrents will be detected, resulting in null difference signals, and hence, the normalized coordinates will be (X, Y) = (0, 0). The photocurrents will change if the beam moves off center, thereby giving rise to difference signals that are directly proportional to the beam displacement from the center of the sensor.

These sensors are very accurate and are ideal for auto-alignment applications. However, care should be taken in the shape and density distribution of the incident beam. These sensors are sensitive to these two parameters. A beam that does not have a Gaussian power distribution will be centered based on the power not on the geometric center of the beam. For these types of beams, a lateral sensor might be better suited.

F.2 PDQ80A Specs

Item #	PDQ80A	PDQ30C
Substrate	Si	InGaAs
Wavelength Range	400 - 1050 nm	1000 - 1700 nm
Photodiode Diameter	Ø7.8 mm	Ø3.0 mm
Gap Size	42 µm	45 µm
Detector Bandwidth	150 kHz	150 kHz
Responsivity	0.45 A/W @ 633 nm	1 A/W @ 1630 nm
Dark Current (V_{Rvrs} = 10 V)	5 nA	2.0 nA Typ, 100 nA Max
Rise Time, Typical	40 ns @ 10 V	24 ns @ 5 V
Breakdown Voltage	15 V	10 V
Damage Threshold	100 mW/cm^2	100 mW/cm^2
Housing Dimensions	2.0" x 1.20" x 0.65"	
Cable Length	5 ft (1.52 m)	
Mounting Threads	8-32 (with M4 Adapter Included)	

Appendix G

Links

Coherent. *Understanding Laser Beam Parameters. Retrieved* July 2011, from
http://www.coherent.com/downloads/UnderstandingLaserBeamParameters.pdf

Coherent. *Best Practices White Paper. Retrieved* July 2011, from
http://www.coherent.com/Downloads/Best_Practices_Whitepaper.pdf

FTDI Company. *FT232R USB UART IC Datasheet Version 2.09. Retrieved* December 2010, from
http://www.ftdichip.com/Support/Documents/DataSheets/ICs/DS_FT232R.pdf

Linear Technologies. *LTC1859 8-Channel, 12-/14-/16-Bit,100ksps SoftSpan A/D Converters with Shutdown. Retrieved* November 2010, from **http://cds.linear.com/docs/Datasheet/185789fa.pdf**

Linear Technologies. *LTC2641/LTC2642 16-/14-/12-Bit VOUT DACs in 3mm × 3mm DFN. Retrieved* November 2010, from **http://cds.linear.com/docs/Datasheet/26412fb.pdf**

Maxim. *CMOS Monolithic Voltage Converter. Retrieved* March 2011, from http://datasheets.maxim-ic.com/en/ds/MAX660.pdf

Microchip. *DsPIC30F6010A/6015 Data Sheet High-Performance, 16-bit Digital Signal Controllers. Retrieved* March 2011, from **http://ww1.microchip.com/downloads/en/DeviceDoc/70150E.pdf**

Microchip. *Dspic Reference Manual Serial Peripheral Interface (SPI). Retrieved* April 2011, from
http://ww1.microchip.com/downloads/en/DeviceDoc/70067E.pdf

Microchip. *PICkit. 2 Programmer/Debugger Use's Guide. Retrieved* March 2011, from
http://ww1.microchip.com/downloads/en/DeviceDoc/51553E.pdf

SPI Laser. *redENERGY G3 Made for. Retrieved* June 2011, from
http://www.spilasers.com/Products/redENERGY_G3.aspx?

Texas Instruments. *MAX232, MAX232I EIA Line Drivers/Receivers. Retrieved* April 2011, from
http://focus.ti.com/lit/ds/symlink/max232.pdf

Thorlabs, Inc. *- Your Source for Fiber Optics, Laser Diodes, Optical Instrumentation and Polarization. Retrieved* June 2011, from **http://www.thorlabs.de/index.cfm?**

USB. *Universal Serial Bus. Retrieved* May 2011, from **http://www.usb.org/home**